Stockholm University

Licenciate thesis

Geology

Vein controlled crystal size distributions of Barrovian index minerals

Alexander Lewerentz

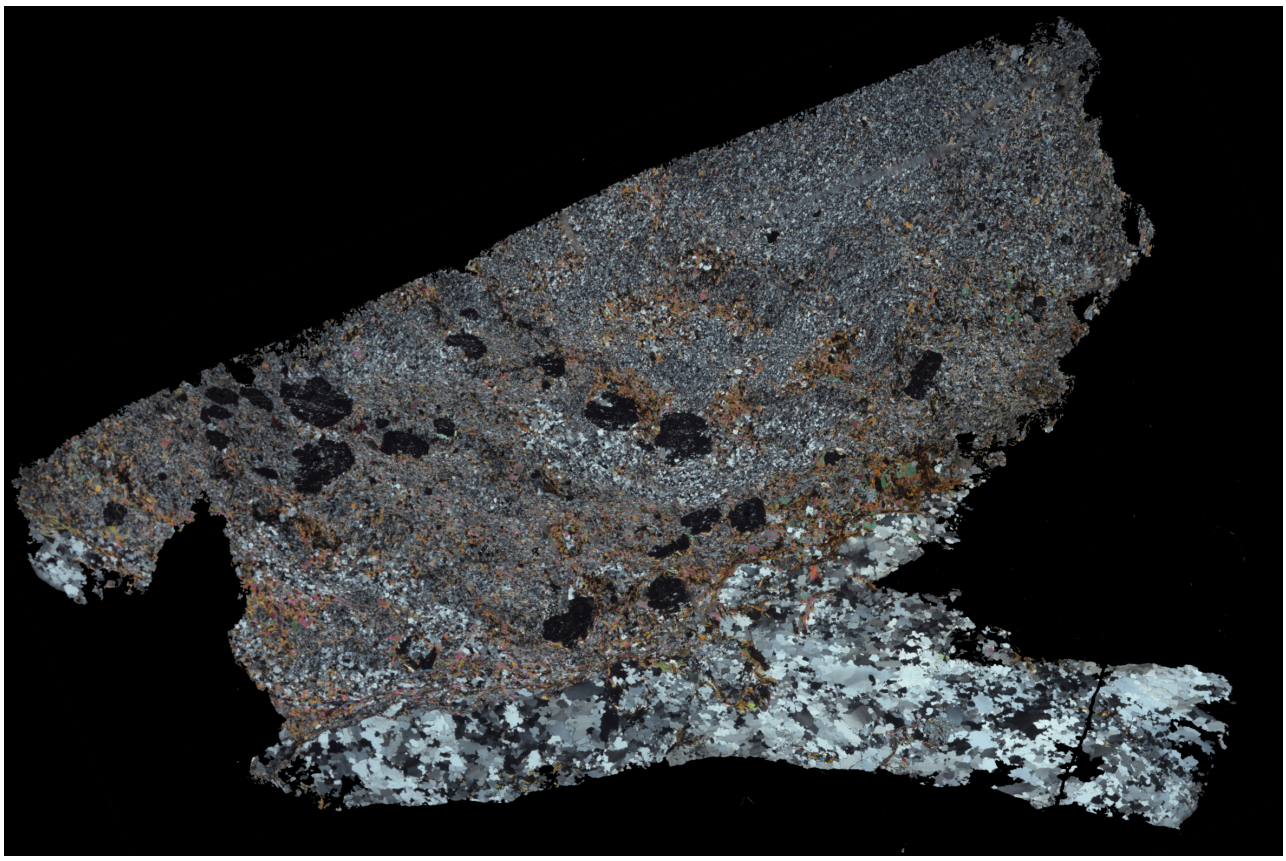

Stockholm 2015

Department of Geological Sciences
Stockholm University
SE-106 91 Stockholm

Vein controlled crystal size distributions of Barrovian index minerals

Alexander Lewerentz

Stockholm 2015

Abstract

The concept of index mineral based metamorphic zones was first introduced by George Barrow in 1912, and Barrovian metamorphism is still applied by metamorphic petrologists. Today the importance of metamorphic fluids for driving metamorphic reactions is widely recognised. Even so, the general view is that Barrovian metamorphism is solely controlled by pressure, temperature, and protolith composition. This thesis aims to establish if and how fluids control index mineral formation and distribution during Barrovian metamorphism. To do so, samples from Barrow's own type locality in Glen Esk, Southeast Scottish Highlands, are used to investigate possible relationships between veining and index mineral distribution. This was done using a combination of petrographic and textural observations and analyses, whole rock chemistry, mineral chemistry, as well as oxygen isotope analyses. These data show a grade dependant association of index mineral distribution and veining: in the chlorite zone and most of the biotite zone, no correlation between veining and index mineral distribution is seen. For the garnet and staurolite zones, index mineral abundance is shown to decrease away from veins. The kyanite zone shows a fairly homogenous kyanite distribution, but also indications of extensive fluid-rock interaction. Based on these observations and the analysis datasets, it is concluded that fluid played a major role in the stabilisation and distribution of the Barrovian index minerals in Glen Esk, and that the fluid control was larger at metamorphic grade.

Sammanfattning

Metamorfa zoner baserade på index mineral introducerades av George Barrow 1912 och dessa används fortfarande idag av petrologer. Ehuru vikten av metmorfa fluider för att driva metamorfa reaktioner har under senare tid blivit allmer erkänd, anses barrovisk metamorfos enbart vara kontrollerad av tryck, temperatur och protolitens kemiska sammansättning. Målet med denna avhandling är att undersöka om och hur metamorfa fluid påverkar bildande och fördelning av indexmineral under barrovisk metamorfos. I studien används prover från Barrows egen typlokal i Glen Esk, sydöstra skotska högländerna, för att utröna möjliga samband mellan åderbildning och indexmineralfördelning med hjälp av en kombination av petrografiska och texturella observationer och analyser, kemisk bergartssammansättning, mineralkemi, samt syreisotopanalys. Dessa påvisar en fördelning av indexmineral som är beroende av metamorf grad: i kloritzonen och mestadels biotitzonen finns ingen korrelation mellan indexmineralfördelning och åderbildning. I granat- och staurolitzonen finns däremot ett starkt samband där indexmineralmängd minskar med ökat avstånd från kvartsådror. Kyantizonen visar emellertid en homogen fördelning av indexmineral, men också indikationer på kraftig reaktion mellan fluid och berg. Med anledning av ovanstående fastslås att metamorfa fluider hade stor påverkan på stabilisering och fördelning av barroviska indexmineral i Glen Esk, samt att fluidpåverkan var högre vid högre metamorf grad.

Contents

1. Introduction

The word *metamorphism* is derived from *metamorphosis*, which is of Greek origin and translates to "*a change of the form or nature of a thing or person into a completely different one*" (Oxford Dictionaries, 2015). The geological meaning of this is the transformation of a rock type into another by mineralogical alteration induced by changes in pressure, temperature or some other shift from chemical equilibria in the system. Today we recognise plate tectonics as the driving force behind metamorphism, but scientists researched the subject of metamorphism long before plate tectonics was widely accepted by the scientific community.

One of the early descriptions of metamorphism was made by Hutton (1788), although not using the exact word but nonetheless distinguishing between primary and secondary rock types. Approximately a hundred years later, Barrow (1893; 1912a) used the term metamorphism when he introduced the metamorphic zones as an explanation for systematic mineralogical and textural variations in metasedimentary rocks found in the Scottish Highlands. This concept exploits the fact that different minerals are thermodynamically stable at different temperature and pressure conditions, which results in a sequence of index minerals that represents gradually increased metamorphic grade.

The Barrovian sequence is only valid for metapelites, i.e. the resulting rock type from metamorphism of a mudstone protolith. Protoliths of any other composition than that of an average pelite will result in metamorphic rocks that do not follow this sequence. Protolith composition together with pressure and temperature are the main controls on Barrovian metamorphism, at least according to the general view. Recently, metamorphic fluids have been recognised as perhaps the most important force driving metamorphic reactions. Even so, the impact of metamorphic fluids on Barrovian metamorphism remains unstudied.

This thesis aims to establish the importance of metamorphic fluid flow for Barrovian metamorphism, and more specifically answer the following questions. Is there a spatial relationship between index mineral distributions and veins? How do fluids affect the mineralogical, chemical and isotopic compositions of rock adjacent to veins? What is the impact on index mineral distribution, and thus the appearance of Barrovian metamorphism? Samples from Barrow's own type locality in Glen Esk, Scotland, are used to answer these questions and thereby constraining controls for index mineral stabilisation. The following datasets are taken into account: petrographic observations, whole rock and mineral chemical composition, equilibrium thermodynamics (pseudosections), and oxygen isotope signatures.

2. Background

2.1 Barrovian metamorphism

George Barrow (1853 – 1932) was one of the pioneers in the study of metamorphic rocks, and is famous for introducing the concept of metamorphic zones, presented in Barrow (1893; 1912a). His work is based on observations from large areas of the SE Scottish Highlands, where Glen Esk, and nearby valleys Glen Lethnot and Glen Clova, served as type localities. Barrow's key observations are a gradual, systematic change in mineralogy and texture of the metasedimentary rocks found in these areas, which he interprets as recording continuously increasing intensity of metamorphism, and from this the concept of metamorphic zones is derived. According to this concept, the first appearance of a certain mineral marks the transition into the next metamorphic zone. Such minerals are known as *index minerals*. The Barrovian metamorphic sequence consists of six metamorphic zones, which are named after their respective index minerals: chlorite, biotite, garnet, staurolite, kyanite and sillimanite, in order of increasing metamorphic grade.

Eskola (1915; 1920; 1929) later refined Barrow's work by introducing the ACF and AKF chemographic diagrams, and thereby linked mineral assemblages to protolith composition. Both diagrams uses systems that are reduced to three components, because this is the maximum number that is easily represented in a two dimensional diagram. The first step in this reduction by grouping components together, meaning that they are treated together as one component under the assumption of equal partitioning within the group, as shown in table 1. The second step is to project the diagram from components or phases that are in excess, in this case both the ACF and AKF diagrams are projected from quartz and H_2O. The ACF diagram is also projected from muscovite and albite, but the AKF diagram from muscovite and plagioclase. A problem with both the ACF and AKF systems is that ignore the effect of varying the relative proportions of FeO and MgO, but this is not appropriate for various metamorphic minerals (e.g. chlorite, biotite, and garnet). As a solution, Thompson (1957) introduced a chemographic diagram specially constructed for metapelites: the AFM diagram which treats FeO and MgO as separate components (fig. 1). This is enabled by projection from quartz, muscovite, and H_2O, in combination with that Na_2O, CaO, and MnO are ignored.

Table 1. Component reduction in the ACF, AKF, and AFM systems

ACF	AKF	AFM
$A = Al_2O_3 + Fe_2O_3 – (Na_2O + K_2O)$	$A = Al_2O_3 – (CaO + Na_2O + K_2O)$	$A = Al_2O_3 - 3K_2O$
$C = CaO$	$K = K_2O$	$F = FeO$
$F = FeO + MgO + MnO$	$F = FeO + MgO + MnO$	$M = MgO$

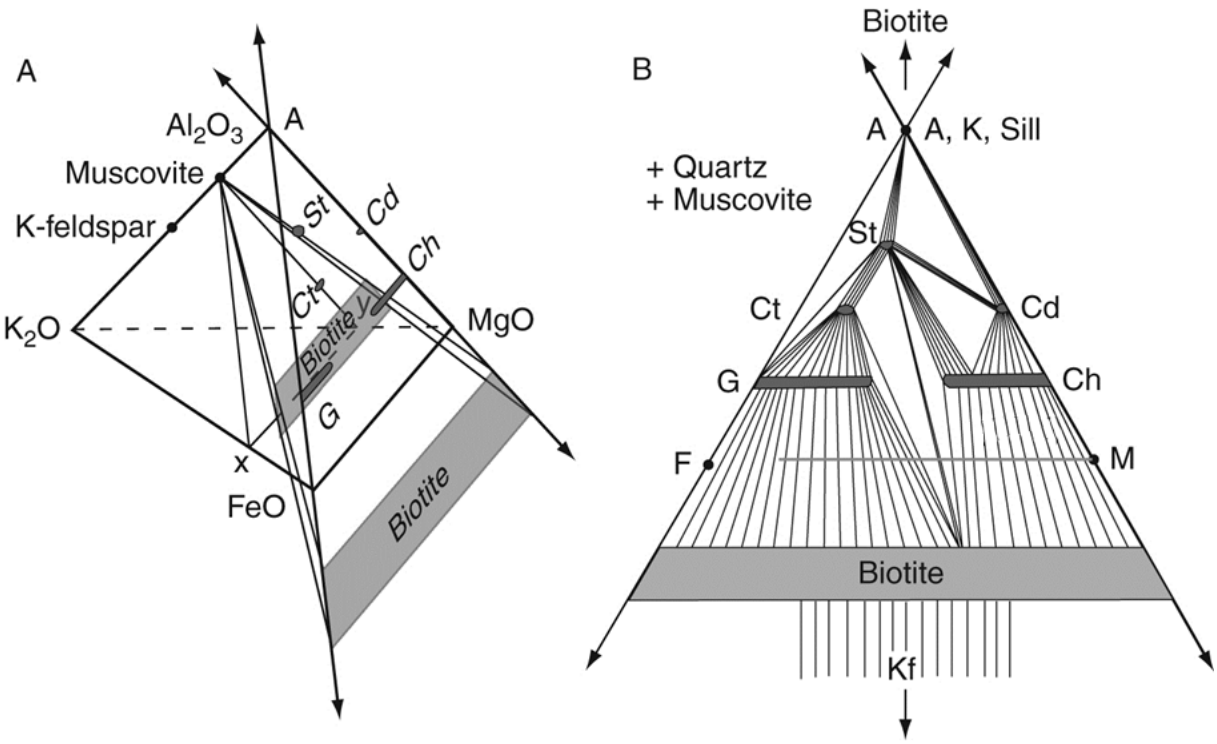

Figure 1: Projection and general construction of Thompson's (1957) A(K)FM diagram, specially designed to link bulk rock composition with mineral assemblages for metapelites (from Philpotts & Ague, 2009). Mineral abbreviations: A = andalusite, K = kyanite, Sill = sillimanite, St = staurolite, Ct = chloritoid, Cd = cordierite, G = garnet, Ch = chlorite.

Chemographic diagrams only consider mineral assemblage stability as a function of bulk rock composition, and do not alone give any information about changes in mineral assemblages and the reactions driving such changes. Equilibrium thermodynamics are widely used to investigate these *metamorphic reactions*, a practice made possible by the compilation of thermodynamic databases containing mineral stability data (cf. Helgeson et al., 1978; Berman et al., 1985; Holland & Powell, 1985; Powell & Holland, 1985). Using such databases, it is possible to construct AFM diagrams for a series of temperatures and thus track the reactions that cause changes in mineral assemblages. Another application is construction of petrogenetic grids, i.e. pressure-temperature (P-T) diagrams of all possible metamorphic reactions (cf. Albee, 1965; Hess, 1969; Thompson, 1976; Koons & Thompson, 1985; Spear & Cheney, 1989). Although a powerful tool for general estimation of P-T conditions and P-T paths during metamorphism, petrogenetic grids do not take bulk rock composition into account, and thereby offer no information of which reactions will take place for a specific rock with a specific composition. This shortfall is overcome by using thermodynamic data bases to construct pseudosections: these are P-T or temperature-composition (T-X) diagrams that take rock composition into account and show which mineral assemblages are stable for a specific rock over a range of P-T or T-X conditions (cf. Hensen, 1971; Powell et al, 1998). P-T pseudosections are especially used for tracing the metamorphic P-T path (fig. 2). T-X pseudosections are utilised to investigate what impact rock or fluid composition has on mineral assemblage stability, and are a good tool in the study of metamorphic fluids.

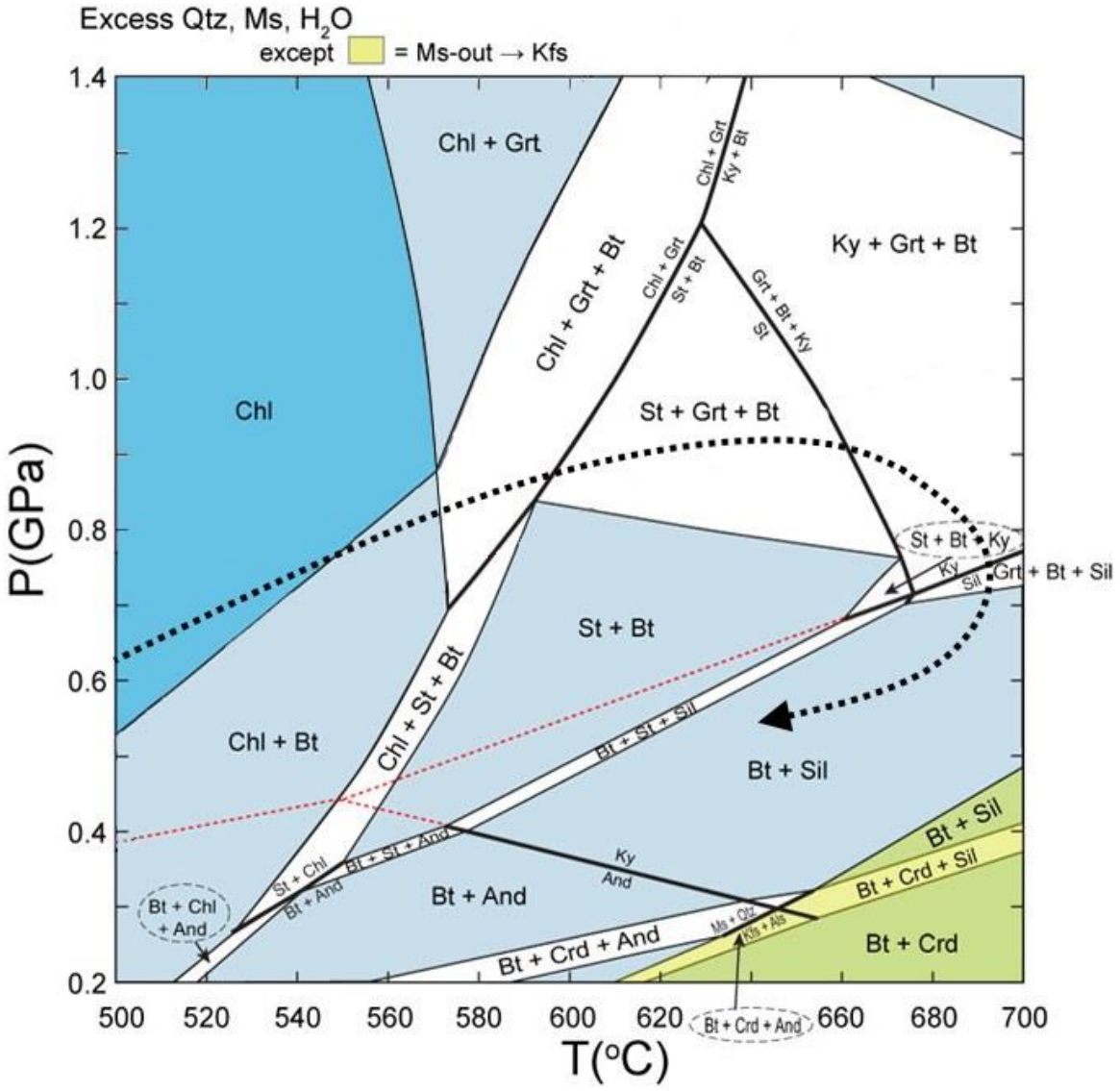

Figure 2: Pseudosection for a rock with typical metapelite composition, constructed using the KFMASH system (modified from Winter, 2010). The dashed black curve represents a hypothetical P-T path that would yield the Barrovian sequence of index minerals. Mineral abbreviations: Chl = chlorite, Bt = biotite, Grt = garnet, St = staurolite, Ky = kyanite, Sil = sillimanite, And = andalusite, Crd = cordierite, Ms = muscovite, Qtz = quartz, and Kfs = K-feldspar.

2.2 Metamorphic fluids

Metamorphic fluids are released from the crust when temperature increases as a result of subduction or burial. They originate from H and C bearing phases that gradually become unstable due to increasing metamorphic grade. The main constituents are H_2O and CO_2, but small amounts of methane and dissolved salts (e.g. Na^+, K^+, and Ca^{2+}) may also be present (Philpotts & Ague, 2009 and references therein). Metamorphic fluid flow is widely recognised as one of the main driving forces for metamorphic reactions. During metamorphic reactions, the reactants and products of these reactions are transported by diffusion, and diffusion rate is the chief kinetic limit on these reactions. The rate of diffusion when fully assisted by fluid is over 9 orders of magnitude faster than diffusion through silicate phases only. Hence, fluids make metamorphic reactions considerably faster (Ridley & Thompson, 1986).

Metamorphic fluids are a relatively recent discovery, and it was first in the late 1950s and early 1960s that the idea was proposed (e.g. Greenwood, 1961; 1962). Metasomatism, the alteration of one phase into another but retaining the original volume, was one of the first studied fluid driven metamorphic processes, for which Thompson (1959) concluded that mass transfer is required and proposed metamorphic fluids as transport medium. Several approaches to assessment of component mobility in metasomatic systems have been proposed. Gresens (1967) used differences in density and component concentration between original and altered minerals/rocks, thus deducing the amount of any given component that needs to be added or removed in order to retain unchanged volume. As a simplification of the same approach, the isocon diagram (fig. 3) was introduced by Grant (1986).

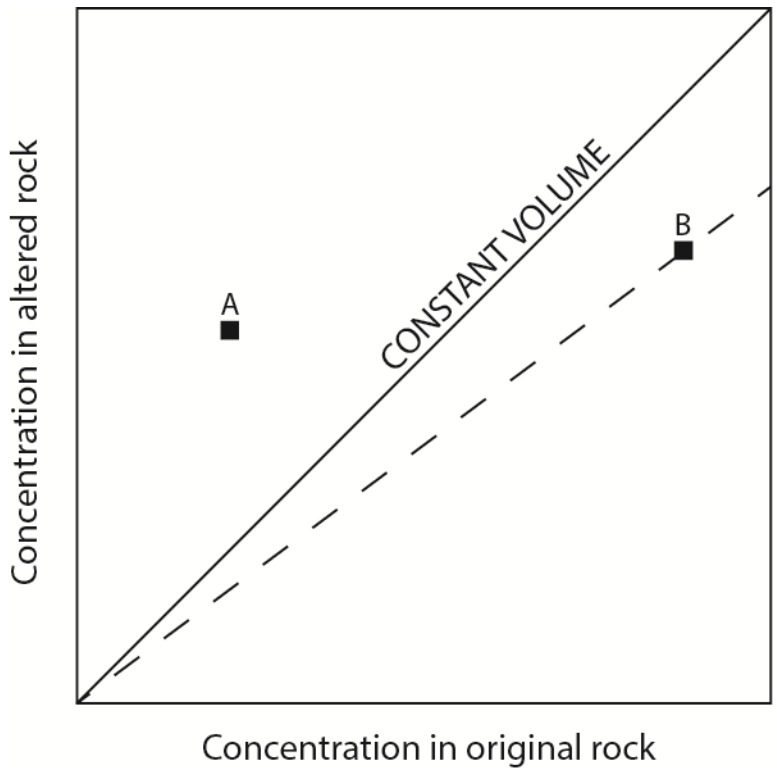

Figure 3: Grant's isocon diagram. If constant volume is assumed, the metasomatic alteration of this rock would have resulted in enrichment of component A, but depletion of component B. If however constant concentration of B is assumed (dashed line), e.g. if so is shown by chemical analysis, it follows that the volume must have increased. By analogy constant concentration of component A would imply a decrease in volume (drawn after Grant, 1986).

Devolatilisation reactions yield large quantities of fluids that are transported through the crust and can thereby interact with the surrounding rock on a regional scale. Over the years, numerous approaches have been proposed for description, evaluation, and quantification of regional scale metamorphic fluid flow. Taylor (1977) used oxygen isotope ratios to construct a volumetric model, the water-rock ratio (W:R), which may be used for evaluation and quantification of fluid driven reactions. The approach yields the relative proportions of fluid and rock that were needed to change the isotopic signature ($\delta^{18}O$) of a rock into that observed in its altered state. This is made possible by that if an external fluid reacts with the surrounding rock, the isotopic signature of the rock will change and equilibrate towards that of the fluid. The degree of equilibration is a direct function of the degree of fluid-rock interaction. Numerous alternatives for calculation of W:R ratios have been proposed over the years. One example is Ferry (1987), who proposed a model based on mass transfer of CO_2 by which the W:R ratio is calculated through the relative proportion of fluid that was needed to carbonate an originally carbonate free rock.

Later studies also focused on how fluids are transported in the crust, and to quantify the actual transportation. On this matter, Bickle & Baker (1990), using oxygen isotope signature profiles that contained alternating layers of schists and marbles, concluded that fluids had been channelled in certain high flux zones. They found that these were predominately positioned within the metapelite sequence, and thus controlled by contrasts in permeability. Furthermore, they also used advective-diffusive transport modelling of the displacement of oxygen isotope fronts to calculate a time integrated fluid flux, i.e. the total amount of fluid that was transported past a specific point over the entire time of active metamorphism. In addition to previous mentioned discoveries, Ague (1994; 2003; 2011) used mass balance calculations, i.e. loss or gain of components analogous to Grant's isocon diagram (fig. 3), to estimate fluid fluxes during Barrovian type metamorphism. He concluded that especially for metapelites, fluids are channelled in vein fracture conduits, which are cm to m scale areas where intense veining occurred during metamorphism. As a result of these, cm to m scale selvages (altered zones), are created in vein adjacent wall rock. In figure 4, a conceptual drawing with different modes for transportation of metamorphic fluids is shown.

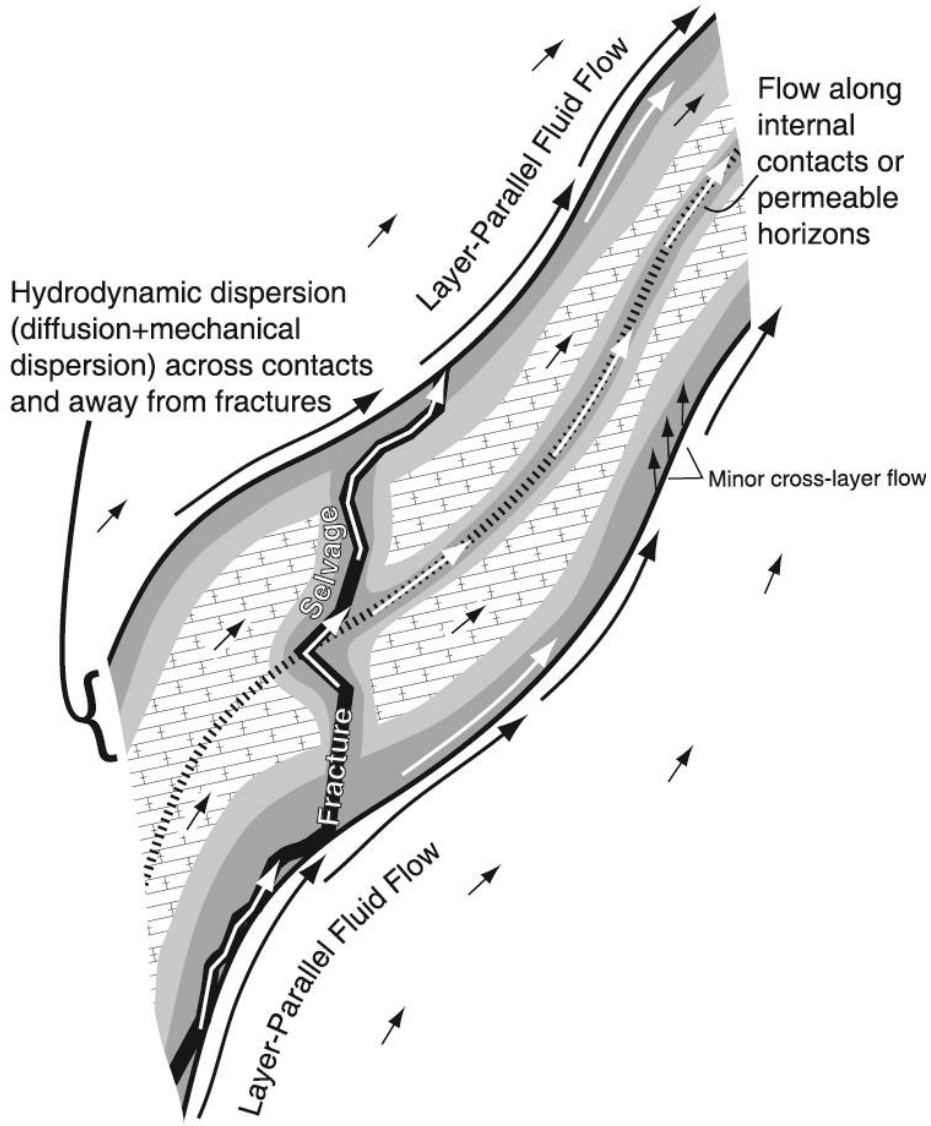

Figure 4: A summary of the different modes for transportation of metamorphic fluids (from Ague, 2003). Diffusive and mechanical dispersion dominate a minor flux component of cross layering flow, and is induced either by devolatilisation reactions or selvage formation. Fluids originating from these processes are channelled into high flux zones, either controlled by permeability contrasts as in the case of layer parallel flow at lithology boundaries or other permeable horizons, or in fractures (veining) which may be either parallel or crosscutting to layering.

2.3 Geological setting

Glen Esk is famous as the type locality of George Barrow's own metamorphic sequence; the actual outcrops he used to propose his theory of metamorphic zones (Barrow, 1893; 1912a; 1912b; Harker, 1912). Situated in the SE Scottish Highlands, Glen Esk hosts rocks from both sides of the Highland Boundary Fault (HBF). At the lower end of the valley in the south, Old Red Sandstone Supergroup sedimentary and volcanic rocks of Siluro-Devonian age are the dominating lithologies. Further to the north and on the other side of the HBF, Ordovician rocks of the Highland Border Complex (HBC) are found. Subdivided into the Margie and North Esk Formations, the HBC consists of weakly metamorphosed limestones, shales, slates,

grits, and conglomerates. The HBC is juxtaposed against rocks belonging to the Dalradian Supergroup along the North Esk Fault (NEF). These are metasedimentary rocks belonging to the Glen Lethnot Grit and Glen Effock Schist Formations (Fig. 5). This metamorphosed turbidite sequence consists of alternating layers of metapelites and metapsammites. Metamorphic grade increases continuously, from chlorite grade near the NEF up to sillimanite grade, northwards across the area. In the north, the sequence is cut off by a granite intrusion.

The area is part of the Caledonian mountain chain, and the Grampian Orogeny has been considered to be the main metamorphic event, taking place at 475-465 Ma and reaching peak metamorphic conditions at ca. 470 Ma (Chew & Strachan, 2014). The cluster of granitic and gabbroic intrusions that is found in the area has been dated to ca. 470 Ma (e.g. Oliver et al., 2000; Dempster et al., 2002; Oliver et al., 2008). Observing temperature anomalies in garnet thermobarometry data, Vorhies & Ague (2011) hypothesised that these intrusions caused a secondary heating event and thus are the cause of peak metamorphic temperatures. For a more detailed description of the regional geology, see for instance Harte (1987), Tanner et al. (2013), and references therein.

Pressure and temperature conditions for peak metamorphism are presented in a number of studies, often accompanied by data from the neighbouring valley, Glen Lethnot, which is considered metamorphically equivalent to Glen Esk. Peak metamorphic conditions are estimated to 510-630°C in the staurolite (st) zone, 6.2 kbar and 610-640°C in the kyanite (ky) zone, as well as 5.5-7.4 kbar and 650-690°C in the sillimanite (sil) zone (Dempster, 1985). Estimates from Baker (1985) are in agreement with these numbers: 5.8-6.1 kbar and 610-630°C (ky), 5.7-5.9 kbar and 650°C (sil). More recent evaluations by Viete et al. (2011) show 4.4 kbar and 540°C (grt), 5.7 kbar and 620°C (st), 5.9-6.1 kbar and 640-670°C (sil), while 6.5-8.5 kbar and 580-660°C for the st zone is presented by Vorhies & Ague (2011).

Typical mineral assemblages are, all of which include muscovite and quartz, chlorite, chlorite+biotite, chlorite+biotite+garnet, biotite+garnet+staurolite±chlorite, biotite+staurolite +kyanite±garnet, and biotite+sillimanite±K-feldspar±garnet±staurolite±kyanite. In addition to these typical assemblages, occasional magnetite, pyrite, haematite, and plagioclase have been reported (Barrow, 1893; Barrow, 1912a; Harte & Hudson, 1979; Harte, 1987). Chlorite is also commonly found in the higher grade zones, here attributed to retrograde metamorphism replacing garnet, and biotite. Other observed retrograde reactions are those of sillimanite, kyanite, and staurolite breaking down into white micas (Harte & Johnson, 1969; Baltatzis & Katagas, 1981).

Previous studies on index mineral distribution in their respective zones have shown confinement to layers of pelitic composition for garnet, staurolite, kyanite, and sillimanite, while chlorite and biotite also appear in rocks of more psammitic composition (Harte & Johnson 1969; Tanner et al. 2013). They also reported that kyanite and sillimanite are found in veins. Using structural and textural observations, Harte & Johnson (1969) suggested that growth of index minerals occurred stepwise as a result of four separate structural events. This idea of stepwise index mineral stabilisation, and implicated rapid changes in metamorphic conditions, is also favoured by Robertson (1994). Vorhies & Ague (2011) attributed the last of these steps, the stabilisation of sillimanite, to a secondary heating event caused by magmatic intrusions where the sillimanite zone rocks as a matter of proximity was affected the most.

3. Materials and methods

3.1 Field measurement and sampling

This thesis is based on studies of the metasedimentary rocks in Barrow's type locality; Glen Esk. Outcrops at several localities were examined in each of the six metamorphic zones. All localities are situated on a semi-linear profile, approximately perpendicular to the NEF (fig. 5). Petrological, mineralogical and structural descriptions and measurements were conducted in the field. Relative proportions of the different rock types present at the localities were estimated using 2-dimensional profiles. At some localities, analysis of crystal size and abundance was undertaken using a 5x5 cm meshed square. At each locality, samples representative for all present lithologies were collected for further analysis.

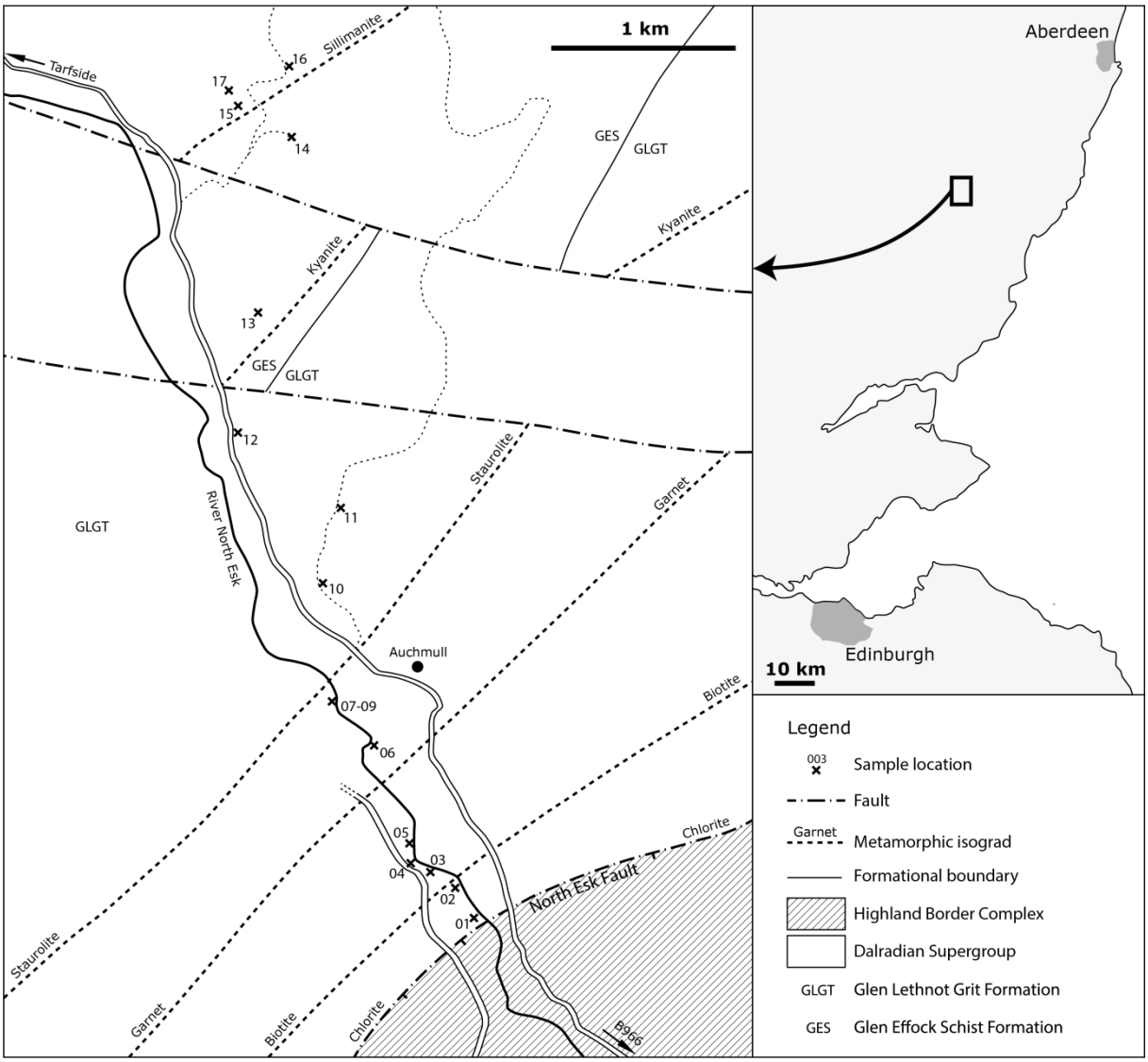

Figure 5: Map showing the field area in Glen Esk, SE Scottish Highlands. The main rock groups and formations, structural boundaries, isograds (drawn from Tanner et al. 2013), and locations of the sample localities are shown.

3.2 Analytical methods

Detailed petrographic and mineralogical descriptions were made using a polarisation microscope fitted with an automated stage for mineral abundance analysis. Mineral abundances were estimated by point counting, whereby minerals were identified in a total of 1000 evenly distributed points for each thin section. The approach of van der Plas & Tobi (1965) was used for estimating uncertainty levels.

Sample preparation for composition analysis began with crushing and milling of the samples. The resulting whole rock powders were then dried in two steps to determine volatile components as loss on ignition (LOI) by comparison of sample weight after (1) >10 h drying at 105°C and (2) >10 h ignition at 1050°C. Following the LOI analysis, the powders were fused into glass discs using a lithium-metaborate-tetraborate flux that is used to lower the melting point of the samples. These glass discs were analysed for major elements using a Rigaku ZSX Primus II sequential X-ray fluorescence (XRF) spectrometer, and for trace elements using a Thermo Fisher X-series II quadropole laser ablation inductively coupled plasma mass spectrometer (LA-ICP-MS), at the Department of Geological Sciences, Stockholm University. Repeat analysis of standard reference material ensures a precision better than 1% for major elements and 5% for trace elements.

Chemical composition of minerals was determined by spot analyses using a JEOL JXA-8530 field emission electron microprobe analyser (EMPA) at the Department of Earth Sciences, Uppsala University, operating in wavelength dispersive (WDS) mode at 15 kV and 20 nA with a beam size of 1-5 µm. Estimated relative 1-σ errors are <0.5 % at >10 wt%, <5% at >1 wt%, 5-20 % at >0.1 wt% and 20-50 % at <0.1 wt%.

Oxygen isotope signatures ($\delta^{18}O$) were determined by laser fluorination of handpicked quartz or kyanite separates using a CO_2 laser and a Finnigan MAT 251 isotope ratio mass spectrometer (IRMS) at the Department of Geoscience, University of Wisconsin-Madison, following the method described by Valley et al. (1995) and Spicuzza et al. (1998). Typical absolute analytical error following this technique is ±0.1‰ $\delta^{18}O$.

3.3 Thermodynamic calculations

Thermodynamic calculations for construction of pseudosections were made using THERMOCALC v3.37 and the ds55 data set (Holland & Powell, 1998a; 1998b), with whole rock chemical compositions from XRF analysis as input data, if necessary corrected for plagioclase and oxide phases. The seven component MnKFMASH system was used. This system includes MnO, K_2O, FeO, MgO, Al_2O_3, SiO_2, and H_2O. H_2O was assumed to be in excess. Solid solution substitution was taken into account by usage of the following models; for cordierite, chloritoid, and staurolite (Mahar et al., 1997; Holland & Powell, 1998b), for chlorite (Mahar et al., 1997; Holland et al., 1998), for garnet and biotite (White et al., 2005), as well as for muscovite (Holland & Powell, 1998b).

4. Discussion of results

Collected observations and analysis data, as well as discussion of these, are fully presented in the attached manuscript. A summary of the most important findings is given here.

In the chlorite zone, chlorite is present in all collected samples in abundances varying from 23 to 36 vol%, and homogeneously distributed within the rocks (fig. 6). Vein density is <1% and the distance between veins is generally several meters or more, which results in only a small proportion of the rock mass being affected by fluid-rock interaction. In addition to this, oxygen isotope data show no signs of equilibration between fluid and country rock (see manuscript for details). The summative interpretation is that the distribution of chlorite as an index mineral is controlled by pressure, temperature, and protolith composition (P-T-x), and hence in agreement with the general view on Barrovian metamorphism.

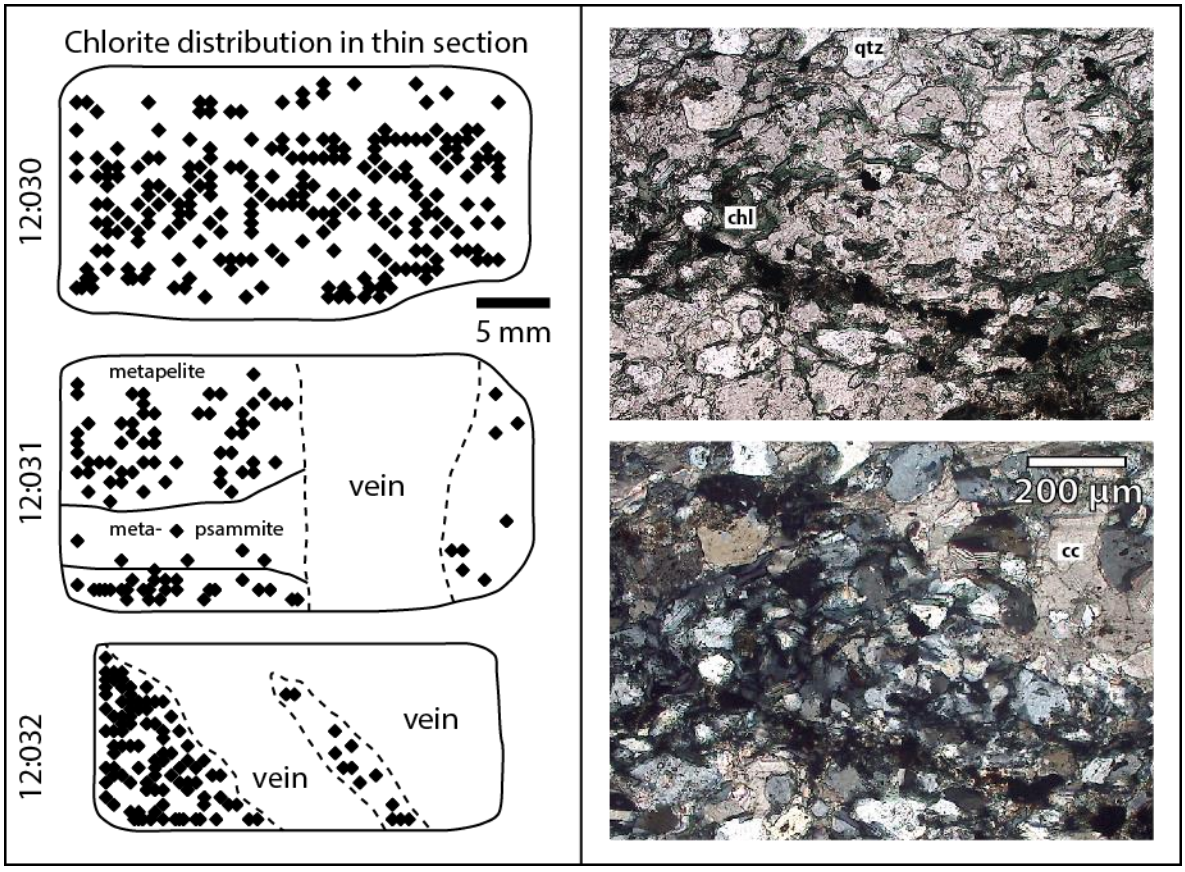

Figure 6: To the left: Spatially plotted chlorite occurrences from thin section point counting, with thin section edges, lithological layers, and veins sketched in, overall showing an homogeneous distribution of chlorite. To the right: Thin section micrographs from sample 12:030 in plane-polarised (above) and cross-polarised light (below). This shows that calcite occurs as an interstitial phase occupying spaces between quartz and chlorite crystals.

Most of the biotite zone is similar to the chlorite zone in terms of index mineral distribution, i.e. biotite size distribution is overall homogenous. However, one of the sampled localities is distinctively different than the rest of the biotite zone (fig. 7). This locality comprises a fold hinge which is intensely veined, with vein densities that reaches above 50% if only accounting for the area closest to the hinge. An estimation of biotite crystal size distribution that was conducted in the field shows the biotite crystals are largest at the fold

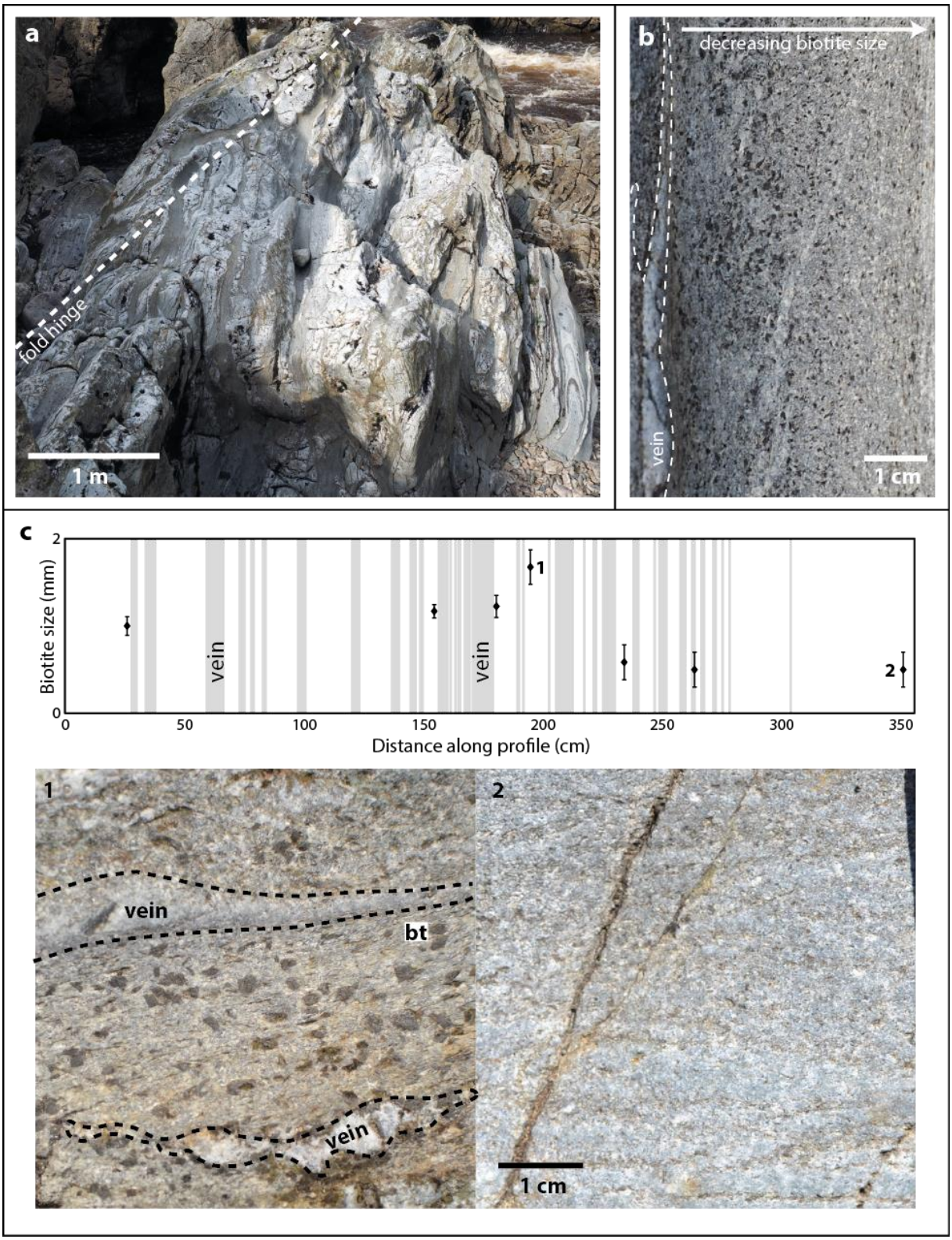

Figure 7a: Field photo of an intensely veined fold hinge in the biotite zone. **7b:** Close-up photo of a small area located near the hinge, showing a decrease in biotite crystal size (black coloured) with increasing distance away from the vein. **7c:** Two dimensional profile of the locality shown in 7a, with field estimation of biotite crystal size presented in seven data points. The hinge is located at x ≈ 175 cm. Below photographs of the small areas used for crystal size estimation are shown, corresponding to the data points marked as 1 and 2, respectively.

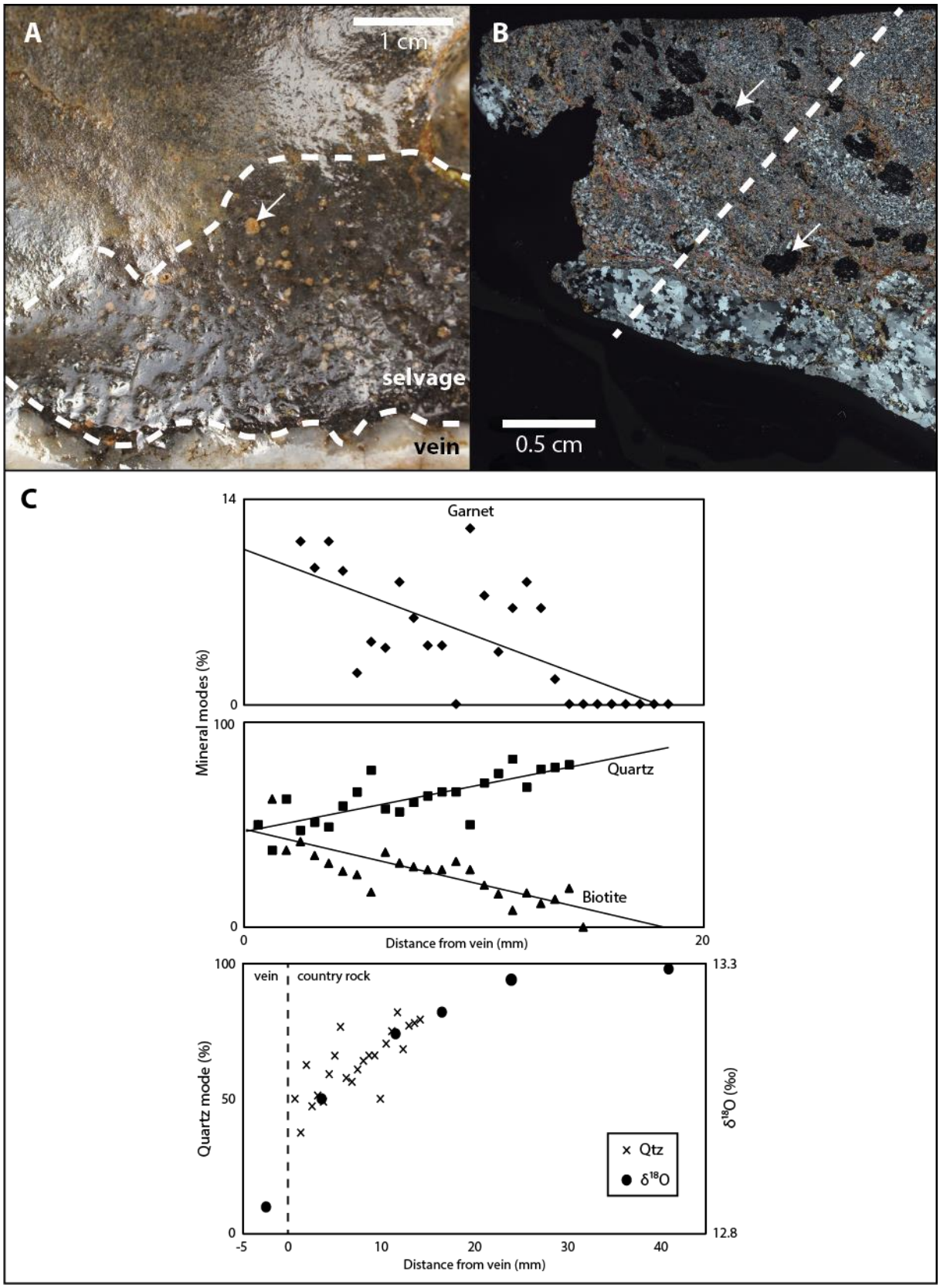

Figure 8A: Field photograph of an outcrop in the garnet zone, typical for the vein adjacent type of garnet occurrence (white arrows), with interpreted approximate boundaries between vein, selvage, and unaltered country rock marked out. **B:** Scan (cross polarised light) of a thin section from the exact same rock as shown in A. Dashed line marks point counting profile. **C:** Above, point counting results from the dashed line in B. Below, oxygen isotope data together with quartz mode from point counting, both from the same sample as B.

hinge and gradual decrease away from the hinge on both limbs. This indicates a locally high degree of fluid-rock interaction. In all, the distribution of biotite as an index mineral is interpreted to be P-T-x controlled in most cases. For the fold hinge locality, crystal size is however fluid controlled (by selvage formation, see below).

In the garnet zone the actual index mineral, garnet, is extremely scarce and most rocks in the garnet zone do not host any garnet. Where found, garnet is restricted to thin metapelite layers or rock adjacent to veins. Adjacent to veins, porphyroblast size is also larger. An example of this vein adjacent garnet occurrence is presented in fig. 8. Mineral point counting shows that garnet abundance increases towards the vein, while quartz mode decreases. These trends are also coincident with a decrease in the oxygen isotope signature of quartz, which is indicative of fluid rock-interaction. The concentration of Mn is an order of magnitude higher in the selvage compared to the unaltered country rock, which is interesting as Mn shifts the garnet stability field towards lowers temperatures (fig. 9). In all, and including trace element data that are available in the attached manuscript, this is interpreted as selvage formation, and thus distribution of garnet as an index mineral is mainly fluid controlled as opposed to the general view of a P-T-x control.

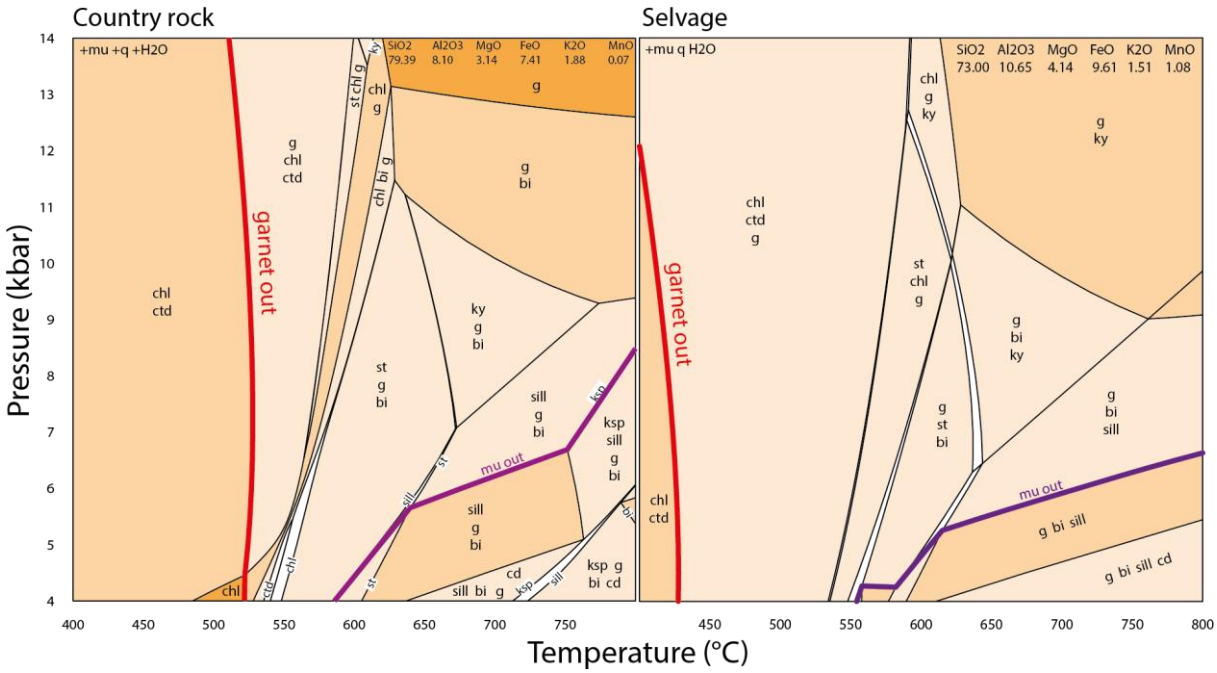

Figure 9: Thermodynamic assessment of the garnet stability using pseudosections, comparing unaltered country rock with selvage for the sample presented in fig. 8. As a result of that MnO is enriched in the selvage (by an order of magnitude), the garnet stability field is expanded towards lower temperatures by ~100°C.

The staurolite zone is very similar to the garnet zoe, and staurolite is restricted to a few intensely veined localities (fig. 10). At these localities, staurolite mainly occurs within cm wide zones adjacent to veins. Point counting shows that staurolite mode decreases away from these veins, coincident with an increase in quartz mode. Selvage formation, analogous to the garnet zone, is interpreted as the main control on distribution of staurolite as an index mineral.

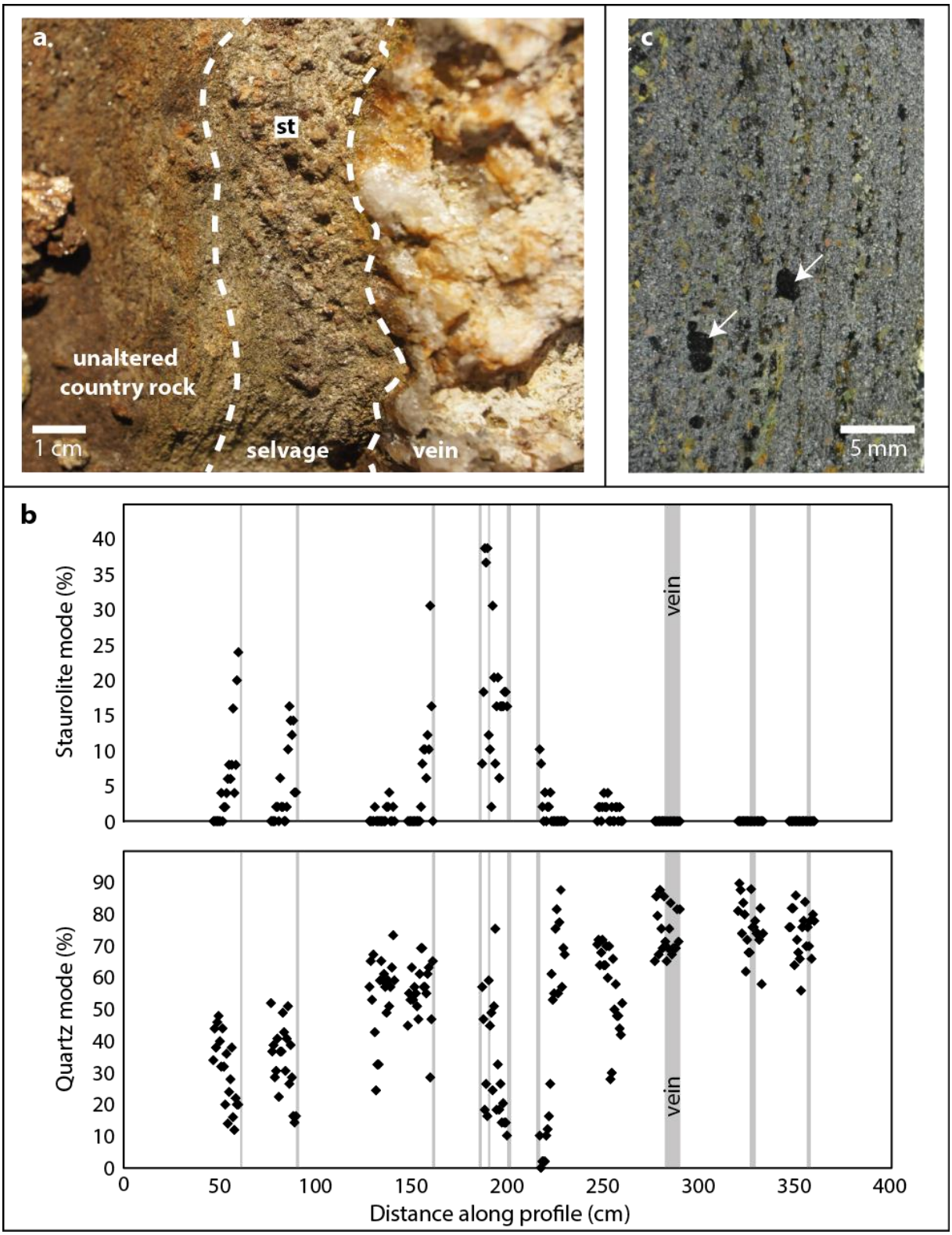

Figure 10a: Field photograph of an outcrop where staurolite bearing vein adjacent zones are found. Staurolite porphyroblasts are a few mm across and show brown colour. The interpreted boundaries between vein, selvage, and unaltered country rock are marked with dashed lines. **5b:** A 2-dimensinoal profile from the locality that A is part of, presented together with quartz and staurolite mode data retrieved by thin section point counting. Generally, staurolite and quartz abundance are inversely correlated as a function of distance from a vein. **5c**: Thin section scan in cross polarised light, showing thin metapelite layers containing surprisingly large garnet crystals (pointed out by small white arrows), as found both in the garnet and staurolite zones.

Kyanite distribution in the kyanite zone is in contrast to the garnet and staurolite zones rather homogenous (fig. 11). Vein density is around 13%, in comparison to 4% and 7% in the garnet and staurolite zones, respectively. This is indicative of even higher fluid-rock interaction than in the two latter. Oxygen isotope data show that the country rock is completely equilibrated with the fluid. Altogether, selvage formation is again attributed as the main control on index mineral distribution, albeit in the case of the kyanite zone, selvages are wider and more narrowly spaced and thus overlapping.

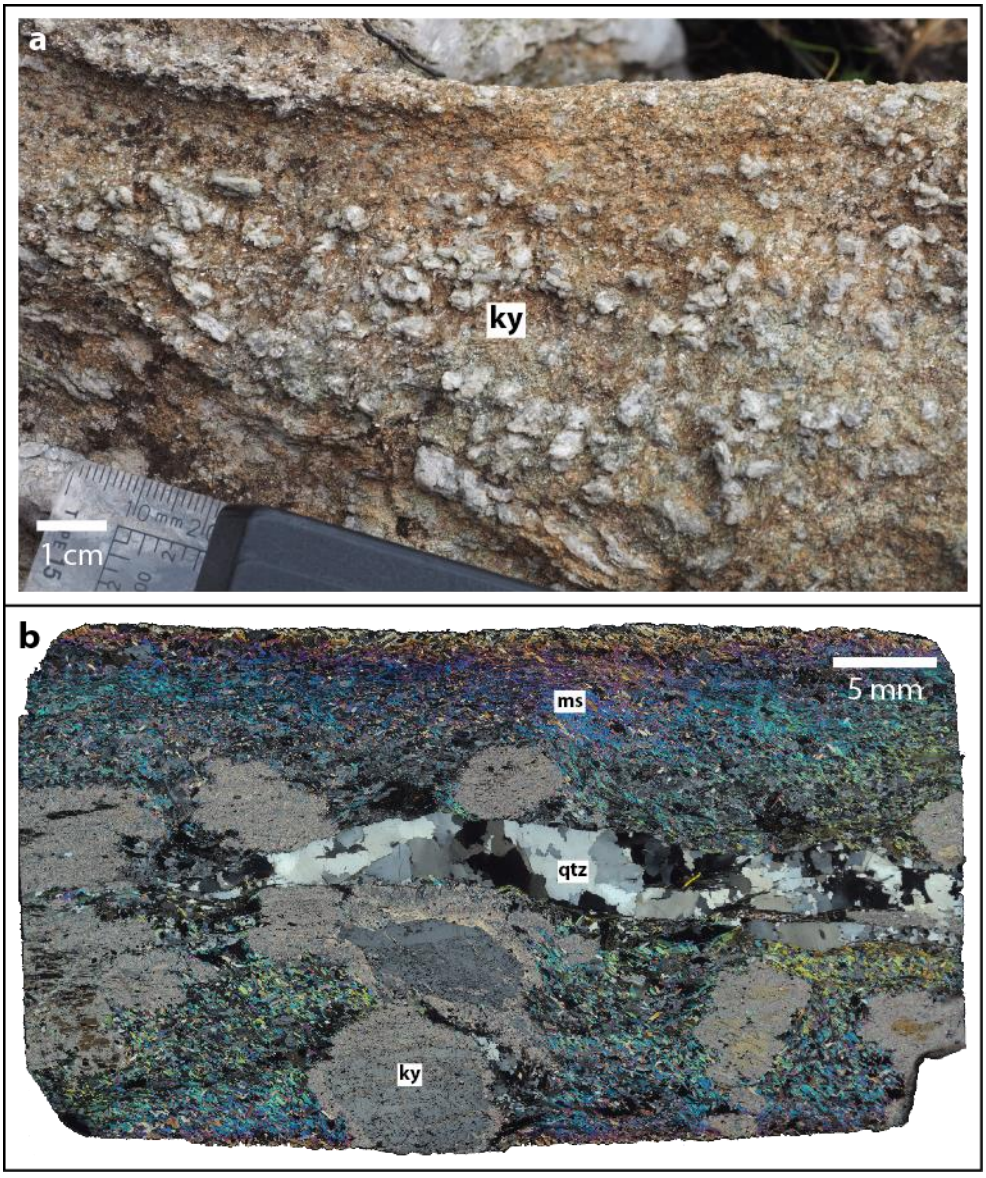

Figure 11a: A field photo from an outcrop in the kyanite zone, showing homogenous kyanite distribution. **11b:** Thin section photoscan of a sample this locality in cross polarised light. Kyanite crystals are rimmed as a result of retrograde breakdown into white micas.

In the sillimanite zone, sillimanite occurs as fibrolite (sillimanite-muscovite intergrowth in fibrous needle bundles), and is again found exclusively in close vicinity to veins (fig. 12). In contrast to this pattern, all other porphyroblasts (biotite, garnet, staurolite, and kyanite) are homogeneously distributed. Together with even higher vein density, this indicates a high degree of fluid-rock interaction, and that overlapping selvages did form during the main phase of metamorphism. A probable interpretation is that sillimanite formation was not contemporaneous with the metamorphic phase that yielded the other porphyroblasts, but rather formed at a later stage. Northward from the sillimanite zone, towards higher metamorphic grade, lays a syn-metamorphic granite intrusion. Vorhies & Ague (2011) suggest that this intrusion was the cause for a secondary heating event, and that sillimanite zone temperatures were reached only as a result of this event. This is a possible cause for the formation of sillimanite, which fits with the observations of sillimanite distribution presented in this study.

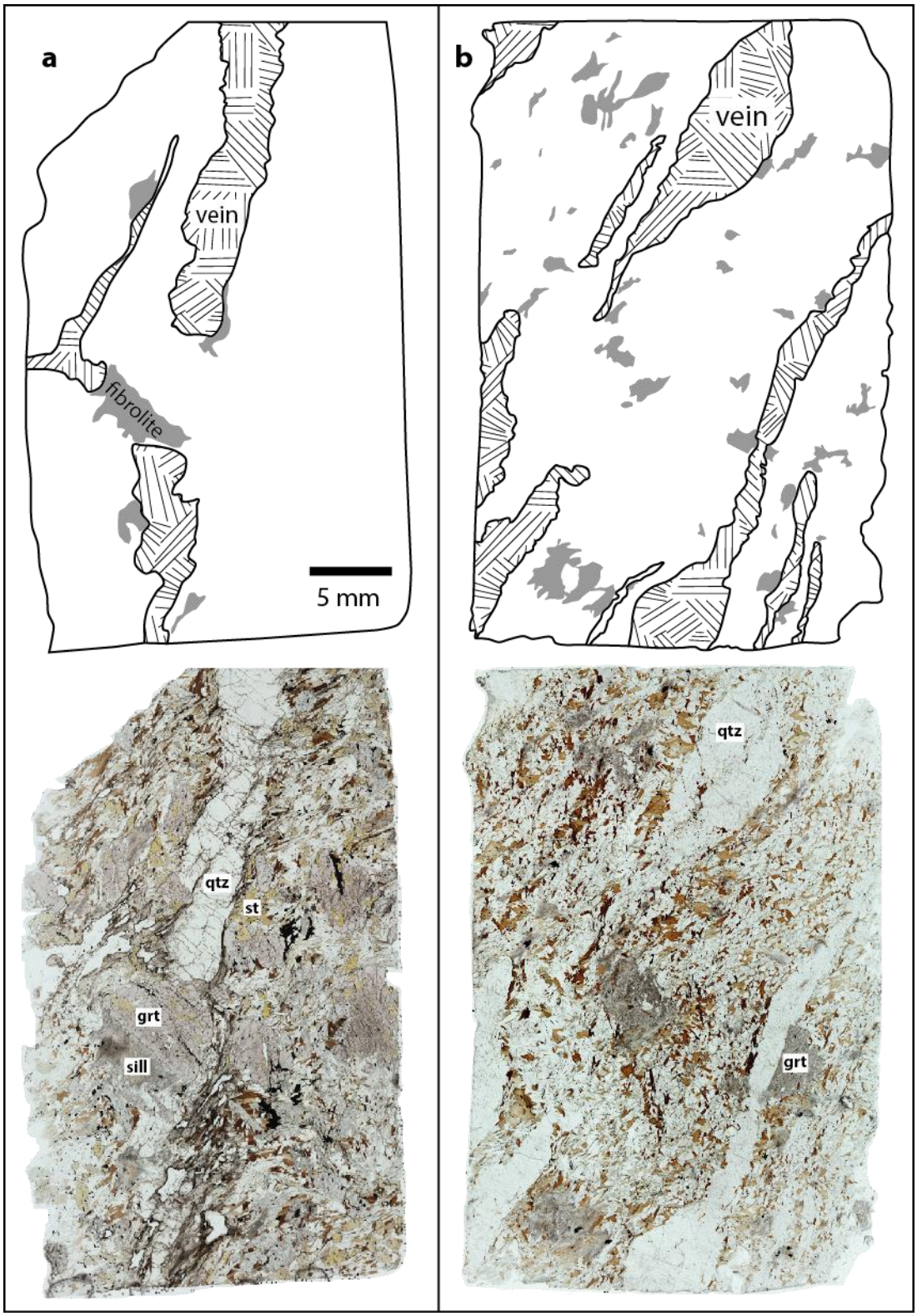

Figure 12: Sketches of two thin sections of samples from the sillimanite zone, where quartz veins and fibrolite (sillimanite-muscovite intergrowth) occurrences are highlighted. Below the thin section scan these sketches were drawn from are shown. Fibrolite is mostly concentrated in close vicinity to the veins.

5. Conclusions

- Stabilisation and distribution of Barrovian index minerals in the chlorite and biotite zones of Glen Esk was mainly controlled by pressure, temperature and whole rock composition.
- Partial fluid-rock interaction and associated localised silica removal adjacent to veins produced index mineral bearing selvages in the garnet and staurolite zones and in intensely veined locality in the biotite zone. This was a primary control of index mineral size distribution in these zones. In addition, MnO played an important role in the stabilisation of garnet, and possibly also staurolite.
- Selvage formation was also the main control on index mineral stabilisation and distribution in the kyanite zone; however, fluid- rock interaction and selvage formation was more extensive and selvages were overlapping resulting in homogeneous index mineral distributions.
- Sillimanite formation was induced by a later event, possibly the syn-metamorphic northward lying granite intrusion. The distribution of sillimanite would in that case mainly be controlled by proximity to this granite.

6. Acknowledgements

I thank my main supervisor, Alasdair Skelton, for suggestions, comments, and other input and help, in all parts of this project. Co-supervisors Charlotte Möller and Patrick Crill are also equally thanked for their feedback. Josefin Linde and Jonas Nilsson are acknowledged for their work on the staurolite zone, a project they undertook as their respective MSc theses. Dan Zetterberg has also been of great help in field, but also with sample preparations and other practical issues. Runa Jacobsson and Cora Wohlgemuth-Überwasser are recognised for assistance with whole rock composition analyses. John Valley and Mike Spicuzza are grateful thanked for making the oxygen isotope analyses possible, and welcoming me at their laboratory in Madison, Wisconsin. For assistance with the electron microprobe in Uppsala, Jaroslaw Majka is also thanked. Pavel Pitra is also thanked for his support on THERMOCALC and the construction of pseudosections. Last but not least, I also thank all other friends and colleges whom I have forgotten to mention, but nevertheless directly or indirectly have contributed to the project in some manner.

7. References

Ague, J.J. (1994). Mass transfer during Barrovian metamorphism of pelites, south-central Connecticut. I: evidence for changes in composition and volume. *American Journal of Science* **294**, 989-1057.

Ague, J.J. (2003). Fluid infiltration and transport of major, minor, and trace elements during regional metamorphism of carbonate rocks, Wepawaug schist, Connecticut, USA. *American Journal of Science* **303**, 753-816.

Ague, J.J. (2011). Extreme channelization of fluid and the problem of element mobility during Barrovian metamorphism. *American Mineralogist* **96**, 333-352.

Albee, A.L. (1965). A petrogenetic grid for the Fe-Mg silicates ofpelitic schists. *American Journal of Science* **263**, 512-536.

Baker, A.J. (1985). Pressures and temperatures of metamorphism in the eastern Dalradian. *Journal of the Geological Society, London* **142**, 137–148.

Baltatzis, E. & Katagas, C. (1981). Margarite pseudomorphs after kyanite in Glen Esk, Scotland. *American Mineralogist* **66**, 213-216.

Barrow, G. (1893). On an intrusion of muscovite-biotite gneiss in the south-eastern Highlands of Scotland, and its accompanying metamorphism. *Quarterly Journal of the Geological Society of London* **49**, 330-358.

Barrow, G. (1912a). On the geology of Lower Dee-side and the southern Highland border. *Proceedings of the Geologists' Association* **23**, 274-290.

Barrow, G. (1912b). Lower Dee-side and the Highland border. *Proceedings of the Geologists' Association* **23**, 268-273.

Berman, R.G. & Brown, T.H. (1985). The heat capacity of minerals in the system K_2O-Na_2O-CaO-MgO-FeO-Fe_2O_3-Al_2O_3-SiO_2-TiO_2-H_2O-CO_2: representation, estimation, and high temperature extrapolation. *Contributions to Mineralogy and Petrology* **89**, 168-183.

Bickle, M.J. & Baker, J. (1990). Advective-diffusive transport of isotopic fronts: an example from Naxos, Greece. *Earth and Planetary Science Letters* **97**, 78-93.

Chew, D.M. & Strachan, R.A (2014). The Laurentian Caledonides of Scotland and Ireland. In: Corfu, F., Gasser, D. & Chew, D.M. (eds.). New Perspectives on the Caledonides of Scandinavia and Related Areas. *Geological Society of London Special Publications* **390**, 45-91.

Dempster, T.J. (1985). Garnet zoning and metamorphism of the Barrovian type. *Contributions to Mineralogy and Petrology* **89**, 30–38.

Dempster, T.J., Rogers, G., Tanner, P.W.G., Bluck, B.J., Muir, R.J., Redwood, S.D., Ireland, T.R. & Paterson, B.A. (2002). Timing of deposition, orogenesis and glaciations within the Dalradian rocks of Scotland: constraints from U–Pb ages. *Journal of the Geological Society, London* **159**, 83–94.

Harker, A. (1912). The North Esk. *Proceedings of the Geologists' Association* **23**, 273.

Harte, B. (1987). Glen Esk Dalradian, Barrovian metamorphic zones. In: N.H., Kneller, B.C., Gillen, C. (Eds.). *Excursion Guide to the Geology of the Aberdeen Area*. Scottish Academic Press (for Geological Society of Aberdeen), Edinburgh, pp. 193–210.

Harte, B., & Hudson, N.F.C. (1979). Pelite facies series and the temperatures and pressures of Dalradian metamorphism in E Scotland. In Harris, A.L., Holland, C.H. & Leake, B.E.

The Caledonides of the British Isles; reviewed. *Geological Society of London – Special Publication* **8**, 323-337.

Harte, B. & Johnson, M.R.W. (1969). Metamorphic history of Dalradian rocks in Glens Clova, Esk and Lethnot, Angus, Scotland. *Scottish Journal of Geology* **5**, 54–80.

Hutton, J. (1788). Theory of the Earth: or an investigation of the laws observable in the composition, dissolution, and restoration of land upon the globe. *Transactions of the Royal Society of Edinburgh* **1**, 209-304.

Eskola, P. (1915). On the relation between the chemical and mineralogical composition in metamorphic rocks of the Orijärvi region. *Bulletin of the Geological Society of Finland* **44**.

Eskola, P. (1920). The mineral facies of rocks. *Norsk Geologisk Tidskrift* **6**, 143-194.

Eskola, P. (1929). On the mineral facies. *Proceedings of the Geological Society, Stockholm* **51**, 157-172.

Ferry, J.M. (1987). Metamorphic hydrology at 13-km depth and 400-550°C. *American Mineralogist* **72**, 39-58.

Greenwood, H.J. (1961). The system $NaAlSi_2O_6$-H_2O-argon. Total pressure and water pressure in metamorphism. *Journal of Geophysical Research* **66**, 3923-3946.

Greenwood, H.J. (1962). Metamorphic reactions involving two volatile components. *Year Book Carnegie Institution of Washington* **61**, 82-85.

Gresens, R.L. (1967). Composition-volume relationships of metasomatism. *Chemical Geology* **2**, 47-65.

Grant, J.A. (1986). The isocon diagram: a simple solution to Gresens' equation for metasomatic alteration. *Economic Geology* **81**, 1976-1982.

Helgeson, H.C., Delany, J.M., Nesbitt, H.W. & Bird, D.K. (1978). Summary and critique of the thermodynamic properties of rock-forming minerals. *American Journal of Science* **278**, 1-299.

Hensen, B.J. (1971). Theoretical phase relations involving cordierite and garnet in system MgO-FeO-Al_2O_3-SiO_2. *Contributions to Mineralogy and Petrology* **33**, 191-214.

Hess, P.C. (1969). The metamorphic paragenesis of cordierite in pelitic rocks. *Contributions to Mineralogy and Petrology* **24**, 191-207.

Holland, T.J.B., Baker, J.M. & Powell, R. (1998). Mixing properties and activity-composition relationships of chlorites in the system MgO-FeO-Al_2O_3-SiO_2-H_2O. *European Journal of Mineralogy* **10**, 395-406.

Holland, T.J.B. & Powell, R. (1985). An internally consistent thermodynamic dataset with uncertainties and correlations: 2. Data and results. *Journal of Metamorphic Geology* **3**, 343–370.

Holland, T.J.B. & Powell, R. (1998a). Calculating phase diagrams involving solid solutions via non-linear equations, with examples using THERMOCALC. *Journal of Metamorphic Geology* **16**, 577–588.

Holland, T.J.B. & Powell, R. (1998b). An internally consistent thermodynamic dataset for phases of petrological interest. *Journal of Metamorphic Geology* **16**, 309-343.

Koons, P.O. & Thompson, A.B. (1985). Non-mafic rocks in the greenschist, blueschist and eclogite facies. *Chemical Geology* **50**, 3-30.

Mahar, E.M., Baker, J.M., Powell, R. Holland, T.J.B. & Howell, N. (1997). The effect of Mn on mineral stability in metapelites. *Journal of Metamorphic Geology* **15**, 223-238.

Oliver, G.J.H., Chen, F., Buchwaldt, R. & Hegner, E. (2000). Fast tectonometamorphism and exhumation in the type area of the Barrovian and Buchan zones. *Geology* **28**, 459–462.

Oliver, G.J.H., Wilde, S.A. & Wan, Y. (2008). Geochronology and geodynamics of Scottish granitoids from the late Neoproterozoic break-up of Rodinia to Palaeozoic collision. *Journal of the Geological Society, London* **165**, 661–674.

Philpotts, A.R. & Ague, J.J. (2009). *Principles of igneous and metamorphic petrology*, 2nd edition. Cambridge University Press, Cambridge, 667 p.

Powell, R. & Holland, T.J.B. (1985). An internally consistent thermodynamic dataset with uncertainties and correlation: 1. Methods and a worked example. *Journal of Metamorphic Geology* **3**, 372-342.

Ridley, J. & Thompson, A.B. (1986). The role of mineral kinetics in the development of metamorphic microtextures. In: Walther, J.V. & Wood, B.J. (Eds.). Fluid-rock interactions during metamorphism. *Advances in Physical Geochemistry* **5**, 195-212. New York, Springer-Verlag, 218 p.

Robertson, S. (1994). Timing of Barrovian metamorphism and 'Older Granite' emplacement in relation to Dalradian deformation. *Journal of the Geological Society, London* **151**, 5–8.

Tanner, P.W.G., Thomas, C.W., Harris, A.L., Gould, D., Harte, B., Treagus, J.E. & Stephenson, D. (2013). The Dalradian rocks of the Highland Border region of Scotland. *Proceedings of the Geologists' Association* **124**, 215-262.

Spear, F.S. & Cheney, J.T. (1989). A petrogenetic grid for pelitic schists in the system SiO_2-Al_2O3-FeO-MgO-K_2O-H_2O. *Contributions to Mineralogy and Petrology* **101**, 149-164.

Spicuzza, M.J., Valley, J.W., Kohn, M.J., Girard, J.P. & Fouillac, A.M. (1998). The rapid heating, defocused beam technique: a CO_2-laser-based method for highly precise and accurate determination of $\delta^{18}O$ values of quartz. *Chemical Geology* **144**, 195-203.

Taylor, H.P. (1977). Water/rock interactions and the origin of H2O in granitic batholiths: Thirtieth William Smith lecture. *Journal of the Geological Society* **133**, 509-558.

Thompson, J.B. (1957). The graphical analysis of mineral assemblages in pelitic schists. *American Mineralogist* **42**, 842-858.

Thompson, J.B. (1959). Local equilibrium in metasomatic processes. In: Abelson, P.H. (Ed.). *Researches in Geochemistry*, Vol. 1, John Wiley (1959), 427–457.

Thompson, A.B. (1976). Mineral reactions in pelitic rocks: II. Calculation of some P-T-X(Fe-Mg) phase relations. *American Journal of Science* **276**, 425-454.

Valley, J.W., Kitchen, N., Kohn, M.J., Niendorf, C.R. & Spicuzza, M.J. (1995): UWG-2, a garnet standard for oxygen isotope ratios: Strategies for high precision and accuracy with laser heating. *Geochimica et Cosmochimica Acta* **59**, 5223-5231.

van der Plas, L. & Tobi, A.C. (1965). A chart for judging the reiliability of point counting results. *American Journal of Science* **263**, 87-90.

Viete, D.R., Hermann, J., Lister, G. & Stenhouse, I. (2011). The nature and origin of the Barrovian metamorphism, Scotland: diffusion length scales in garnet and inferred thermal time scales. *Journal of the Geological Society, London* **168**, 115–132.

Vorhies, S.H. & Ague, J.J. (2011). Pressure-temperature evaluation and thermal regimes in the Barrovian zones, Scotland. *Journal of the Geological Society, London* **168**, 1147–1166.

White, R.W., Pomroy, N.E. & Powell, R., 2005. An in-situ metatexite-diatexite transition in upper amphibolite facies rocks from Broken Hill, Australia. *Journal of Metamorphic Geology* **23**, 579-602.

Winter, J.D. (2010). *An introduction to igneous and metamorphic petrology*, 2nd edition. Prentice Hall, Upper Saddle River, 702 p.

"Metamorphosis". Oxford Dictionaries Online, Oxford University Press. Web. 22 April 2015. <http://www.oxforddictionaries.com/definition/english/metamorphosis>

Manuscript

Vein controlled index mineral crystal size distribution in Barrow's metamorphic zones, Glen Esk, Scotland

Alexander Lewerentz[1], Alasdair Skelton[1], Josefin K. Linde[1], Jonas Nilsson[1], Charlotte Möller[2], Patrick Crill[1] & Michael J. Spicuzza[3]

1: Department of Geological Sciences, Stockholm University, 106 91 Stockholm, Sweden
2: Department of Geology, Lund University, Sölvegatan 12, 223 62 Lund, Sweden
3: Department of Geoscience, University of Wisconsin, Madison, Wisconsin 53706, USA

ABSTRACT

The concept of index mineral based metamorphic zones was first introduced by George Barrow a little more than 100 years ago, and the Barrovian metamorphic zones are still used as framework by metamorphic petrologists. Today the importance of metamorphic fluids for driving metamorphic reactions is widely recognised. Even so, the general view is that Barrovian metamorphism is solely controlled by pressure, temperature, and protolith composition. This paper aims to establish if and how fluids control index mineral formation and distribution during Barrovian metamorphism. To do so, we use samples from Barrow's type localities in Glen Esk, Southeast Scottish Highlands, and study possible relationships between veining and index mineral distribution. In addition to petrographic and textural observations and analyses, we also use whole rock chemistry, mineral chemistry, and oxygen isotope analyses. At low grade, in the chlorite zone and most of the biotite zone, no correlation between veining and index mineral distribution is seen. At higher grade, the garnet and staurolite zone, index mineral abundance is shown to decrease away from veins. The kyanite zone shows a fairly homogenous kyanite distribution, but there are also indications of extensive fluid-rock interaction such as high vein density. Based on these observations and the geochemical datasets, we conclude that fluid flow played a major role in the stabilisation and distribution of the Barrovian index minerals in Glen Esk, and that the importance of fluid flow was larger at higher the metamorphic grades.

INTRODUCTION

The concept of metamorphic zones was first introduced by Barrow (1893; 1912a), as an explanation for systematic mineralogical and textural variations in metasedimentary rocks found in the Scottish Highlands. Understanding the importance of mineral assemblages, Eskola (1915; 1920; 1929) refined the concept by introducing the three component AKF and ACF chemographic diagrams, and the facies based classification system. Both the AKF and ACF system ignore the effect of variation in relative proportions of FeO and MgO, which is not appropriate for various mafic minerals in most rocks. As a solution to the problem Thompson (1957) presented the A(K)FM diagram, which treats Mg and Fe as separate components. To enable the use of thermodynamics to constrain metamorphic reactions, numerous thermodynamic data bases have been compiled (cf. Helgeson et al., 1978; Berman et al., 1985; Holland & Powell, 1985; Powell & Holland, 1985). Such databases are used to construct petrogenetic grids (cf. Albee, 1965; Hess, 1969; Thompson, 1976; Koons & Thompson, 1985; Spear & Cheney, 1989), but also pseudosections, i.e. P-T or T-X diagrams showing stable mineral assemblages for a specific bulk rock composition (cf. Hensen, 1971; Powell et al., 1998). Petrogenetic grids and pseudosections are commonly utilised for deducing pressure-temperature paths for metamorphic rocks, and also to assess the role of metamorphic fluids.

Metamorphic fluids were first hypothesised as the cause behind certain reactions observed in metamorphic rocks by e.g. Greenwood (1961; 1962), and Thompson (1959) realised that metasomatic reactions require mass transfer. To assess component mobility in metasomatic reactions, Gresens (1967) used contrasts in density and component concentration between rocks or minerals, and Grant (1986) later proposed the isocon diagram to further refine Gresens' work. In addition to causing small-scale fluid-driven metasomatic reactions, metamorphic fluids were proposed to act on a regional scale, thus explaining regional scale loss or gain of components. To describe, evaluate and quantify the role of such regional metamorphic fluids, a number of methods and models have been applied throughout the years. Using oxygen isotope fractionation, Taylor (1977) constructed a volumetric model for description and quantification of fluid driven reactions, the water-rock ratio (W:R). Another approach using mass transfer of CO_2 to calculate a fluid-rock ratio was later proposed by Ferry (1987). Utilising oxygen isotope signatures, Bickle & Baker (1990) suggested that metamorphic fluids can be channelled in certain high-flux zones driven by rock permeability contrasts, and used isotopic front displacement to derive a time integrated fluid flux based on advective-diffusive transport modelling. Ague (1994; 2003; 2011) applied mass balance calculations to Barrovian type metamorphism, concluding that fluids are channelled in vein fracture conduits.

Today the importance of fluids for driving metamorphic reactions is widely recognised. This paper aims to establish the role of fluids during Barrovian type metamorphism in Barrow's own metamorphic sequence in Glen Esk, SE Scottish Highlands. More specifically, we aim to answer the following questions. Is there a spatial relationship between index mineral distributions and veins? How did fluids affect the mineralogical, chemical and isotopic compositions of rock adjacent to veins? What was the impact on index mineral distribution, and thus the appearance of Barrovian metamorphism? To answer these questions and constrain controls for index mineral stabilisation we take into integrate petrographic observations, whole rock and mineral chemical composition, equilibrium thermodynamic modelling (pseudosections), and oxygen isotope signatures.

GEOLOGICAL SETTING

Glen Esk is famous as the type locality of George Barrow's own metamorphic sequence; the actual outcrops he used to pro-

pose his theory of metamorphic zones (Barrow, 1893; 1912a; 1912b; Harker, 1912). Situated in the SE Scottish Highlands, Glen Esk hosts rocks from both sides of the Highland Boundary Fault (HBF). At the lower end of the valley in the south, Old Red Sandstone Supergroup sedimentary and volcanic rocks of Siluro-Devonian age are the dominating lithologies. Further to the north and on the other side of the HBF, Ordovician rocks of the Highland Border Complex (HBC) are found. Subdivided into the Margie and North Esk Formations, the HBC consists of weakly metamorphosed limestones, shales, slates, grits, and conglomerates. The HBC is juxtaposed against rocks belonging to the Dalradian Supergroup along the North Esk Fault (NEF). These are metasedimentary rocks belonging to the Glen Lethnot Grit and Glen Effock Schist Formations (Fig. 1). This metamorphosed turbidite sequence consists of alternating layers of metapelites and metapsammites. Metamorphic grade increases continuously northwards in the area, from chlorite grade near the NEF up to sillimanite grade. In the north, the sequence is cut by a granite intrusion.

The area is part of the Caledonides, with Grampian Orogeny considered as the main metamorphic event at 475-465 Ma, and reaching peak metamorphic conditions at ca. 470 Ma (Chew & Strachan, 2014). Granitic and gabbroic intrusions in the area have been dated to ca. 470 Ma (e.g. Oliver et al., 2000; Dempster et al., 2002; Oliver et al., 2008). Vorhies & Ague (2011) hypothesised that these intrusions caused a secondary heating event and thus are the cause of peak metamorphic temperatures. Pressure and temperature conditions for peak metamorphism are presented in a number of studies, often accompanied by data from the neighbouring valley, Glen Lethnot, which is considered metamorphically equivalent to Glen Esk. These estimates are presented in Table 1. For a more detailed description of the regional geology, see for instance Harte (1987), Tanner et al. (2013), and references therein.

Typical mineral assemblages are **chlorite**, chlorite+**biotite**, chlorite+biotite+**garnet**, bitite+garnet+**staurolite** ±chlorite, biotite+staurolite+**kyanite**±garnet, and biotite +**sillimanite**±K-feldspar±garnet± staurolite± kyanite, all of which also contain quartz and muscovite. In addition to these typical assemblages, occasional magnetite, pyrite, haematite, and plagioclase have been reported (Barrow, 1893; Barrow, 1912; Harte & Hudson, 1979; Harte, 1987). Chlorite is also commonly found in the higher grade zones, here attributed to retrograde metamorphism replacing garnet, and biotite. Other inferred retrograde reactions include the breakdown of kyanite and staurolite to form white micas (Harte & Johnson, 1969; Baltatzis & Katagas, 1981).

Previous studies on index mineral distribution in their respective zones have shown confinement to layers of pelitic composition for garnet, staurolite, kyanite, and sillimanite, while chlorite and biotite also appear in rocks of more psammitic composition (Harte & Johnson 1969; Tanner et al. 2013). They also reported that kyanite and sillimanite are found in veins. Using structural and textural observations, Harte & Johnson (1969) suggested that growth of index minerals occurred stepwise as a result of four separate structural events. This idea of stepwise index mineral stabilisation, and implicated rapid changes in metamorphic conditions, is also favoured by Robertson (1994). Vorhies & Ague (2011) attributed the last of these steps, the stabilisation of sillimanite, to a secondary heating event caused by magmatic intrusions where the sillimanite zone rocks as a matter of proximity was affected the most.

MATERIALS AND METHODS

Field measurement and sampling

This paper is based on observations and material collected from each of Barrow's six metamorphic zones. In addition to field descriptions, two-dimensional profiles were made to estimate relative lithological abundances within the outcrops, and in some cases in field point counting was undertaken us-

ing a 5 by 5 cm meshed square for estimation of mineral abundances and sizes. Samples were collected to be representative of all lithological variation seen at each outcrop. All sampled outcrops are situated on a semi-linear profile line, which is approximately perpendicular to the NEF. The localities included in this study are shown in Figure 1 and presented in Table 2.

Analytical methods

Petrographic analysis and estimation of mineral modes were conducted using a polarised light microscope fitted with an automated stage for point counting. For each thin section, minerals were identified in a total of 1000 evenly distributed points. Uncertainty levels were estimated using the approach of van der Plas & Tobi (1965). All point counting data are reported in Table 3.

Whole rock major and trace element chemistry was determined by analysis of rock powder lithium-metaborate-tetraborate fused glass discs, using a Rigaku ZSX Primus II sequential X-ray fluorescence (XRF) spectrometer and a Thermo Fisher X-series II quadrupole laser ablation inductively coupled plasma mass spectrometer (LA-ICP-MS) at the Department of Geological Sciences, Stockholm University. Repeat analysis of standard reference material ensures a precision better than 1% for major elements and 5% for trace elements. Volatile components were measured as loss on ignition (LOI), calculated for each sample from its weight after (1) >10 h drying at 105°C and (2) >10 h ignition at 1050°C. These analyses are reported in table 4.

Chemical composition of minerals was determined by spot analyses using a JEOL JXA-8530 field emission electron microprobe (EMPA) at the Department of Earth Sciences, Uppsala University, operating in wavelength dispersive (WDS) mode at 15 kV and 20 nA with a beam size of 1-5 µm. Estimated relative 1-σ errors are <0.5 % at >10 wt%, <5% at >1 wt%, 5-20 % at >0.1 wt% and 20-50 % at <0.1 wt%. All mineral compositions are reported in Table 5.

Oxygen isotope ratios ($\delta^{18}O$) were determined by laser fluorination of handpicked quartz or kyanite separates using a CO_2 laser and a Finnigan MAT 251 isotope ratio mass spectrometer (IRMS) at the Department of Geoscience, University of Wisconsin-Madison, following the method described by Valley et al. (1995) and Spicuzza et al. (1998). Values are standardized by replicate analyses of the UWG-2 garnet standard (Valley et al. 1995) and reported in standard permil notation relative to VSMOW (Vienna-Standard Mean Ocean Water). Typical absolute analytical error following this technique $\delta^{18}O$ is ±0.1‰. All analyses are reported in Table 6.

Thermodynamic calculations

Thermodynamic calculations for construction of pseudosections were made using THERMOCALC v3.37 and the ds55 data set (Holland & Powell, 1998a; 1998b), with whole rock chemical compositions from XRF analysis as input data, if necessary corrected for plagioclase and oxide phases. The seven component MnKFMASH system was used. This system includes MnO, K_2O, FeO, MgO, Al_2O_3, SiO_2, and H_2O. H_2O was assumed to be in excess. Solid solution models used for cordierite, chloritoid, and staurolite include Mahar et al. (1997) and Holland & Powell (1998b), for chlorite Mahar et al. (1997) and Holland et al. (1998), for garnet and biotite White et al. (2005), and for muscovite Holland & Powell (1998b).

RESULTS

Field and petrographic observations

The chlorite zone

Chlorite zone rocks are dominantly fine-grained phyllitic metapelites (Fig. 2). Most veins are composed of both quartz and carbonate, but occasionally solely composed of

either of these. Vein orientations are both parallel to and crosscutting the foliation. At locality 02, vein density was estimated to <1%.

Thin section point counting results show that the chlorite zone rocks contain quartz, chlorite, and muscovite, as well as minor amounts of plagioclase, pyrite and tourmaline (Table 3). Interstitial calcite was found in all samples in amounts from 3 to 25 vol%. Within the chlorite zone, chlorite was identified in all collected samples at concentrations varying between 23 and 36 vol%. Microscopy confirmed quartz and calcite as vein phases.

The biotite zone

The biotite zone outcrops show alternating layers of fine-grained metapsammities and metapelites, as well as variations in between. Rock texture changes from phyllitic to schistose with increasing distance from the NEF. Biotite porphyroblasts are up to 5 mm in size, but usually less than 2 mm. Veins are almost entirely composed of quartz, but locally contain small amounts of carbonate, and orientated both parallel to and crosscutting the foliation. Vein densities at localities 03 and 04 were estimated to 5% and <1%, respectively. At locality 05, vein width measurement and in-field point counting across a fold hinge and its two limbs show increased vein density and biotite grain size as a function of distance from the hinge (Fig. 3). This fold hinge is an area of intense veining with a vein density of 31% if including what is exposed of the limbs, and >50% if only considering the area closest to the hinge.

Thin section point counting (Table 3) shows that these rocks contain quartz, muscovite, biotite, and chlorite, with minor plagioclase and K-feldspar. Interstitial calcite is present, but less abundant than in the chlorite zone. Accessory minerals include zircon, hematite, pyrite, and tourmaline. Biotite abundance is highly variable and ranges from absent to 34 vol%. Quartz and calcite are confirmed as vein phases.

The garnet zone

Rocks in the garnet zone are predominately fine-grained schistose metapsammites with scarce thin layers of metapelites. Porphyroblasts of garnet and biotite are found, both in sizes up to 2 mm. Garnet is rarely observed and where found, restricted to pelitic layers. Detailed examination of locality 09 shows that garnet is only present close to a quartz vein and decreases in size away from the vein (Fig.4). Similar observations were made at localities 07 and 08. The veins that we observed in the garnet zone are solely composed of quartz, with the exception of one carbonate bearing vein. Vein orientation is exclusively parallel to foliation. Vein density at locality 08 was estimated to 4%.

Thin section point counting shows quartz, muscovite, biotite, chlorite, and garnet as major phases (Table 3). Minor phases include pyrite, hematite, amphibole, epidote, plagioclase, apatite, and tourmaline. Garnet is absent in most samples. In sample 12:001, the garnet mode decreases away from the vein. This decrease correlates with an increase in quartz mode (Fig. 4). Samples with very thin pelitic layers (<2 mm), sandwiched between thicker metapsammite layers, occasionally host garnets with diameters equal to, or wider than the layer itself (compare with staurolite zone; Fig. 5a). Quartz and calcite are confirmed as vein phases, together with rare occurrences of plagioclase, zoisite, and amphibole.

The staurolite zone

In the staurolite zone, fine- to medium-grained schistose metapsammites dominate, with only occasional thin layers of metapelites, i.e. much like the garnet zone. Porphyroblasts of biotite, garnet, and staurolite, up to a maximum of 10 mm but usually not larger than 5 mm in size, are restricted in occurrence to these metapelite layers. Veins are mainly composed of quartz with occasional

small amounts of sulphides or oxides, and are orientated parallel to the foliation. Vein density at locality 10 was estimated to 7%.

Thin section point counting shows that metapsammite layers typically contain quartz and muscovite, minor amounts of chlorite and biotite, as well as plagioclase and opaque phases as accessories. In addition, metapelite layers generally contain abundant muscovite, chlorite, and biotite, as well as small amounts of tourmaline (Table 3). Staurolite is found together with garnet in some, but not all of the metapelite layers. Garnets are sometimnes found to exceed the width of their thin host metapelite layers, as described for the garnet zone (Fig. 5a). Garnet occurrences in staurolite absent rocks are extremely rare. At locality 10, staurolite porphyroblasts are concentrated near veins (Fig. 5b), and compilation of thin section point counting results from a profile of this locality shos that staurolite mode is higher adjacent to veins (Fig. 5c).

The kyanite zone

Kyanite zone rocks included in this study are mainly schistose and gneissose metapelites. Where found, kyanite porphyroblasts are usually ca. 1-2 cm but occasionally reach 5 cm in length. Kyanite porphyroblasts occur abundantly and are rather evenly distributed at locality 13, but are completely absent at locality 14. In contrast to biotite, garnet, and staurolite zones, where the spatial distribution of index minerals was related to veining, we found no relationship between the abundance of kyanite porphyroblasts and vein density at locality 13. Quartz is the main vein mineral, although radially grown kyanite aggregates with single crystal sizes up to several cm in length, and more rarely K-feldspar, are also observed in veins at locality 13. Vein density was estimated to 13% at locality 13 (Fig. 8).

In thin section, muscovite, quartz, biotite, kyanite, opaque phases, plagioclase, chlorite, and tourmaline were identified in these rocks (Fig. 6; Table 3). In addition to this, minor amounts (up to 2 vol. %) of extremely fine-grained garnet (<50 µm) were found. Kyanite grains commonly show a replacement rim of white micas, but most pseudomorphs retain a core of unaltered kyanite.

The sillimanite zone

The rocks in the sillimanite zone include layers of both metapsammites and metapelites. Staurolite porphyroblasts up to a few mm in size occasionally occur. Quartz is the main vein mineral, but tourmaline is also present. Vein density at locality 17 was estimated to 17%.

Thin section point counting results (Table 3) show that quartz, muscovite, and biotite are present in all rocks. In addition to this, varying amounts of chlorite, garnet, staurolite, kyanite, plagioclase, tourmaline, epidote, as well as oxides and sulphides are also observed. Two phases of garnet are present, one porphyroblastic, and one fine-grained similar to the garnet described from the kyanite zone. Veins are found to contain quartz, plagioclase, and tourmaline.

Sillimanite was not found in any of the localities situated on the chosen profile. We therefore include localities 18 and 19, although off profile, as these rocks do contain sillimanite. Two main types of rocks are found at this locality: (1) quartz rich (psammitic), non-veined, and sillimanite absent, and (2) quartz poor (pelitic), intensely veined, and sillimanite bearing. Sillimanite is exclusively found as fibrolite, in small patches (<50 µm) throughout the pelitic rock mass, and as larger patches (up to 1 cm) when adjacent to veins (Fig. 7). Other mineralogical and petrological properties are very similar to what is described above about locality 17, including homogenous distribution of other porphyroblasts (garnet, staurolite, and kyanite).

Regional trends

Based on field and petrographic observation along the ca. 6 km long profile (Fig. 1), some trends are evident as a function increased metamorphic grade (distance from the NEF; Fig. 8). Rock texture changes from phyllitic in the chlorite zone to schistose in the garnet, staurolite, and kyanite zones to gneissose in the sillimanite zone. Both matrix and porphyroblast crystal size generally increase from <1 mm in the chlorite zone to 10-50 mm in the sillimanite zone. Vein density increases from <1% in the chlorite zone to 17% in the sillimanite zones, while vein width and spacing decrease. Regardless of metamorphic grade or mineral constituents, most veins in Glen Esk show a blocky texture; however, occasional stretched crystals and wall rock array inclusions are also observed. In the chlorite zone, vein density and the crystal size distribution of the index mineral chlorite were unrelated. In the biotite, garnet, and staurolite zones, both size and abundance of the respective index minerals were higher adjacent to veins. This was seen on scales of mm, cm and dm. In the kyanite and sillimanite zones, vein density and the crystal size distribution of the respective index mineral were again unrelated. Another regional trend was an overall decrease in quartz mode and increase in muscovite mode with distance from the NEF.

Analytical results

Whole rock chemistry

Whole rock chemical compositions are presented in Table 4. Our dataset contains analyses of 39 rock samples from the 18 sampled localities (Fig. 1). In terms of MnKFMASH components, our samples range between 30.27-85.45 wt.% SiO_2, 7.18- 32.62 wt.% Al_2O_3, 1.78-35.56 wt.% Fe_2O_3, 0.35-11.48 wt.% MgO, 0.01-1.30 wt.% MnO, and 0.06-9.17 wt.% K_2O. SiO_2 and Al_2O_3 are inversely correlated as expected for interlayered metapsammites and metapelites. If only considering the samples we identified as metapelites, these average to 55.9±2.97 wt% SiO_2, 21.71±1.69 wt% Al_2O_3, 10.30±1.68 wt.% Fe_2O_3, 2.85±0.53 wt.% MgO, 0.19±0.08 wt.% MnO, as well as 4.32±0.62 wt.% K_2O, which is similar to the average pelitic rock as reported by Ague (1991). No clear regional trends as a function of distance from the NEF are seen in this dataset.

On an outcrop-scale, sample 12:001 from the garnet zone is especially interesting. This garnet bearing rock contains less SiO_2 and K_2O, but more MnO than the adjacent garnet absent rock; however, the relative proportions of Al_2O_3, FeO, and MgO in these rocks are almost identical. These AFM components represent a first order control of the presence/absence (but not the mode) of the Barrovian index minerals (Thompson, 1957). In terms of trace elements, these two subsamples show different concentrations of mobile elements e.g. Y, and Sr, but equal concentrations of immobile elements e.g. Ti, Zr, and Th (Fig. 9).

Mineral compositions

Mineral compositions from electron microprobe analyses are presented in Table 5. Muscovite contains varying amounts of Mg and Fe, however always within limits of the muscovite-celadonite series. Chlorite is an intermediate member of the clinochlore-chamosite series. Biotite is an intermediate member of the phlogopitic-annite series, and is generally closer to the phlogopite end member in the lower grade zones. Plagioclase compositions range between 53 and 97 % Ab, and are generally more albitic further from the NEF.

Paired core-rim and profile analyses of garnets from the garnet and staurolite zones generally show higher amounts of the spessartine and grossular components in the core than in the rim, and vice versa for the pyrope and almandine components (Fig. 10). This is consistent with prograde growth zonation of garnet (Kohn, 2003). Comparison of the two zones shows that the amounts of the pyrope and almandine components are generally higher in the staurolite zone, whereas the

amounts of the spessartine and grossular components are lower. The fine-grained garnets found in the kyanite zone, however, show an inverse growth zonation for the spessartine, grossular, and pyrope components, and are generally very Mn-rich (X(spessartine) > 40%).

All staurolite composition data are from samples from locality 10, and these yield an average of X_{Fe} = 0.84±0.01 (95% conf., n = 39. MnO content in staurolite is variable and correlates well with both staurolite mode and whole rock MnO content (Fig. 10).

Oxygen isotopes

Oxygen isotope ratios were utilised to investigate vein-wall rock interaction. We include pairs of vein and vein-adjacent wall rock $\delta^{18}O_{Qtz}$ analyses from the chlorite and biotite zones, as well as two cm scale $\delta^{18}O_{Qtz/Ky}$ profiles from the garnet and kyanite zones (Fig. 11). In the chlorite and biotite zones, the vein isotopic signature is different from that of the vein-adjacent wall rock. The garnet zone profile shows that $\delta^{18}O$ of the wall rock gradually increase away from the vein. The kyanite zone profile, on the other hand, shows no change in $\delta^{18}O_{Qtz}/_{Ky}$ after Qtz- Ky isotopic fractionation for a calculated fluid is taken into account.

DISCUSSION

Controls on index mineral distribution

Chlorite zone

In the chlorite zone, index mineral distribution is generally homogenous and vein density is low. No mineralogical or petrological differences are observed between vein adjacent country rock and country rock situated far from veins. Stable isotope data from the chlorite zone shows that country rock and veins are out of isotopic equilibrium (Fig. 11). This indicates that veins in the chlorite zone mainly transported fluids of external origin, and that no or extremely little fluid-rock interaction took place, implying that vein-channelised metamorphic fluids had little or no effect on the crystal size distributions of index minerals. The homogenous chlorite distribution irrespective of proximity to veins and rock composition (pelitic/psammitic) could indicate that pressure and temperature are the most important factors controlling index mineral distribution, and that both fluid-rock interaction and rock composition were of less importance; however, the small amount of available outcrop to sample makes it impossible to test the role of rock composition statistically. For the chlorite zone, our data support the classic view of a pressure, temperature, and composition (P-T-x) controlled Barrovian index mineral distribution.

Biotite zone

The biotite zone is generally very similar to the chlorite zone in terms of index mineral and vein distribution. Mineralogical and petrological observations, as well as oxygen isotope data (Fig. 11), in most cases indicate extremely little or no fluid-rock interaction. In contrast to the homogenous chlorite distribution in the chlorite zone, biotite abundance is highly variable and is generally higher in metapelite layers, which indicates that bulk composition of the rock is of importance. Our observations from the biotite zone generally support P-T-x controlled Barrovian index mineral distribution.

Locality 05 is different from all other localities we examined in the biotite zone. This fold hinge is an area of intense veining, with a vein density of at places >50%, i.e. at least one order of magnitude higher than the biotite zone in general. The smaller vein spacing and high vein density suggest this is an area of higher fluid flux, and therefore a greater portion of the country rock may have been affected by fluid-rock interaction, but also that the hinge served as a conduit for channelisation of fluids as suggested by

Ague (2011). In-field crystal size distribution analysis shows increased biotite size and possibly also abundance towards the fold hinge, the most intensely veined part of the locality (Fig. 3). We interpret this as evidence for fluid-rock interaction having influenced index mineral size distributions in the biotite zone. The fact that biotite also occurs in the less veined rocks suggests that biotite stabilisation is P-T-x controlled also at this locality; however, we attribute localised fluid-rock interaction as the main control on size and abundance. Similar observations have been reported by Skelton (1997), in which areas of intense veining correlate with increased garnet crystal size, who also attributes this to a higher degree of fluid-rock interaction. Fluid controlled index mineral distribution as a mechanism is further discussed in the following section.

Garnet and staurolite zones

In the garnet and staurolite zones, index mineral distribution is extremely heterogeneous, and in most outcrops the index mineral in question is not even present. Where found, however, the abundance of both garnet and staurolite is shown to be spatially related to veins (Figs. 4 & 5) or thin (~1 mm) metapelite layers (Fig. 5). General quartz content somewhat correlates to the staurolite abundance in the profiled locality 10 (Fig. 5), which is indicative of a bulk rock compositional control on staurolite distribution, but the impact by distance from each individual vein is by far the largest. As a function of proximity to veins, not only does index mineral size and abundance increase, but in most cases quartz abundance decreases. Coincident with these mineralogical trends in the garnet zone, oxygen isotope data from locality 09 show a gradual decrease in $\delta^{18}O$ towards vein values (Fig. 11b).

The simplest explanation for the observed heterogeneous index mineral distribution is that veining predominately occurs in metapelitic layers because these are mechanically weaker than metapsammites. This would imply that occurrence of index minerals was controlled by protolith composition and not necessarily related to veining. However, our staurolite zone samples were taken across a 4 m gradual transition from metapelite to metapsammite which is seen as an overall increase in quartz content with distance (Fig. 5). No correlation is seen between vein density and this trend. This argues against preferential veining of metapelitic rocks. Also, in the garnet zone, we see no difference between the concentrations of immobile elements (e.g. Ti, Zr, and Th) between garnet bearing and garnet absent rock in sample 12:001 (Fig. 9). Furthermore, $\delta^{18}O$ decreases towards the vein (Fig. 11). This is indicative of chemical transport either towards or away from the vein. Spatial coincidence between this isotopic gradient and decreasing quartz abundance (Fig. 11) points to silica removal by fluid-assisted diffusive/advective transport towards the vein. This together with the previous arguments points to fluid-rock interaction as responsible for the formation of cm-scale altered zones (selvages) within the country rock. Similar observations and interpretations have been made by Ague (2003), Masters & Ague (2005), and Ague (2011). Following the vein classification scheme offered by Bons et al. (2002), the veins in Glen Esk are either syntaxial veins or stretching veins, both indicative of an advection dominated mode of fluid transportation within the veins.

For sample 12:001 from the garnet zone FeO, MgO, Al_2O_3, and MnO are enriched in the selvage subsample compared to the country rock, but K_2O, and SiO_2 are depleted. The relative proportions of FeO, MgO, and Al_2O_3 are identical in the two subsamples, which indicates that this enrichment is fully attributable to silica depletion and that no amount of these components was added to the rock during selvage formation (Fig. 9). The concentration of MnO, on the other hand, is an order of magnitude higher in the selvage than in the surrounding rock. One possible explanation is that MnO was added to this selvage from the surrounding rocks. We thus suggest a model whereby

MnO was transported by fluid-assisted diffusion/advection towards the vein, accompanied by SiO_2, K_2O, and ^{18}O. Thermodynamic modelling (Fig. 12) shows that the increased concentration of MnO in the selvage would have expanded the stability field of garnet to lower temperature. Growth of garnets in the vein selvage served as a MnO sink. This coincides with enrichment of AFM components which we infer was due to loss of silica into the vein. Such a model would thus explain not only why we almost exclusively observe garnet in vein adjacent rock, but also why the garnet mode decreases away from these veins. The correlation between staurolite MnO content and both whole rock MnO content and staurolite mode indicates that Mn may be of importance also in the staurolite zone (Fig. 10). Based on this, and the coincident variation in staurolite and quartz mode discussed above, we therefore propose an analogous model for staurolite stabilisation and distribution in the staurolite zone. Fluid-rock interaction may also explain the occurrence of unusually large garnets in thin metapelite layers (~1 mm) sandwiched between thicker metapsammite layers (Fig. 5), found in both the garnet and staurolite zones. We suggest that fluid was channelized along the more permeable metapelite layers (cf. Bickle & Baker, 1990; Ague, 2003; Ague, 2011). Garnet formation might thus have been assisted by coupled removal of silica and addition of Mn along these layers in a manner analogous to that which is proposed above.

In both zones, we also observed examples where vein adjacent rock did not host garnet or staurolite respectively. We offer two possible explanations for these observations, which either alone or together resulted in a lack of index minerals. Firstly, this could be an effect of differences in vein properties. Wider veins generally yield higher fluid fluxes and thereby less fluid-rock interaction. Skelton (1997) spatially correlated increased garnet abundance and crystal size with narrower veins, and vice versa for wider veins. Vein density might also be of importance, larger distances between the veins imply a smaller total volume of country rock in direct contact with the fluid. In the staurolite zone, staurolite is generally absent where vein density is lower and veins are wider (Fig. 5). Secondly, we would like to propose that there is a critical mass of AFM components that needs to be reached, before these index minerals crystallise. Following the work of Thompson (1957) and thereby assuming chemical equilibrium, in theory the Barrovian index minerals should form as soon as the tiniest concentration of AFM components is present. In other words, variation in AFM components would not change the stability, but only the abundance of these minerals. In nature, however, equilibrium might not always be the case. For reactions involving the AFM components, we propose that higher SiO_2 content in the protolith may imply disequilibrium because (1) AFM components are more widely separated and no reaction will take place unless they are in contact, (2) the protolith contains less H_2O, which limits the amount of fluids produced during metamorphism and thereby also the amount of medium for diffusive transportation of AFM components, and (3) metapsammites are less permeable than metapelites and therefore diffusion is slower. These three factors, individually and together, may thus kinetically limit the index mineral forming reactions to an extent where it is thermodynamically favourable to continue the growth of already existing minerals, rather than to form new minerals.

We attribute fluid induced removal of silica from the country rock, and subsequent relative enrichment of the AFM components, to be the general control on index mineral stabilisation and distribution. However, MnO is likely to be an additional factor controlling stabilisation of garnet in the garnet zone, and possibly also staurolite in the staurolite zone. Although selvage formation is the probable explanation for most cases of index mineral stabilisation, it is still possible that some rock layers are of the right composition to stabilise these minerals without the influence of any external fluid. Sample 13:002 may be such an example, in which we found garnets (although in lower amounts than in sample

12:001), and we see no correlation between abundance and spatial relationship to veins.

Kyanite zone

In the kyanite zone, kyanite is abundant and evenly distributed at locality 13. It is not possible to texturally, mineralogically, nor chemically distinguish rock adjacent to veins from rock far from veins. Kyanite zone oxygen isotope signatures show an absolutely flat trend away from a vein (Fig. 11). If corrected for kyanite-quartz fractionation calculated as an average of different fractionation coefficients for kyanite-H_2O and quartz-H_2O (Clayton et al. 1972; Shiro & Sakai 1972; Bottinga & Javoy 1973; Matsuhisa et al 1979; Richter & Hoernes 1988; Zheng 1993), country rock kyanite $\delta^{18}O$ values are within error equal to vein quartz $\delta^{18}O$ values, indicating that the country rock completely equilibrated with the fluid during metamorphism. The general trend of increased vein density and decreased vein spacing as a function of increased metamorphic grade (fig. 8) provide corroborative evidence of more extensive fluid-rock interaction in these higher grade rocks. We thereby propose the same general mechanism for index mineral distribution in the kyanite zone as in the garnet and staurolite zones, i.e. fluid induced silica depletion of the country rock, albeit that selvages are wider and therefore overlapping resulting in a homogeneous index mineral distribution.

Kyanite is absent at locality 14, despite that these rocks are as pelitic and intensely veined as those at locality 13. We see no reason for kyanite not forming in these rocks, as rock compositions are well within the stability fields for these mineral. A possible explanation is that formation of kyanite indeed took place, but that later retrograde overprinting removed both the kyanite grains and their textures. The degree of retrogression is higher in the kyanite zone than in the lower grade zones. Evidence of retrograde reactions is widely found, including (where applicable) partial to complete replacement of kyanite and staurolite by white micas, partial replacement of garnet by biotite and chlorite, presence of very fine-grained and inversely zoned Mn-rich garnet interpreted as retrograde growth, as well as the presence of chlorite. In general these observations are in accordance with previous studies (Harte & Johnson 1969; Baltatzis & Katagas 1981); however, the fine grained Mn-rich garnet has not to our knowledge been reported before.

Sillimanite zone

At first glance, sillimanite distribution at locality 18 seems controlled in the same manner as in the garnet and staurolite zones, i.e. locally concentrated in vein adjacent selvages. In contrast to the garnet and staurolite zones, sillimanite is the only porphyroblast that follows this pattern, and the size distribution of garnet, staurolite, and kyanite is homogeneous. The latter is an indication that wide and overlapping selvages were formed, analogous to what we argue for the kyanite zone. An implication of this, however, is that sillimanite growth cannot have been controlled by the same mechanism as the other porphyroblasts. If that was the case it would also be evenly distributed. One possible explanation is that sillimanite was stabilised due to a later event that only affected the sillimanite zone. Vorhies & Ague (2013) suggested that sillimanite grade metamorphism in Glen Esk was reached due to a secondary heating event caused by the adjacent synmetamorphic granite intrusion, meaning that sillimanite stabilised as a result of contact metamorphism rather than regional scale orogenic metamorphism. This is also consistent with our observation of sillimanite at locality 18 but not at locality 17. Locality 18 is positioned much closer to the granite.

CONCLUSIONS

We conclude that:

- Stabilisation and distribution of Barrovian index minerals in the chlorite and biotite zones of Glen Esk was

mainly controlled by pressure, temperature and whole rock composition.

- Partial fluid-rock interaction and associated localised silica removal adjacent to veins produced index mineral bearing selvages in the garnet and staurolite zones and in intensely veined locality in the biotite zone. This was a primary control of index mineral size distribution in these zones. In addition, MnO played an important role in the stabilisation of garnet, and possibly also staurolite.
- Selvage formation was also the main control on index mineral stabilisation and distribution in the kyanite zone; however, fluid- rock interaction and selvage formation was more extensive and selvages were overlapping resulting in homogeneous index mineral distributions.
- Sillimanite formation post-dated formation of the other Barrovian minerals. This may be related to secondary heating associated with the syn-metamorphic northward lying granite intrusion as proposed by Vorhies & Ague (2013). The distribution of sillimanite would in that case mainly be controlled by proximity to this granite.

REFERENCES

Ague, J.J. (1991). Evidence for major mass transfer and volume strain during regional metamorphism of pelites. *Geology* **19**, 855-858.

Ague, J.J. (1994). Mass transfer during Barrovian metamorphism of pelites, south-central Connecticut. I: evidence for changes in composition and volume. *American Journal of Science* **294**, 989-1057.

Ague, J.J. (2003). Fluid infiltration and transport of major, minor, and trace elements during regional metamorphism of carbonate rocks, Wepawaug schist, Connecticut, USA. *American Journal of Science* **303**, 753-816.

Ague, J.J. (2011). Extreme channelization of fluid and the problem of element mobility during Barrovian metamorphism. *American Mineralogist* **96**, 333-352.

Albee, A.L. (1965). A petrogenetic grid for the Fe-Mg silicates ofpelitic schists. *American Journal of Science* **263**, 512-536.

Baker, A.J. (1985). Pressures and temperatures of metamorphism in the eastern Dalradian. *Journal of the Geological Society, London* **142**, 137–148.

Baltatzis, E. & Katagas, C. (1981). Margarite pseudomorphs after kyanite in Glen Esk, Scotland. *American Mineralogist* **66**, 213-216.

Barrow, G. (1893). On an intrusion of muscovite-biotite gneiss in the south-eastern Highlands of Scotland, and its accompanying metamorphism. *Quarterly Journal of the Geological Society of London* **49**, 330-358.

Barrow, G. (1912a). On the geology of Lower Dee-side and the southern Highland border. *Proceedings of the Geologists' Association* **23**, 274-290.

Barrow, G. (1912b). Lower Dee-side and the Highland border. *Proceedings of the Geologists' Association* **23**, 268-273.

Berman, R.G. & Brown, T.H. (1985). The heat capacity of minerals in the system K_2O-Na_2O-CaO-MgO-FeO-Fe_2O_3-Al_2O_3-SiO_2-TiO_2-H_2O-CO_2: representation, estimation, and high temperature extrapolation. *Contributions to Mineralogy and Petrology* **89**, 168-183.

Bickle, M.J. & Baker, J. (1990). Advective-diffusive transport of isotopic fronts: an example from Naxos, Greece. *Earth and Planetary Science Letters* **97**, 78-93.

Bons, P.D., Elburg, M.A. & Gomez-Rivas, E. (2012). A review of the formation of tectonic veins and their microstructures. *Journal of Structural Geology* **43**, 33-62.

Bottinga, Y. & Javoy, M. (1973). Comments on oxygen isotope geothermometry. *Earth and Planetary Science Letters* **20**, 250-265.

Chew, D.M. & Strachan, R.A (2014). The Laurentian Caledonides of Scotland and Ireland. *In*: Corfu, F., Gasser, D. & Chew, D.M. (eds.). New Perspectives on the Caledonides of Scandinavia and Related Areas. *Geological Society of London Special Publications* **390**, 45-91.

Clayton; R.N., O'Neil, J.R. & Mayeda, T.K. (1972). Oxygen isotope exchange between quartz and water. *Journal of Geophysical Research* **77**, 3057-3067.

Dempster, T.J. (1985). Garnet zoning and metamorphism of the Barrovian type. *Contributions to Mineralogy and Petrology* **89**, 30–38.

Dempster, T.J., Rogers, G., Tanner, P.W.G., Bluck, B.J., Muir, R.J., Redwood, S.D., Ireland, T.R. & Paterson, B.A. (2002). Timing of deposition, orogenesis and glaciations within the Dalradian rocks of Scotland: constraints from U–Pb ages. *Journal of the Geological Society, London* **159**, 83–94.

Eskola, P. (1915). On the relation between the chemical and mineralogical composition in metamorphic rocks of the Orijärvi region. *Bulletin of the Geological Society of Finland* **44**.

Eskola, P. (1920). The mineral facies of rocks. *Norsk Geologisk Tidskrift* **6**, 143-194.

Eskola, P. (1929). On the mineral facies. *Proceedings of the Geological Society, Stockholm* **51**, 157-172.

Ferry, J.M. (1987). Metamorphic hydrology at 13-km depth and 400-550°C. *American Mineralogist* **72**, 39-58.

Gresens, R.L. (1967). Composition-volume relationships of metasomatism. *Chemical Geology* **2**, 47-65.

Grant, J.A. (1986). The isocon diagram: a simple solution to Gresens' equation for metasomatic alteration. *Economic Geology* **81**, 1976-1982.

Greenwood, H.J. (1961). The system NaAlSi2O6-H2O-argon. Total pressure and water pressure in metamorphism. *Journal of Geophysical Research* **66**, 3923-3946.

Greenwood, H.J. (1962). Metamorphic reactions involving two volatile components. *Year Book Carnegie Institution of Washington* **61**, 82-85.

Harker, A. (1912). The North Esk. *Proceedings of the Geologists' Association* **23**, 273.

Harte, B. (1987). Glen Esk Dalradian, Barrovian metamorphic zones. *In*: N.H., Kneller, B.C., Gillen, C. (Eds.). *Excursion Guide to the Geology of the Aberdeen Area*. Scottish Academic Press (for Geological Society of Aberdeen), Edinburgh, pp. 193–210.

Harte, B., & Hudson, N.F.C. (1979). Pelite facies series and the temperatures and pressures of Dalradian metamorphism in E Scotland. *In* Harris, A.L., Holland, C.H. & Leake, B.E. The Caledonides of the British Isles; reviewed. *Geological Society of London – Special Publication* **8**, 323-337.

Harte, B. & Johnson, M.R.W. (1969). Metamorphic history of Dalradian rocks in Glens Clova, Esk and Lethnot, Angus, Scotland. *Scottish Journal of Geology* **5**, 54–80.

Helgeson, H.C., Delany, J.M., Nesbitt, H.W. & Bird, D.K. (1978). Summary and critique of the thermodynamic properties of rock-forming minerals. *American Journal of Science* **278**, 1-299.

Hensen, B.J. (1971). Theoretical phase relations involving cordierite and garnet in system MgO-FeO-Al_2O_3-SiO_2. *Contributions to Mineralogy and Petrology* **33**, 191-214.

Hess, P.C. (1969). The metamorphic paragenesis of cordierite in pelitic rocks. *Contributions to Mineralogy and Petrology* **24**, 191-207.

Holland, T.J.B., Baker, J.M. & Powell, R. (1998). Mixing properties and activity-composition relationships of chlorites in the system MgO-FeO-Al2O3-SiO2-H2O. *European Journal of Mineralogy* **10**, 395-406.

Holland, T.J.B. & Powell, R. (1985). An internally consistent thermodynamic dataset with uncertainties and correlations :

2. Data and results. *Journal of Metamorphic Geology* **3**, 343–370.

Holland, T.J.B. & Powell, R. (1998a). Calculating phase diagrams involving solid solutions via non-linear equations, with examples using THERMOCALC. *Journal of Metamorphic Geology* **16**, 577–588.

Holland, T.J.B. & Powell, R. (1998b). An internally consistent thermodynamic dataset for phases of petrological interest. *Journal of Metamorphic Geology* **16**, 309-343.

Kohn, M.J., (2003). Geochemical zoning in metamorphic minerals. In Rudnick, R.L. (ed.), *The Crust*. Holland, E.D. & Turekian, K.K. (eds.), *Treatise on Geochemistry* **3**, Elsevier, Amsterdam, pp. 229-261

Koons, P.O. & Thompson, A.B. (1985). Non-mafic rocks in the greenschist, blueschist and eclogite facies. *Chemical Geology* **50**, 3-30.

Mahar, E.M., Baker, J.M., Powell, R. Holland, T.J.B. & Howell, N. (1997). The effect of Mn on mineral stability in metapelites. *Journal of Metamorphic Geology* **15**, 223-238.

Masters, R.L. & Ague, J.J. (2005). Regional-scale fluid flow and element mobility in Barrow's metamorphic zones, Stonehaven, Scotland. *Contributions to Mineralogy and Petrology* **150**, 1-18.

Matsuhisa, Y., Goldsmith, J.R. & Clayton, R.N. (1979). Oxygen isotopic fractionation in the system quartz-albite-anorthite-water. *Geochimica Cosmochimica Acta* **43**, 1131-1140.

Oliver, G.J.H., Chen, F., Buchwaldt, R. & Hegner, E. (2000). Fast tectonometamorphism and exhumation in the type area of the Barrovian and Buchan zones. *Geology* **28**, 459–462.

Oliver, G.J.H., Wilde, S.A. & Wan, Y. (2008). Geochronology and geodynamics of Scottish granitoids from the late Neoproterozoic break-up of Rodinia to Palaeozoic collision. *Journal of the Geological Society, London* **165**, 661–674.

Powell, R. & Holland, T.J.B. (1985). An internally consistent thermodynamic dataset with uncertainties and correlation: 1. Methods and a worked example. *Journal of Metamorphic Geology* **3**, 372-342.

Powell, R, Holland, T.J.B. & Worley, B. (1998). Calculating phase diagrams involving solid solutions via non-linearequations, with examples using THERMOCALC. *Journal of Metamorphic Geology* **16**, 577-588.

Richter, R. & Hoernes, S. (1988). The application of the increment method in comparison with experimentally derived and calculated O-isotope fractionations. *Chemie der Erde* **48**, 1-18.

Robertson, S. (1994). Timing of Barrovian metamorphism and 'Older Granite' emplacement in relation to Dalradian deformation. *Journal of the Geological Society, London* **151**, 5–8.

Shiro, Y. & Sakai, H. (1972). Calculation of the reduced partition function ratios of alpha-, beta-quartz and calcite. *Bulletin of the Chemical Society of Japan* **45**, 2355-2359.

Skelton, A.D.L. (1997). The effect of metamorphic fluid flow on the nucleation and growth of garnets from Troms, North Norway. *Journal of Metamorphic Geology* **15**, 85-92.

Spear, F.S. & Cheney, J.T. (1989). A petrogenetic grid for pelitic schists in the system SiO_2-Al_2O_3-FeO-MgO-K_2O-H_2O. *Contributions to Mineralogy and Petrology* **101**, 149-164.

Spicuzza, M.J., Valley, J.W., Kohn, M.J., Girard, J.P. & Fouillac, A.M. (1998). The rapid heating, defocused beam technique: a CO_2-laser-based method for highly precise and accurate determination of $\delta^{18}O$ values of quartz. *Chemical Geology* **144**, 195-203.

Tanner, P.W.G., Thomas, C.W., Harris, A.L., Gould, D., Harte, B., Treagus, J.E. & Stephenson, D. (2013). The Dalradian rocks of the Highland Border region of Scotland. *Proceedings of the Geologists' Association* **124**, 215-262.

Taylor, H.P. (1977). Water/rock interactions and the origin of H_2O in granitic batholiths: Thirtieth William Smith lecture. *Journal of the Geological Society* **133**, 509-558.

Thompson, A.B. (1976). Mineral reactions in pelitic rocks: II. Calculation of some P-T-X(Fe-Mg) phase relations. *American Journal of Science* **276**, 425-454.

Thompson, J.B. (1957). The graphical analysis of mineral assemblages in pelitic schists. *American Mineralogist* **42**, 842-858.

Thompson, J.B. (1959). *Local equilibrium in metasomatic processes*. In: Abelson, P.H. (Ed.). *Researches in Geochemistry*, Vol. 1, John Wiley (1959), 427–457.

Valley, J.W., Kitchen, N., Kohn, M.J., Niendorf, C.R. & Spicuzza, M.J. (1995): UWG-2, a garnet standard for oxygen isotope ratios: Strategies for high precision and accuracy with laser heating. *Geochimica et Cosmochimica Acta* **59**, 5223-5231.

van der Plas, L. & Tobi, A.C. (1965). A chart for judging the reiliability of point counting results. *American Journal of Science* **263**, 87-90.

Viete, D.R., Hermann, J., Lister, G. & Stenhouse, I. (2011). The nature and origin of the Barrovian metamorphism, Scotland: diffusion length scales in garnet and inferred thermal time scales. *Journal of the Geological Society, London* **168**, 115–132.

Vorhies, S.H. & Ague, J.J. (2011). Pressure-temperature evaluation and thermal regimes in the Barrovian zones, Scotland. *Journal of the Geological Society, London* **168**, 1147–1166.

White, R.W., Pomroy, N.E. & Powell, R., 2005. An in-situ metatexite-diatexite transition in upper amphibolite facies rocks from Broken Hill, Australia. *Journal of Metamorphic Geology* **23**, 579-602.

Zheng, Y.F. (1993). Calculation of oxygen isotope fractionation in anhydrous silicate minerals. *Geochimica Cosmochimica Acta* **57**, 1079-1091.

Acknowledgements

Dan Zetterberg is thanked assistance in field and with sample preparation. Runa Jacobsson and Cora Wohlgemuth-Überwasser are thanked for whole rock analyses, and so is Jaroslaw Majka for assistance at the electron microprobe analyser. Pavel Pitra is thanked for support on THERMOCALC and pseudo-section construction. We thank John Valley for assistance and funding in stable isotope analysis at UW-Madison and for a review of an early version of this paper.

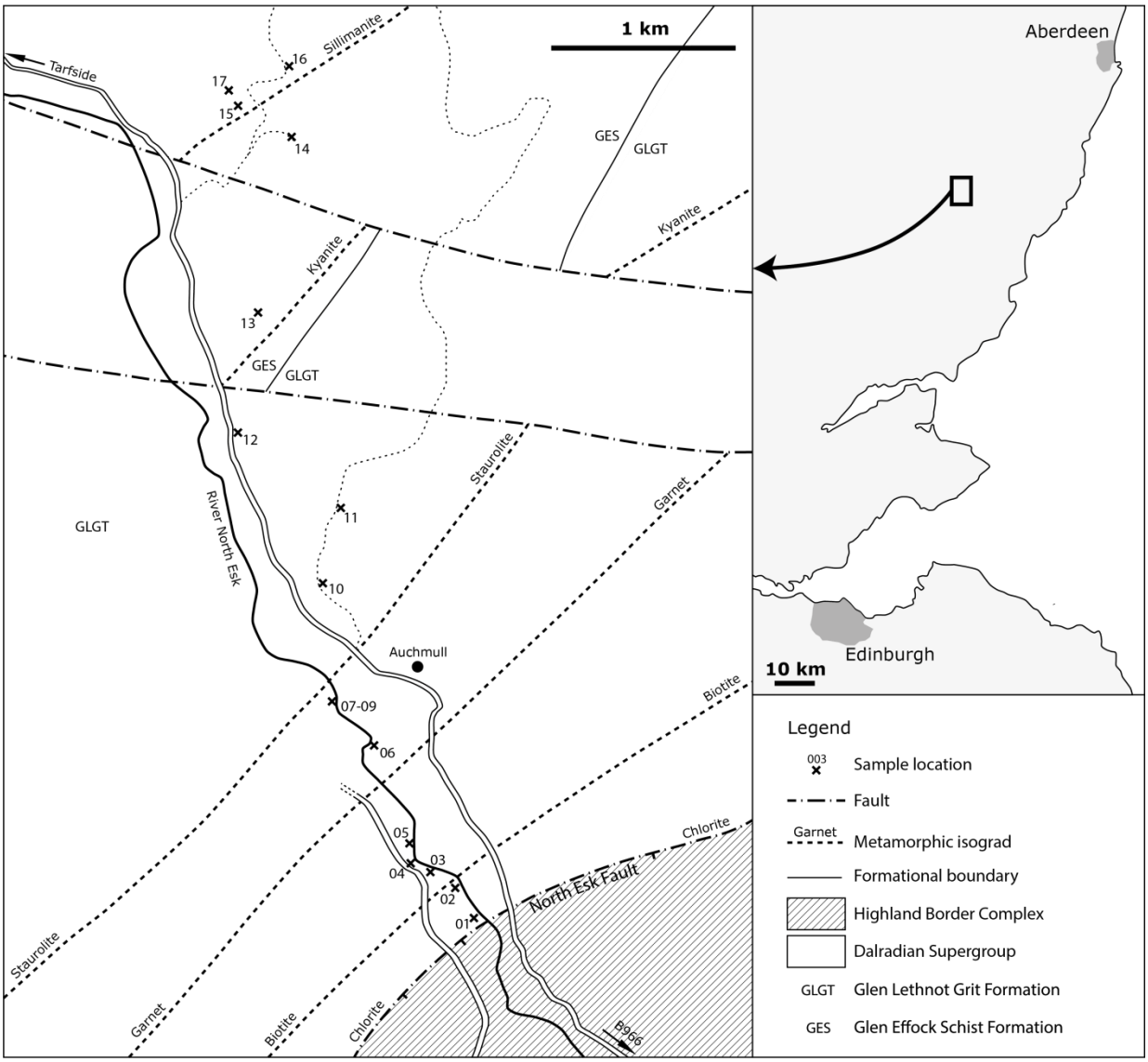

Figure 1: Map showing the field area in Glen Esk, SE Scottish Highlands. The main rock groups and formations, structural boundaries, isograds are indicated (drawn from Tanner et al. 2013), and locations of the sample localities are shown.

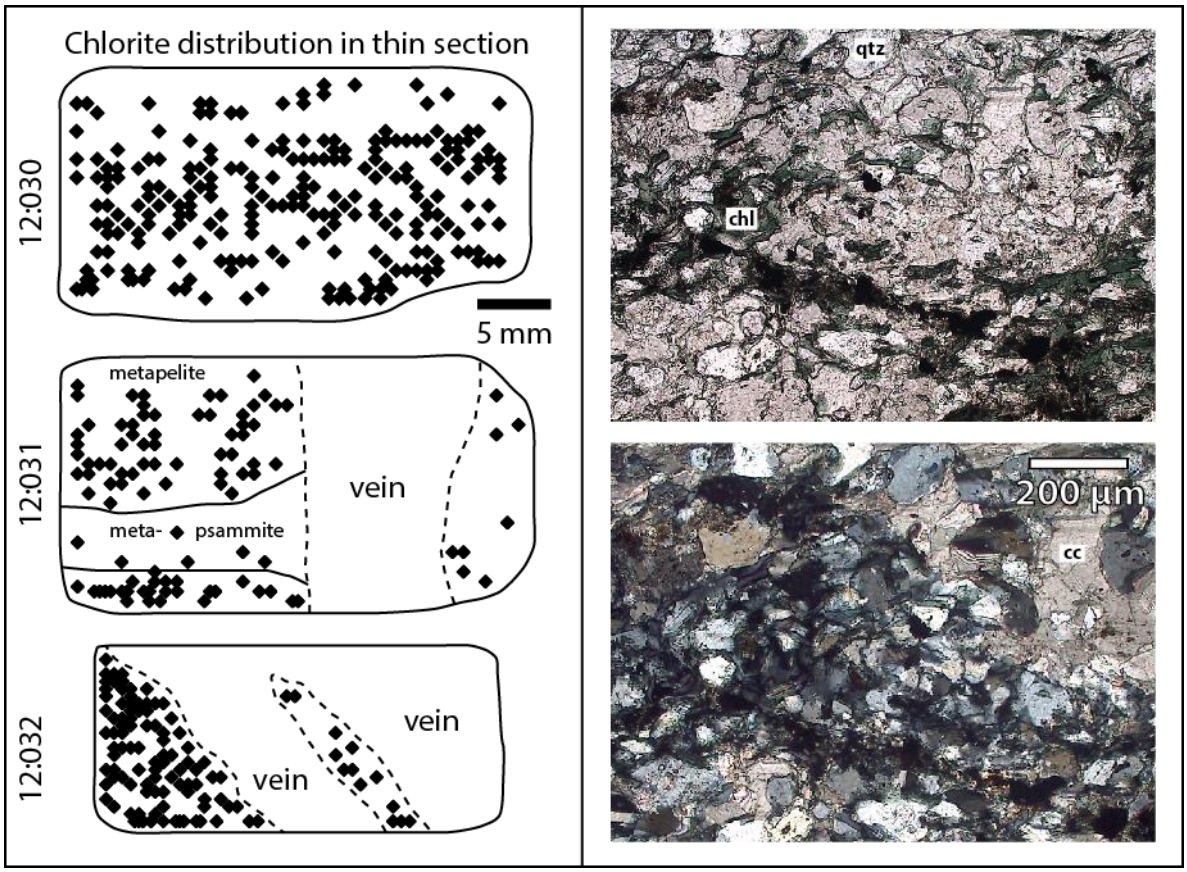

Figure 2: Left: Spatial distribution of chlorite in thin sections (based on point counting; thin section edges, lithological layers, and veins sketched in) showing an overall homogeneous distribution. Right: Photomicrographs of sample 12:030 in PPL (above) and XPL (below), showing that calcite is interstitial to quartz and chlorite.

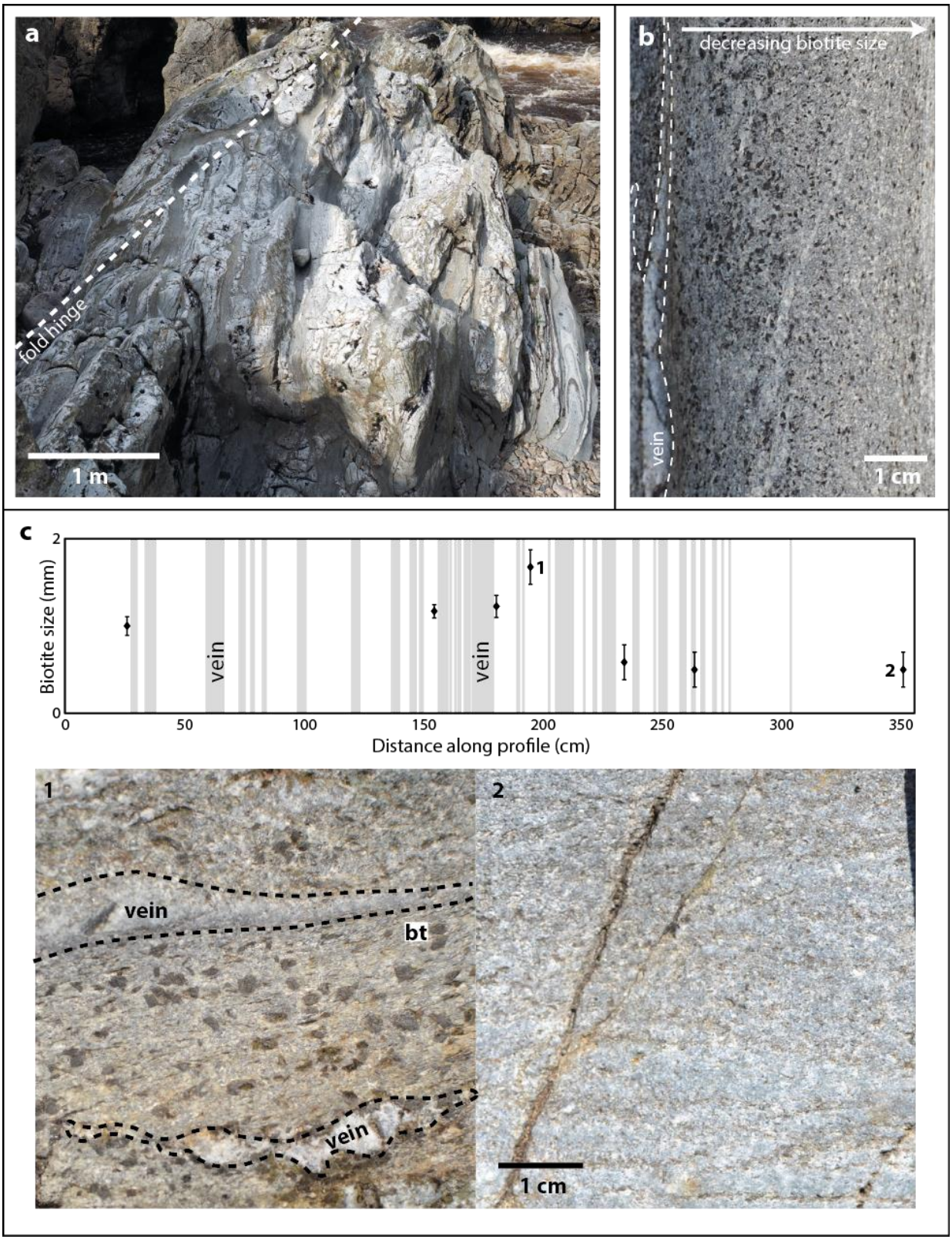

Figure 3a: Field photo of an intensely veined fold hinge in the biotite zone. **3b:** Close-up photo of a small area located near the hinge, showing a decrease in biotite crystal size (black coloured) with increasing distance away from the vein. **3c:** Profile across the fold hinge (in Fig. 7a), with vein widths shown in light grey and in-field estimation of biotite grain size presented in seven data points. The hinge is located at x ≈ 175 cm. Below: photographs of areas used for crystal size estimation corresponding to the data points marked as 1 and 2, respectively.

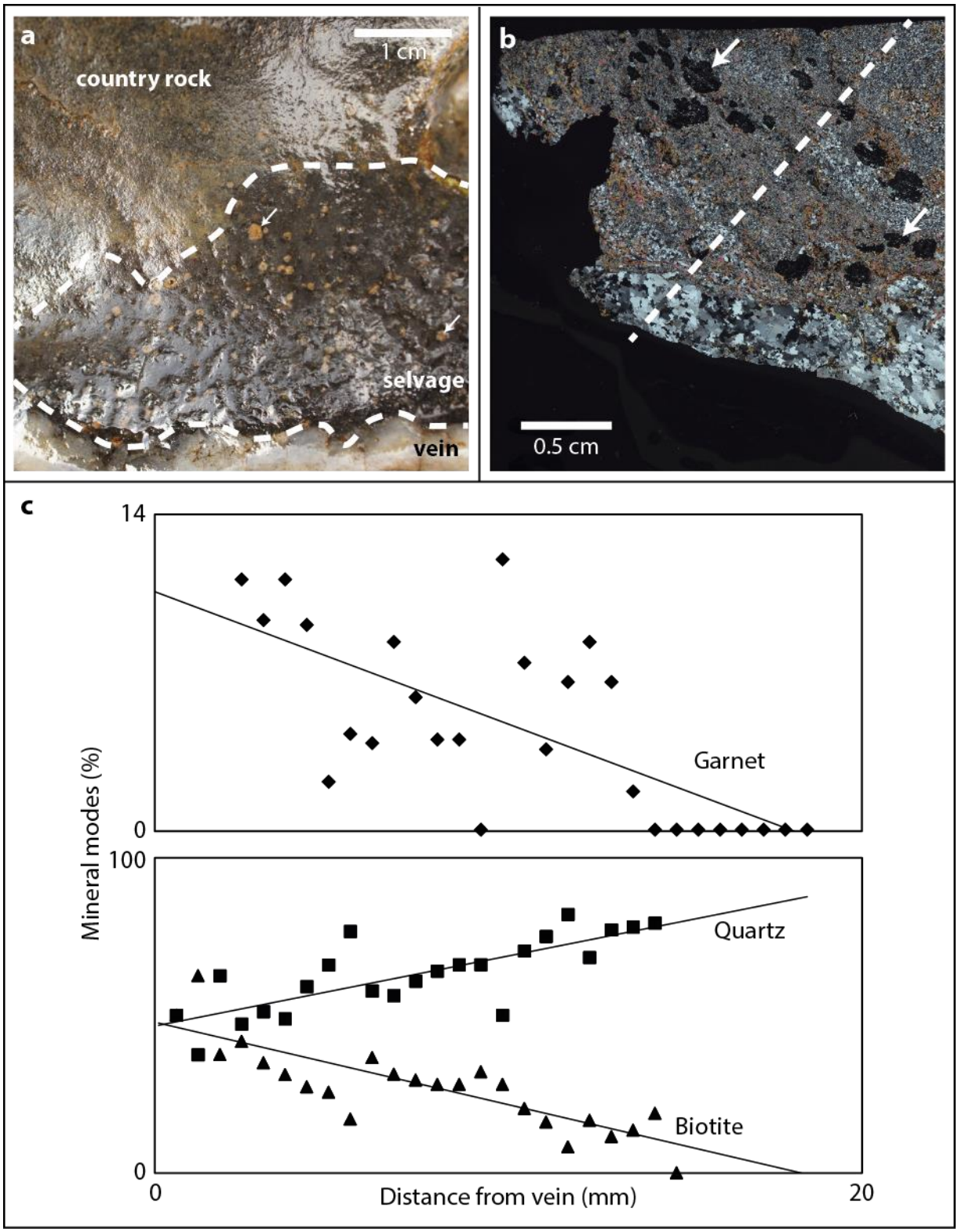

Figure 4a: Field photograph of an outcrop in the garnet zone, typical for the vein-adjacent type of garnet. Dashed line marks approximate boundaries between vein, selvage, and unaltered country rock. Small white arrows mark garnet. 4**b:** Scanned thin section, from the rock in (a), in XPL. Dashed line marks point counting profile. 4**c:** Mineral modes along the dashed line in (b), showing decreasing quartz and increasing garnet and biotite contents towards the vein.

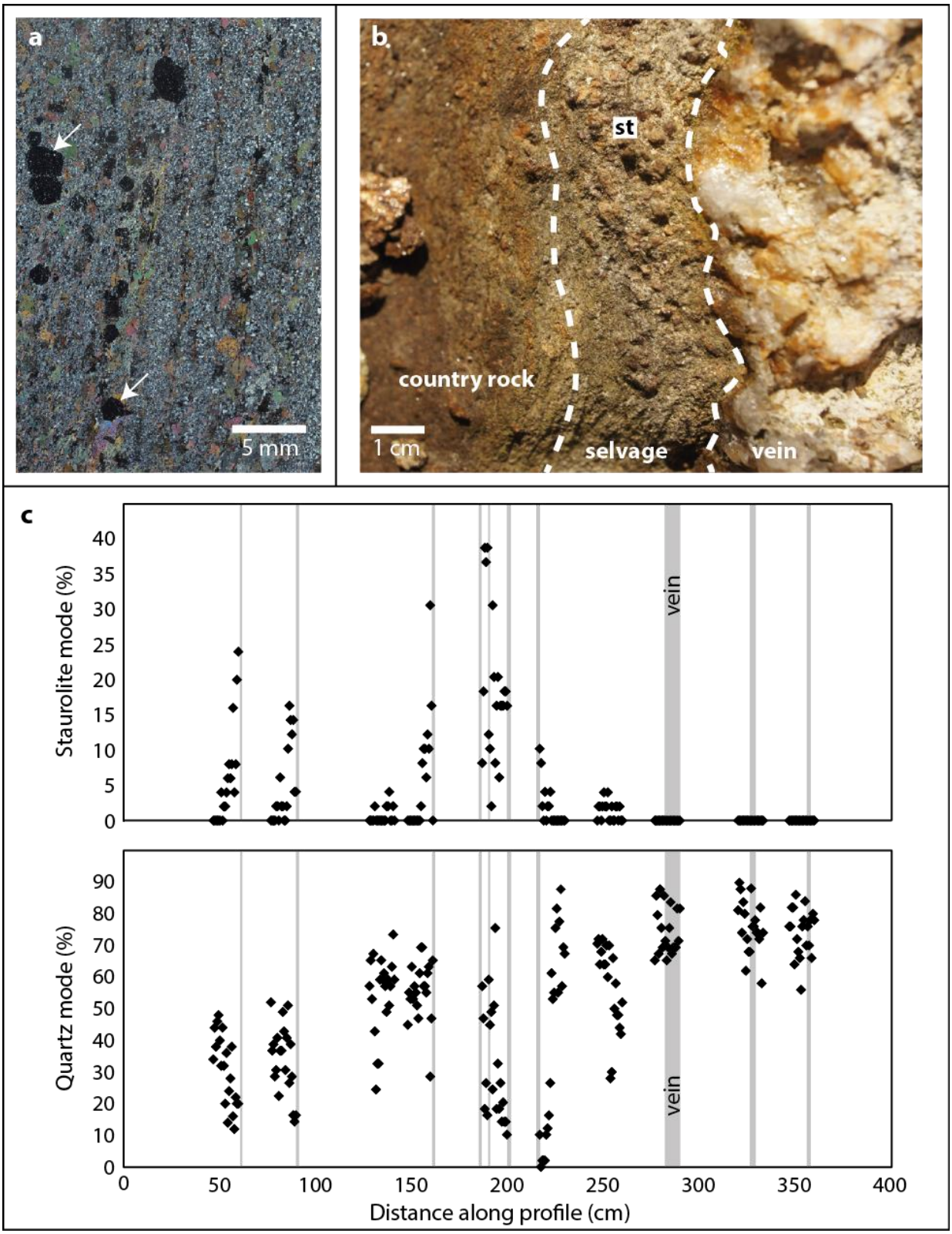

Figure 5a: Thin section scan in cross polarised light, showing metapelite laminae with large garnet crystals (arrows), as found both in the garnet and staurolite zones. **5b**: Outcrop with staurolite bearing vein adjacent zones. Staurolite porphyroblasts are brown and a few mm across. Boundaries between vein, selvage, and country rock are marked with dashed lines. **5c:** Profile from the outcrop in part shown in (a), but extending further in both directions, with staurolite and quartz abundance data from thin section point counting. Generally, staurolite and quartz abundance are inversely correlated as a function of distance from a vein.

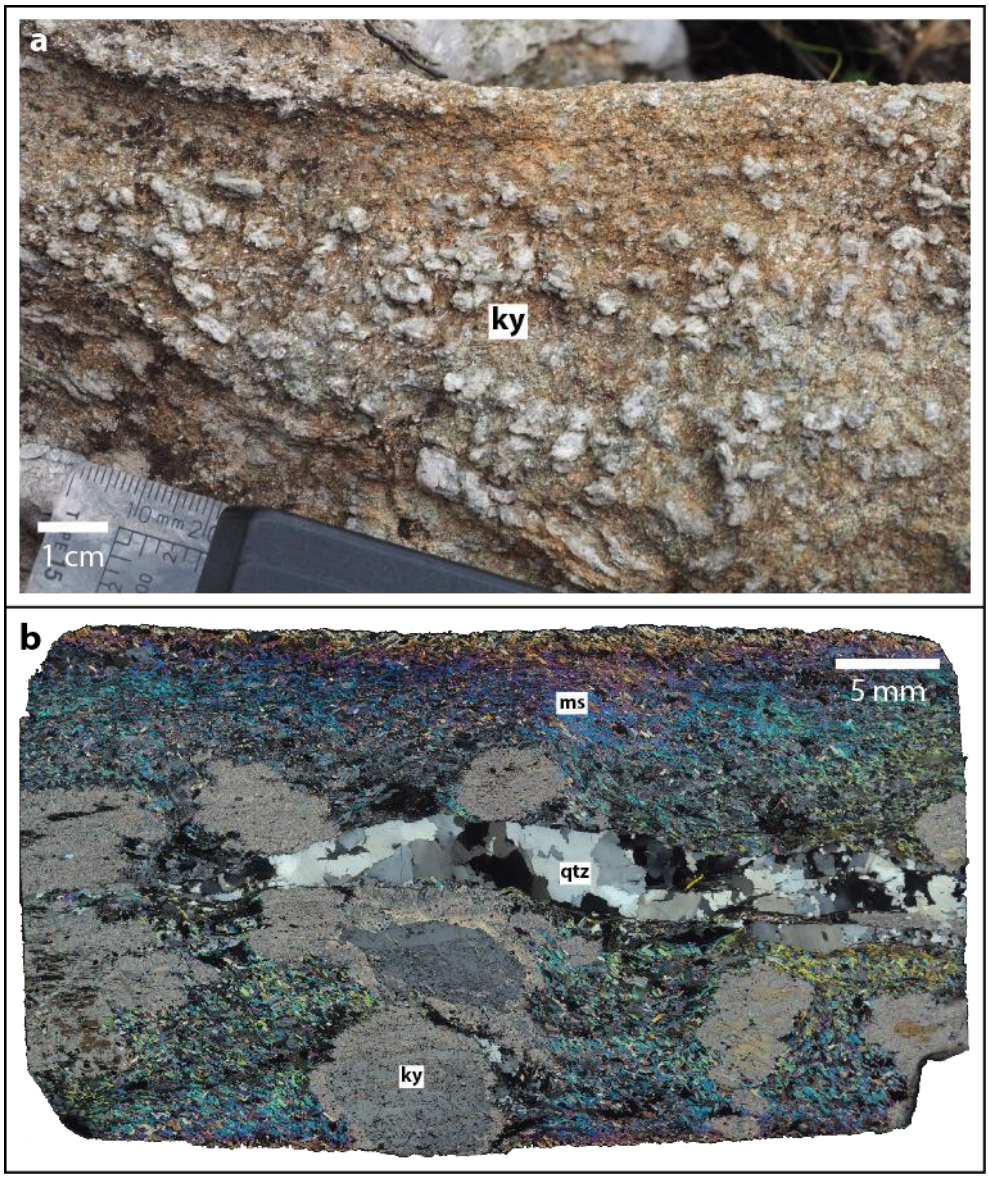

Figure 6a: Outcrop in the kyanite zone, illustrating homogeneous kyanite distribution. 6b: Scanned thin section (XPL) of a sample from the same locality. Kyanite crystals are rimmed by retrograde white mica.

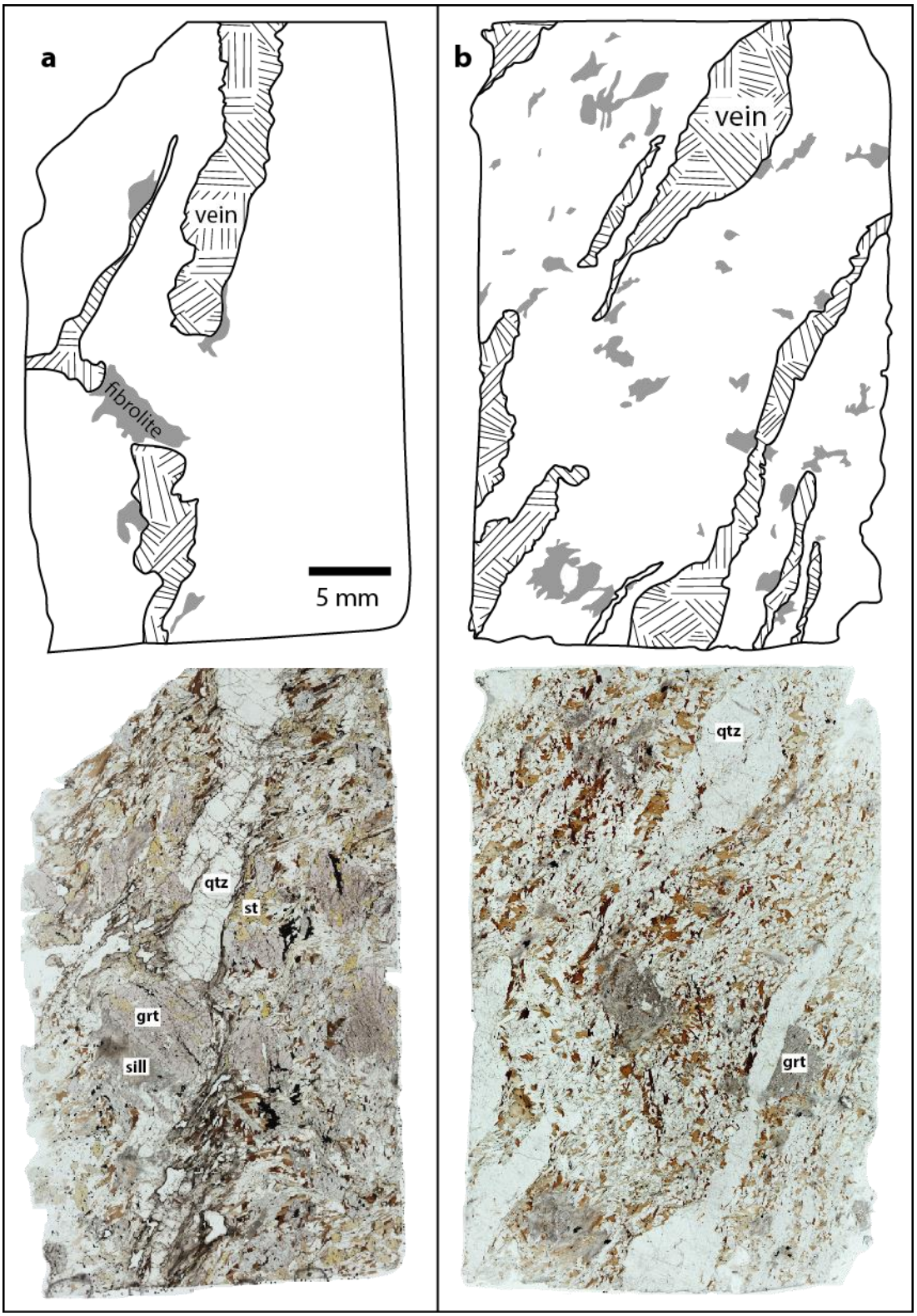

Figure 7: Two thin sections of samples from the sillimanite zone, with sketches highlighting quartz veins and fibrolite occurrences. Fibrolite is concentrated in vicinity to the veins.

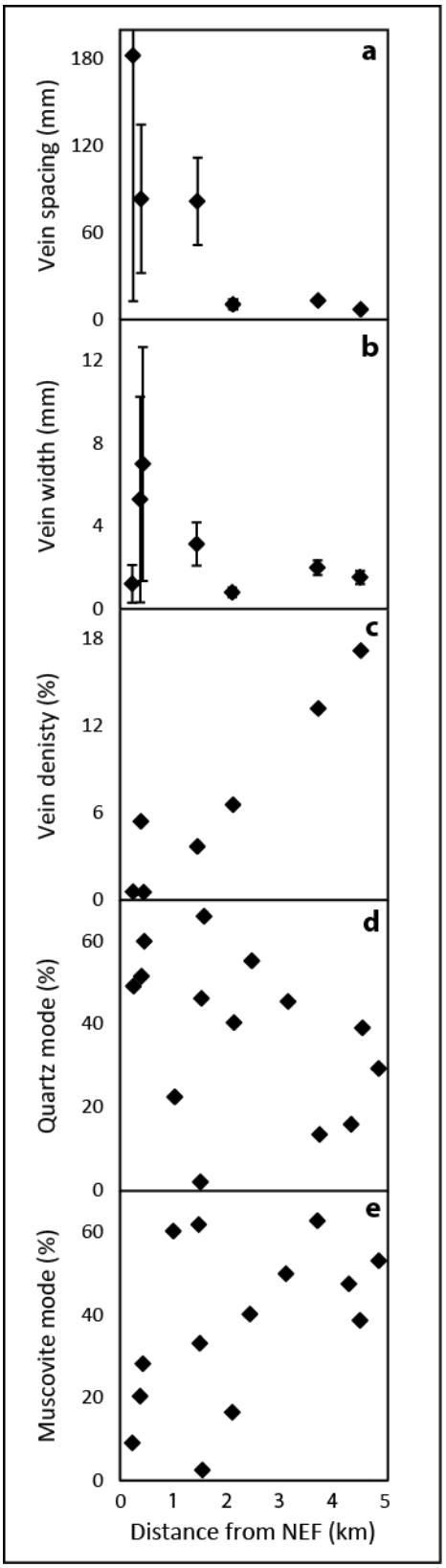

Figure 8: Regional trends. Vein spacing (a) and width (b) decrease as a function of distance from the NEF, but vein density (c) increase. As veins gradually become narrower and more tightly spaced, this implies increased number of veins in order to accommodate the increased volume of vein (vein density).Outcrop averaged values for mineral modes show a general decrease in quartz mode (d) but increase in muscovite mode (e), as a function of distance from NEF.

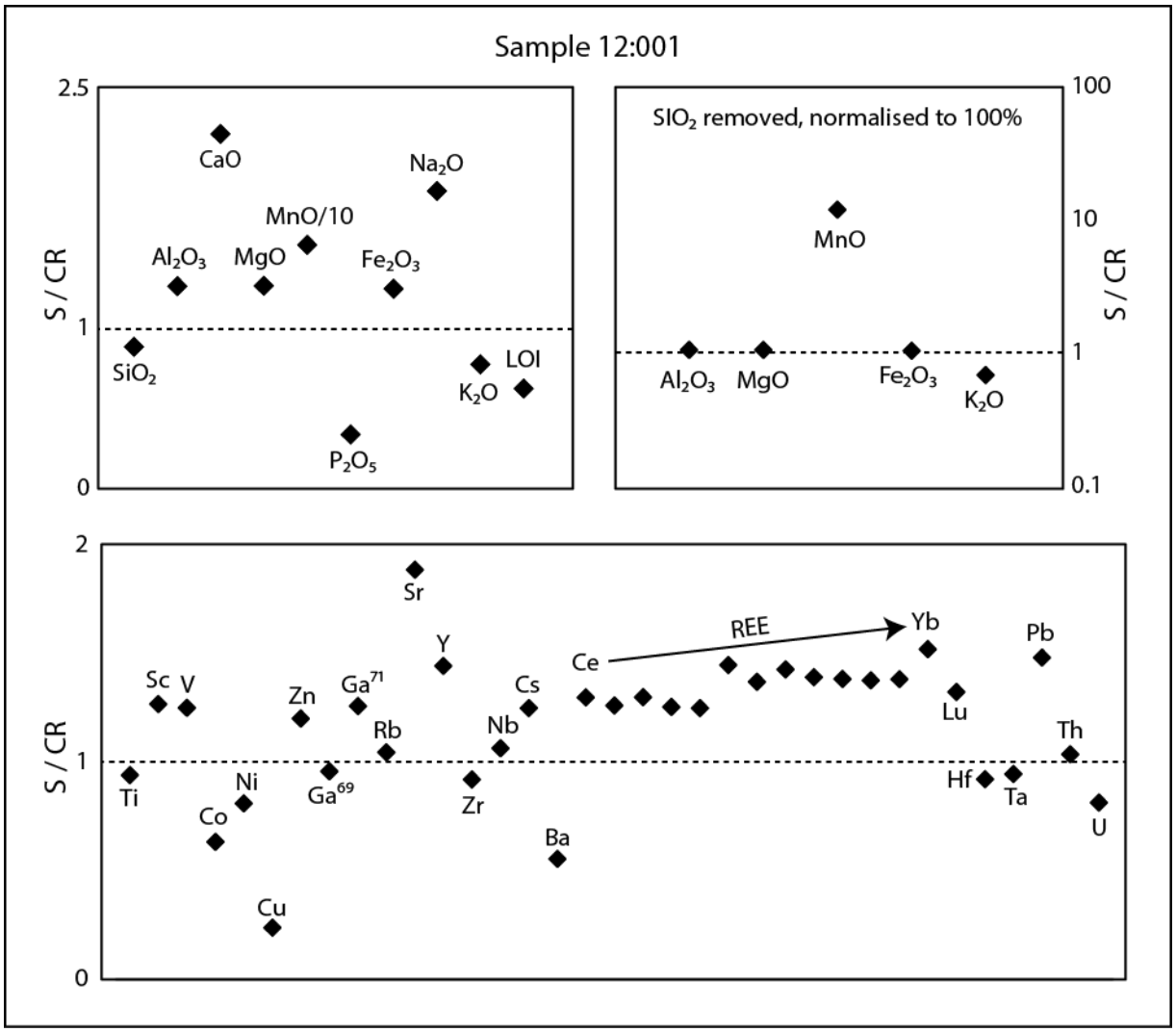

Figure 9: Top left diagram shows the major oxide concentrations for sample 12:001 (locality 09) as the ratio of the selvage divided by the unaltered country rock (e.g.. S/CR = 2 for any oxide means that the selvages contain twice the amount of that oxide). Note that SiO_2 is slightly lower in the selvage (S/CR = 0.88). The top right shows the MnKFMASH components but with SiO_2 removed and normalised to 100% (ignoring H_2O), thus assessing how much of the apparent loss that may be explained by pure silica depletion. Bottom chart is analogous to the top left, but for trace elements, showing S/CR ≈ 1 for immobile elements (e.g. Ti, Zr, and Th), and S/CR ≠ 1 for mobile elements (e.g. Sr, and the REEs).

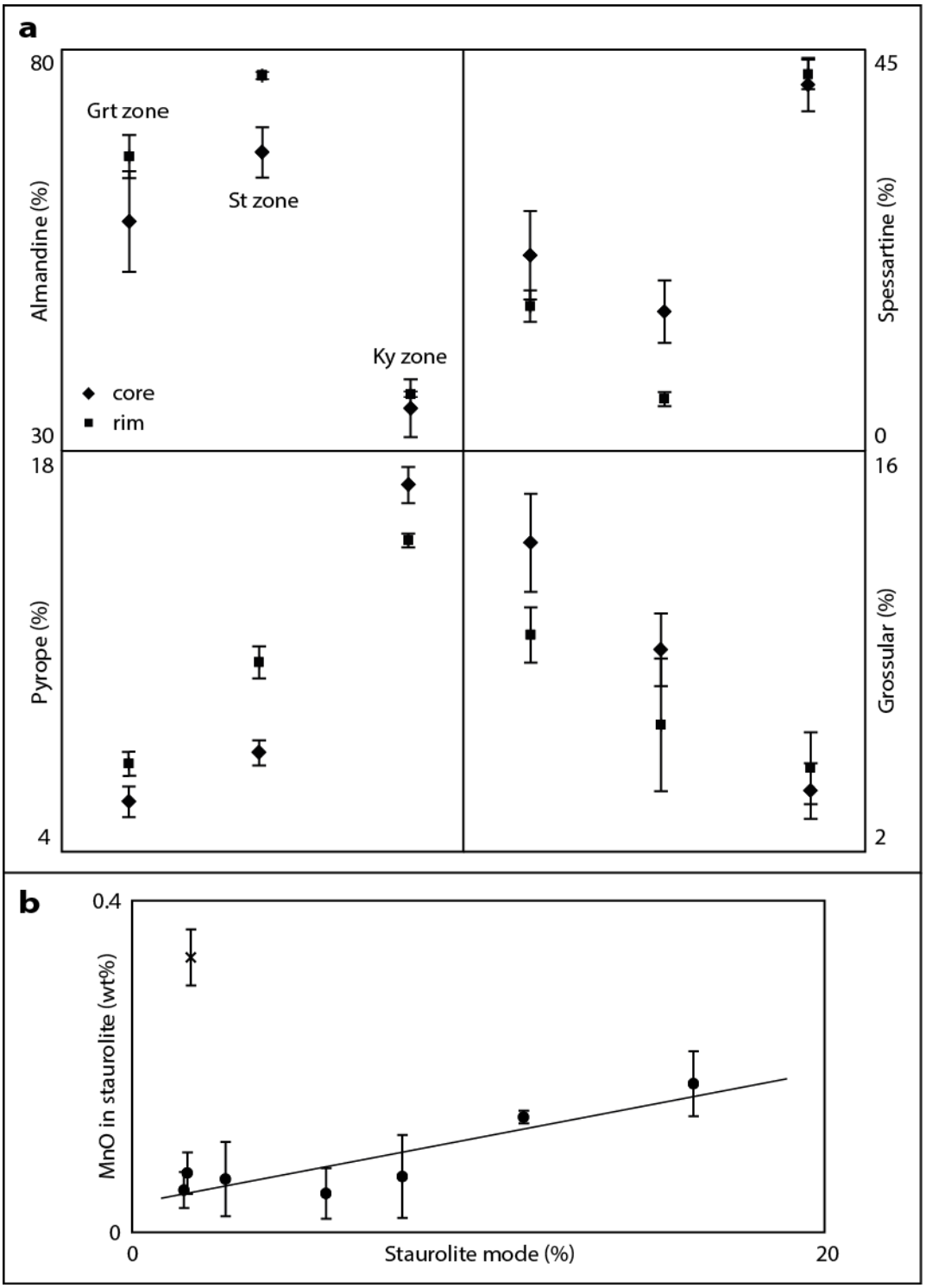

Figure 10a: Average core and rim garnet compositions, for the garnet, staurolite, and kyanite zones, respectively. Garnet compositions in the garnet and staurolite zones reflect prograde growth, such as decrease in spessartine component from core to rim. In the kyanite zone, garnets show an opposite core-rim composition relationship, indicative of retrograde growth. Because of this, the kyanite zone garnets cannot be compared with the other zones in terms of e.g. regional trends. **10b:** MnO content in staurolite (averaged for each sample?), versus modal amount of staurolite mode for individual samples.

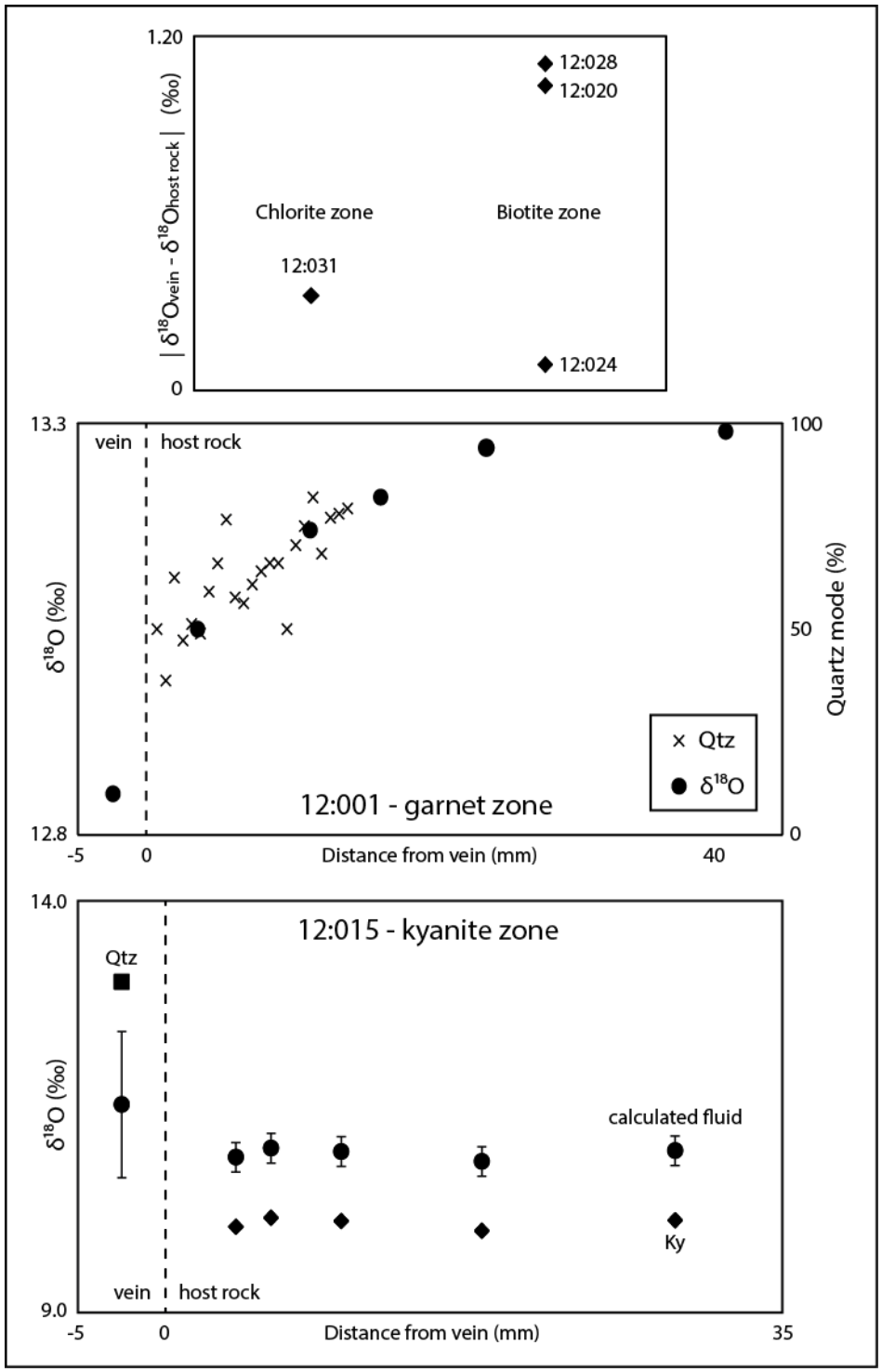

Figure 11: Oxygen isotopes. The top chart shows the absolute difference between quartz d18O in veins and vein adjacent host rock for the chlorite and biotite zones. In the middle, quartz oxygen isotope data from locality 09 in the garnet zone is presented, showing a decrease in d18O towards the vein, a trend that is coincident with a decrease in quartz mode. The bottom diagram shows an oxygen isotope profile from the kyanite zone. Quartz was analysed from the vein, while kyanite was used for the host rock. The host rock trend is flat, and if corrected for Qtz-Ky fractionation at 625°C, vein and host rock signatures are indifferent within error. Error bars represent the maximum and minimum amount of fractionation retrieved from the different calculations models that were used.

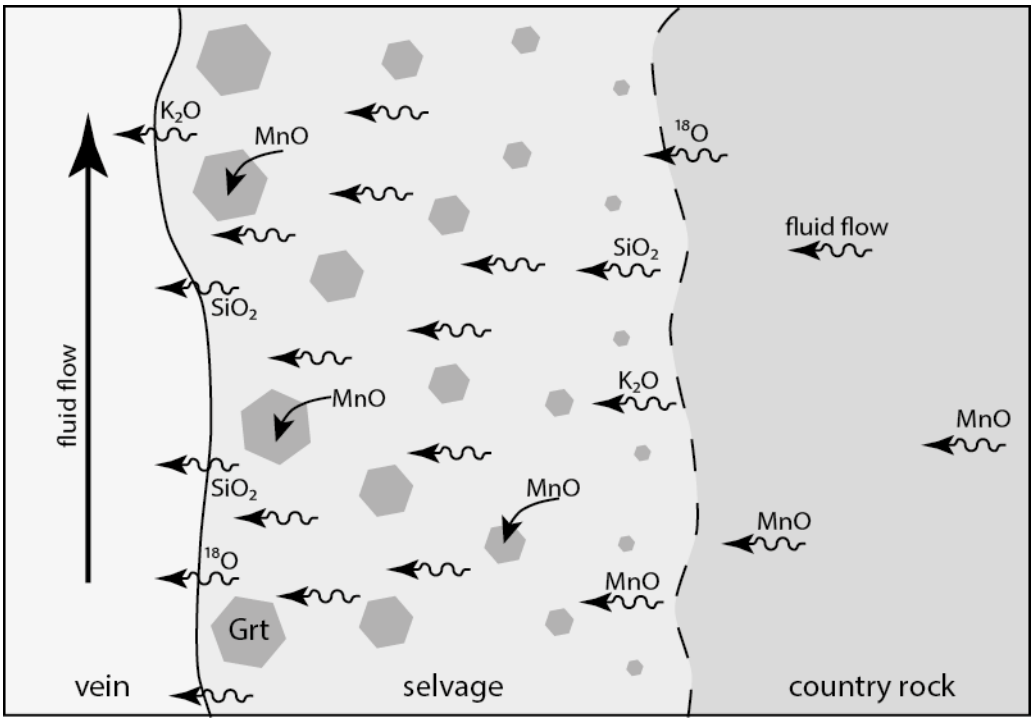

Figure 12: Conceptual model fluid control of garnet crystal size distribution in the garnet zone (e.g. locality 09). The width of the sketch represents ~10 cm. Cross-layer fluid flow in the surrounding rock is directed towards the vein, and is activated by fluid flow within the vein. SiO2, K2O, and 18O is mobilised and transported towards and into the vein, which implies that these components becomes more depleted the smaller distance to the vein the rock is situated. MnO is also mobilised, but at the vein-selvage interface MnO will stabilise garnet, which upon nucleation and further growth will act as a Mn-sink.

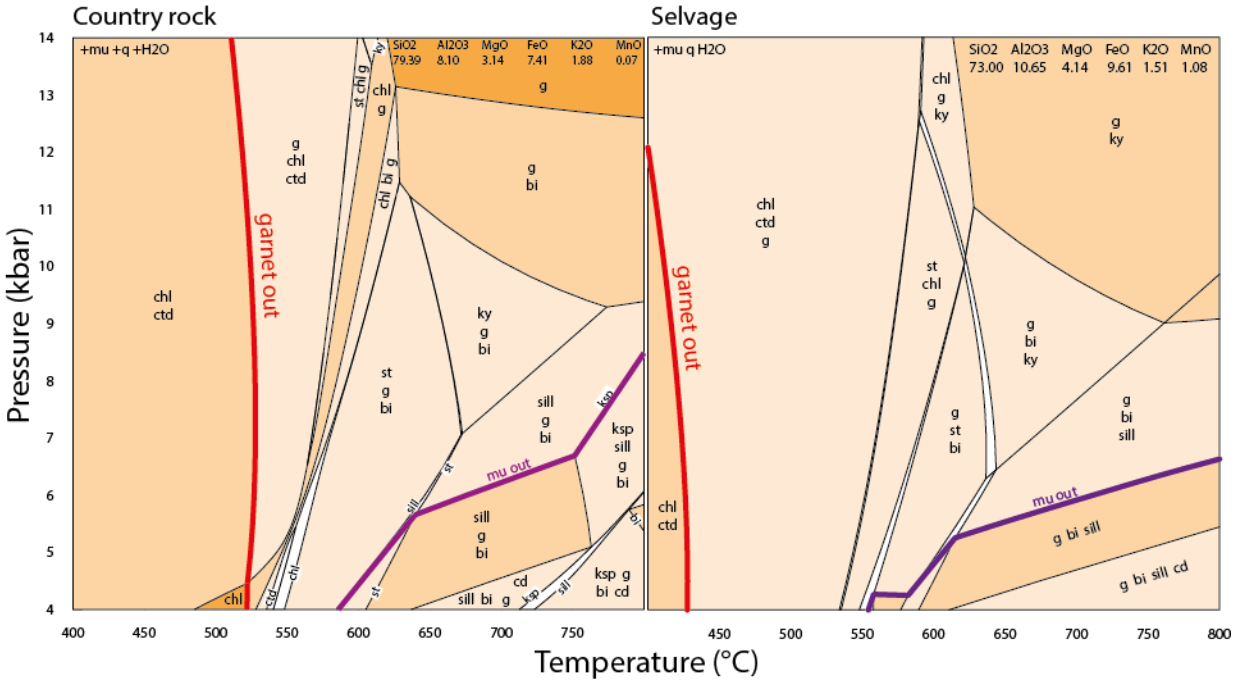

Figure 13: Peudosection comparison of the unaltered country rock and the selvage from locality 09. The garnet stability field is considerably larger in the selvage, as the garnet out line is shifted ~100°C towards lower temperatures.

Table 1. Estimates of peak metamorphic conditions in Glen Esk

Met. zone	P (kbar)	T (°C)	Reference
Garnet	4.4	540	*Viete et al. (2011)*
Staurolite	n.d.	510-630	*Dempster (1985)*
	5.7	620	*Viete et al. (2011)*
	6.5-8.5	580-660	*Vorhies & Ague (2011)*
Kyanite	5.8-6.1	610-630	*Baker (1985)*
	6.2	610-640	*Dempster (1985)*
Sillimanite	5.5-7.4	650-690	*Dempster (1985)*
	5.7-5.9	650	*Baker (1985)*
	5.9-6.1	640-670	*Viete et al. (2011)*

Table 2. List of sampled localities

Met. zone	Locality*	WGS84 (N : W)	Samples
Chlorite	01	56.84945 : 2.68015	14:015
	02	56.85018 : 2.68080	12:030-032
Biotite	03	56.85087 : 2.68340	12:028-029
	04	56.85082 : 2.68503	12:023-027
	05	56.85213 : 2.68512	14:014
Garnet	06	56.85737 : 2.68932	12:020-022
	07	56.85891 : 2.69226	13:002
	08	56.85898 : 2.69240	12:016-019 & 13:001
	09	56.85927 : 2.69260	12:001
Staurolite	10	56.86550 : 2.69368	12:002-005 & JJ-samples
	11	56.87332 : 2.70162	12:006
	12	56.86923 : 2.69245	12:036-038
Kyanite	13	56.87948 : 2.69953	12:013-015
	14	56.88812 : 2.69643	12:011-012
Sillimanite	15	56.88989 : 2.70142	13:015-018
	16	56.89120 : 2.69690	12:007-010
	17	56.89075 : 2.70227	14:003-005
	18	56.89485 : 2.72552	IP-64
	19	56.89463 : 2.89788	IP-68

*Localities 01, 03, 08 & 13 are the very same as studied by Barrow (1893; 1912).

Table 3. Thin section point counting results

			Mineral modes (%)												
Met. zone	**Sample**	**Comment**	**Qtz**	**Ms**	**Chl**	**Bi**	**Grt**	**St**	**Ky**	**Sil**	**Opq**	**Pl**	**Cal**	**Tur**	**Other**
Chl	AL-12-GE-030	country rock (cr)	43.7	5.1	23.0						1.6	1.5	25.1		
	AL-12-GE-031	cr	51.4	17.0	24.6						0.5	1.0	5.0	0.5	
		vein	71.4										28.6		
	AL-12-GE-032		52.0	5.0	35.8						1.7	2.6	2.6	0.3	
		vein	68.7										31.3		
Bt	AL-12-GE-023	cr	80.9	8.9	6.9	1.3						1.9			
	AL-12-GE-024	cr	26.1	65.4	0.5	7.4						0.5			
	AL-12-GE-025	cr	83.8	3.4	0.2	2.0					0.4	3.0			7.2
	AL-12-GE-026	cr	73.1	14.9	2.8	6.5					0.7	1.2			0.8
	AL-12-GE-027	cr	35.4	48.3	2.1	12.9					1.3				
	AL-12-GE-028	cr	72.3	9.8	2.7	8.5					0.5	3.2	3.0		0.2
		vein	99.0	0.3									0.8		
	AL-12-GE-029	cr	30.6	30.8	2.9	33.9					1.0	0.7			0.1
Grt	AL-12-GE-001	selvage	65.9	2.5	0.1	24.4	5.6				1.3			0.3	
	AL-12-GE-016	cr	71.5	17.0	5.6	3.8					1.8	0.2			0.1
	AL-12-GE-017	cr	24.0	45.6	5.3	0.6	0.1				5.3		0.7	7.1	11.3
		vein	89.5	1.8	0.3							8.5			
	AL-12-GE-018-1	cr	79.8	11.0	3.4	4.4	0.1				1.3				
	AL-12-GE-018-2	cr	41.2	47.4	1.9	8.2					1.3				
	AL-12-GE-019	cr	50.2	33.6	1.9	10.8					3.3	0.2			
	AL-12-GE-020	cr	15.3	63.1	12.8	6.4					1.5			1.0	
	AL-12-GE-021	cr	4.8	70.6	11.7						2.0		10.4	0.5	
	AL-12-GE-022	cr	47.0	47.0	2.1	3.0					0.7			0.1	
	AL-13-GE-001A	cr	29.2	41.4	11.3	10.0	0.4				1.9			1.4	4.3
	AL-13-GE-001B	cr	40.0	27.5	12.5	12.6	0.9				1.4			0.1	5.1
	AL-13-GE-001C	cr	32.8	41.7	6.7	14.6	1.6				1.5			0.2	0.8
	AL-13-GE-002	cr	2.0	61.8	21.6	12.2	0.5				1.8			0.1	
St	AL-12-GE-002	cr	8.2	54.1	4.2	27.9	2.8	0.1			2.7			0.1	
		vein	99.0	1.0											
	AL-12-GE-003A	selvage	9.7	53.5	0.8	17.0	2.2	11.3			3.4			2.1	
	AL-12-GE-003B	cr	14.2	42.7	0.6	18.1	3.3	16.2			3.2			1.7	
	AL-12-GE-003C	vein	99.6	0.3							0.1				
		selvage	48.3	42.9	0.4		5.8				2.1	0.4			

			Mineral modes (%)												
Met. zone	**Sample**	**Comment**	**Qtz**	**Ms**	**Chl**	**Bi**	**Grt**	**St**	**Ky**	**Sil**	**Opq**	**Pl**	**Cal**	**Tur**	**Other**
	AL-12-GE-004	cr	44.3	25.0	1.5	17.2	4.7	6.3			1.0				
	AL-12-GE-005	cr	22.7	52.2	1.9	9.5	5.5	2.0			4.3	0.8		1.3	
		vein	88.0	10.8	1.2										
	AL-12-GE-006A	cr (pelitic)	5.8	89.3	0.3	4.6									
		cr (psammitic)	83.7	12.4		2.5						1.4			
	AL-12-GE-006B	cr (matrix)	1.0	97.9	0.7	0.5									
		cr (clasts)	87.9	3.3		0.2						8.6			
	AL-12-GE-006C	vein	99.8	0.1								0.1			
	AL-12-GE-036	cr	90.8	7.6	0.1	0.7					0.5	0.3			
	AL-12-GE-037	cr	19.5	72.7	5.9	1.5					0.4				
	AL-12-GE-038	vein	90.2	6.7							1.6	1.3	0.1		0.1
	JJ-A1-1	cr	45.2	17.6	1.1	26.8	0.8					8.4			
	JJ-A1-2	cr	33.8	8.2	4.1	44.6	4.7				2.0	2.6			
	JJ-A1-3	cr	44.9	3.2	4.3	9.1	4.9	0.1			0.5	33.0			
	JJ-B11-1	cr	36.3	11.9	2.7	44.4	1.7	1.5			1.3	0.2			
	JJ-B11-10	cr	56.4	8.3	0.6	22.6	6.3	0.2			1.2	4.4			
	JJ-B11-10	cr	56.4	8.3	0.6	22.6	6.3	0.2			1.2	4.4			
	JJ-B11-11-12	cr	76.0	3.1	0.0	12.0	3.0				0.8	5.0			
	JJ-B11-12-13	cr	74.2	1.0	0.9	17.9	3.2				0.6	2.2			
	JJ-B11-2-3	cr	30.4	20.8	3.3	36.9	2.3	5.6			0.7				
	JJ-B11-3-4	cr	34.4	9.0	2.5	41.9	7.2	4.5				0.5			
	JJ-B11-5	cr	54.8	1.7	0.3	33.8	7.4	0.6			0.7	0.7			
	JJ-B11-8	cr	39.2	13.3	1.5	32.3	4.1	1.6			1.5	6.5			
	JJ-B11-9	cr	61.3	3.1	0.6	28.7	3.2	1.3				1.8			
	JJ-B12-4-5	cr	46.2	5.4	1.0	36.0	3.3	4.6			2.1	1.4			
	JJ-B12-6	cr	27.8	17.7	3.8	27.0	5.8	15.5			1.4	1.0			
	JJ-B21-11	cr	44.5	5.6	0.3	19.7	1.3	1.7			4.3	22.6			
	JJ-B21-12	cr	40.7	11.2	1.5	10.4	2.1	2.1			4.5	27.5			
	JJ-B21-8	cr	35.9	15.9	0.8	30.8	2.6	8.4			3.3	2.3			
	JJ-B21-9	cr	25.9	32.4	8.0	5.8	2.8	3.0			3.1	19.0			
	JJ-B31-1	cr	37.8	5.7	2.2	30.0	2.3	2.7			1.1	18.2			
	JJ-B31-2	cr	40.1	3.9	5.2	43.7	1.5				0.1	5.5			
	JJ-B31-3	cr	47.5	4.0	1.2	35.6	1.9				0.6	9.2			
	JJ-B41-0-1	cr	40.8	4.8	2.7	34.2	3.9	3.6			1.3	8.7			
	JJ-B41-1	cr	42.4	2.3	1.7	42.3	2.6	5.3			0.7	2.7			
	JJ-B41-3	cr	33.7	19.5		38.4	0.8	3.8			1.0	2.8			
	JJ-B41-5	cr	26.9	31.4	0.4	32.4	2.2	2.7			1.2	2.8			

			Mineral modes (%)												
Met. zone	**Sample**	**Comment**	**Qtz**	**Ms**	**Chl**	**Bi**	**Grt**	**St**	**Ky**	**Sil**	**Opq**	**Pl**	**Cal**	**Tur**	**Other**
	JJ-B41-6	cr	47.0	1.9	0.5	29.4	9.4	7.8			1.0	3.0			
Ky	AL-12-GE-011	cr	24.5	46.3	4.7	20.0	0.3				1.7	2.3		0.2	
		vein	99.0	0.7	0.0	0.3									
	AL-12-GE-012-1	cr	12.6	55.8	1.6	22.8					0.5	6.5			0.3
		vein	100.0	0.0											
	AL-12-GE-012-2	cr	10.4	40.5	4.5	12.6					1.5	30.6			
		vein	100.0	0.0											
	AL-12-GE-013	cr	6.8	62.9	5.5		2.0		8.8		13.5	0.1		0.3	0.1
	AL-12-GE-014	cr	19.3	58.3	10.1	1.0	0.6		2.1		6.3	1.7		0.5	
		vein	94.6	5.0	0.2		0.2								
	AL-12-GE-015	cr	14.0	67.0	7.3		0.1		5.7		5.2	0.5		0.2	
		vein	97.3	0.9	1.8										
Sil	AL-12-GE-007	cr	59.5	31.9	0.8	7.0					0.7	0.1			
	AL-12-GE-008	vein	27.9	4.6	1.9	0.2					1.5	31.6		0.8	31.5
	AL-12-GE-009	cr	15.4	64.8	10.3	0.1	0.1		0.2		1.2	6.4		0.7	0.7
	AL-12-GE-010	cr	12.7	62.5	18.5	0.4					4.2	0.7			0.9
	AL-12-GE-010		86.4	0.5		0.4						12.5			0.2
	AL-13-GE-015	cr	78.7	9.3	0.1	1.8	0.1				0.1				9.8
	AL-13-GE-016	cr	18.7	32.7	1.3	21.4	0.1				0.5	25.1			
	AL-13-GE-017	cr	50.9	37.8	0.9	5.0					0.6	4.8			
	AL-13-GE-018	cr	7.8	74.7	1.1	7.4					0.9	7.6		0.5	

Table 4. Whole rock chemical compositions (wt%)

Met. zone	Sample	SiO2	Al2O3	Fe2O3	CaO	MgO	MnO	P2O5	Na2O	K2O	TiO2	LOI
Chlorite	12-030	57.27	12.66	6.05	15.99	1.62	0.24	0.06	4.98	0.26	0.87	12.29
	12-031	52.19	24.45	9.94	1.28	2.64	0.09	0.22	1.33	6.15	1.72	5.28
	12-032	72.21	12.98	7.16	1.27	1.65	0.08	0.11	1.60	2.24	0.69	3.32
Biotite	12-021	64.29	16.81	9.48	1.11	2.69	0.11	0.04	1.39	3.02	1.06	3.96
	12-022	59.71	20.79	9.15	0.48	2.54	0.08	0.07	1.86	4.06	1.24	3.73
	12-023	30.27	21.89	35.56	0.13	11.48	0.33	0.00	0.00	0.15	0.20	9.92
	12-024	53.43	26.03	7.01	0.27	1.98	0.03	0.13	0.20	9.17	1.75	4.99
	12-025	85.45	7.18	3.23	0.16	0.57	0.03	0.00	2.09	0.91	0.38	1.17
	12-026	80.87	9.01	5.54	0.18	1.62	0.04	0.00	0.75	1.68	0.33	2.17
	12-027	58.48	21.96	7.64	1.51	2.12	0.09	0.16	2.46	4.26	1.33	3.15
	12-028	80.43	10.09	3.52	0.23	0.87	0.02	0.02	2.58	1.69	0.54	1.45
	12-029	64.85	18.47	6.41	0.32	1.95	0.03	0.07	2.79	4.08	1.03	3.14
Garnet	12-001 (cr)	72.08	12.49	7.24	1.10	1.91	0.07	0.04	1.62	2.68	0.77	2.11
	12-001 (selvage)	63.52	15.73	9.00	2.42	2.42	1.11	0.01	3.01	2.07	0.72	1.30
	12-002	44.60	28.69	12.37	1.06	4.00	0.08	0.15	1.87	5.72	1.47	5.63
	12-016	74.60	12.71	5.53	0.77	1.53	0.06	0.02	2.18	1.92	0.69	2.04
	12-017	45.73	26.74	10.26	5.72	3.19	0.20	0.08	2.19	4.18	1.71	3.82
	12-018	59.49	20.78	8.25	0.90	2.32	0.08	0.06	2.23	4.65	1.24	2.88
	12-019	60.84	20.87	7.52	0.87	2.17	0.08	0.05	1.95	4.48	1.16	2.98
	13-001	69.05	15.16	6.48	1.88	1.71	0.04	0.06	2.32	2.48	0.81	1.73
	13-001	53.26	22.53	10.60	3.04	3.06	0.15	0.07	2.63	3.44	1.21	3.29
	13-002	55.15	21.26	12.40	0.58	3.02	0.18	0.11	0.94	5.11	1.27	3.77
Staurolite	12-003A	41.63	32.62	12.67	1.01	3.90	0.32	0.13	1.29	4.72	1.70	4.32
	12-003B	44.20	30.80	12.44	1.00	3.32	0.35	0.15	1.35	4.73	1.67	4.09
	12-004	59.19	20.17	10.55	0.94	3.01	0.16	0.11	1.10	3.68	1.09	2.34
	12-005	51.33	24.55	11.44	1.24	2.54	0.24	0.08	2.41	4.55	1.61	3.33
	12-006A	60.46	21.95	6.26	0.41	1.91	0.05	0.04	1.14	6.69	1.07	3.24
	12-006B	78.94	11.88	3.03	0.37	0.90	0.02	0.10	1.18	3.07	0.50	1.82
	12-036	79.40	12.05	1.78	0.35	0.43	0.01	0.00	4.29	1.25	0.43	1.08

Met. zone	Sample	SiO2	Al2O3	Fe2O3	CaO	MgO	MnO	P2O5	Na2O	K2O	TiO2	LOI
	12-037	51.25	27.80	7.33	0.40	2.16	0.03	0.25	0.97	8.03	1.79	5.06
	12-038	74.55	14.09	3.89	0.39	0.76	0.03	0.11	2.86	2.72	0.60	2.38
	JJ-A1-1	62.08	16.86	10.25	1.07	2.90	0.08	0.08	2.36	3.53	0.79	1.93
	JJ-A1-2	62.39	17.37	9.29	1.16	2.68	0.09	0.09	2.58	3.43	0.92	1.92
	JJ-A1-3	85.86	7.97	2.00	0.78	0.30	0.01	0.00	2.51	0.52	0.06	0.86
	JJ-B11-1	59.23	20.79	8.93	0.94	2.96	0.07	0.18	1.50	4.41	1.00	2.64
	JJ-B11-10-1	55.63	23.23	7.72	2.35	2.41	0.10	0.05	5.31	2.18	1.02	2.28
	JJ-B11-10-2	63.62	17.87	7.21	2.29	2.16	0.08	0.05	4.16	1.67	0.89	1.64
	JJ-B11-11	73.82	12.32	5.55	2.53	1.44	0.13	0.04	2.66	0.99	0.51	0.51
	JJ-B11-12-13	71.43	13.35	5.97	2.94	1.61	0.16	0.04	2.80	1.13	0.55	0.64
	JJ-B11-2-3	57.71	20.74	11.36	0.79	2.94	0.15	0.07	1.15	4.03	1.07	2.07
	JJ-B11-3-4	58.61	20.33	10.70	0.89	2.77	0.18	0.14	1.17	4.16	1.06	2.01
	JJ-B11-5	58.44	19.34	10.69	1.53	2.87	0.11	0.08	2.49	3.41	1.05	1.53
	JJ-B11-8	54.45	24.77	9.56	1.29	2.10	0.28	0.07	2.19	3.84	1.45	1.94
	JJ-B11-9	71.64	13.85	6.57	1.30	1.61	0.08	0.05	2.32	2.04	0.55	1.03
	JJ-B12-3-4	67.71	16.03	5.28	2.62	1.61	0.08	0.07	4.47	1.29	0.85	0.86
	JJ-B12-4-5	58.25	18.10	11.93	1.95	2.89	0.18	0.06	3.02	2.65	0.98	9.40
	JJ-B12-6	65.41	18.08	7.20	1.11	2.13	0.06	0.06	2.19	2.84	0.92	1.97
	JJ-B21-10	59.29	20.96	6.04	3.88	2.21	0.08	0.21	4.51	1.83	0.99	2.85
	JJ-B21-11	69.81	14.39	5.12	3.33	1.82	0.04	0.31	3.34	1.26	0.60	1.85
	JJ-B21-12	62.86	18.61	6.14	3.82	1.97	0.09	0.21	4.17	1.31	0.82	2.43
	JJ-B21-8-9	49.01	26.98	8.37	3.34	2.78	0.34	0.34	3.61	3.83	1.41	3.36
	JJ-B21-9	73.50	12.91	3.94	5.62	1.01	0.29	0.20	1.07	1.00	0.46	1.69
	JJ-B31-2	60.29	21.21	7.01	1.40	2.38	0.10	0.30	2.78	3.49	1.05	3.04
	JJ-B31-3	59.75	21.10	7.04	1.67	2.45	0.15	0.28	3.83	2.72	1.03	3.00
	JJ-B41-0-1	60.71	20.21	8.95	1.50	2.69	0.17	0.07	2.00	2.64	1.07	2.38
	JJ-B41-1	60.58	20.48	8.95	1.14	2.55	0.17	0.10	1.49	3.42	1.12	2.49
	JJ-B41-2	60.64	20.78	8.58	0.95	2.74	0.07	0.11	1.27	3.83	1.05	1.40
	JJ-B41-3	59.29	20.31	10.10	1.08	2.91	0.14	0.09	1.35	3.55	1.19	2.40
	JJ-B41-5	56.60	22.60	10.58	1.08	2.55	0.21	0.06	1.30	3.57	1.45	2.24
	JJ-B41-6	61.02	17.83	9.68	2.13	2.85	0.13	0.06	3.04	2.27	1.00	2.16

Met. zone	Sample	SiO2	Al2O3	Fe2O3	CaO	MgO	MnO	P2O5	Na2O	K2O	TiO2	LOI
Kyanite	12-011	63.72	17.12	7.44	1.42	2.31	0.10	0.05	2.98	3.81	1.06	1.85
	12-012	51.77	23.76	9.68	1.10	2.83	0.10	0.00	3.89	5.47	1.38	2.89
	12-013	37.28	24.60	23.68	0.38	3.93	1.30	0.01	0.76	5.25	2.81	4.01
	12-014	63.18	17.59	9.39	1.03	2.35	0.15	0.14	1.80	3.17	1.20	2.74
	12-015	43.78	29.06	13.90	0.94	2.40	0.28	0.22	2.09	5.73	1.60	3.91
Sillimanite	12-007	72.84	13.90	5.15	0.34	1.51	0.06	0.06	2.56	2.80	0.80	1.96
	12-008	49.31	25.29	11.59	0.66	3.50	0.11	0.04	3.04	4.93	1.54	4.15
	12-009	49.90	25.80	10.19	0.57	3.08	0.11	0.14	3.59	5.30	1.32	3.92
	12-010	62.12	18.47	8.57	0.87	2.56	0.13	0.19	2.24	3.58	1.27	3.10
	13-015	82.98	8.48	2.78	3.67	0.35	0.05	0.09	0.12	1.15	0.35	1.03
	13-016-1	62.98	17.21	7.77	1.96	2.33	0.12	0.01	3.50	3.07	1.05	2.56
	13-016-2	68.42	14.54	6.98	1.18	1.82	0.10	0.01	3.05	2.77	1.12	1.74
	13-017	77.31	11.30	4.78	0.49	1.04	0.06	0.08	2.16	2.04	0.75	1.96
	13-018	48.57	28.29	8.15	0.50	3.19	0.10	0.06	2.18	7.55	1.42	5.22

Table 5. Electron microprobe analysis data

Mineral	Met. zone	Sample	Comment	Na2O	Al2O3	SiO2	MgO	CaO	MnO	K2O	TiO2	Cr2O3	FeO	Total
Muscovite	Chlorite	12-030		0.43	28.35	49.23	2.22	0.02	0.05	10.27	0.13	0.00	3.73	94.44
				0.57	31.01	47.02	1.57	0.00	0.02	9.96	0.15	0.00	3.96	94.26
				0.46	31.49	47.02	1.25	0.06	0.00	10.55	0.29	0.09	3.59	94.80
	Biotite	12-027		0.55	32.92	48.42	1.26	0.06	0.04	10.26	0.19	0.02	2.20	95.93
	Garnet	12-001		0.74	36.05	46.69	0.79	0.06	0.08	8.87	0.73	0.03	1.53	95.56
		13-001A		0.30	27.52	49.64	1.98	0.21	0.00	6.00	0.12	0.01	7.43	93.21
		13-001B		0.33	29.61	44.59	1.75	0.04	0.07	9.46	1.19	0.08	4.95	92.07
				0.17	28.73	47.32	2.02	0.02	0.01	10.71	1.18	0.05	4.28	94.47
	Staurolite	12-003A		1.45	35.85	45.26	0.59	0.01	0.02	8.82	0.32	0.09	1.55	93.96
				1.52	35.47	45.88	0.68	0.00	0.03	8.72	0.14	0.02	1.18	93.64
				1.35	34.23	46.26	0.80	0.03	0.03	8.65	0.26	0.02	1.39	93.01
				1.68	34.78	45.51	0.65	0.00	0.00	8.42	0.24	0.02	1.19	92.49
		12-003B		1.73	35.35	45.78	0.72	0.00	0.02	8.60	0.29	0.08	1.27	93.84
				1.60	35.97	46.75	0.81	0.01	0.00	8.94	0.25	0.00	1.20	95.54
				1.49	36.47	45.60	0.72	0.16	0.00	8.30	0.30	0.04	2.15	95.23
				1.68	36.25	46.64	0.61	0.00	0.09	8.86	0.27	0.05	1.36	95.81
		JJ-A11		0.64	32.71	45.95	1.30	0.00	0.00	10.09	0.30	0.02	1.72	92.72
				1.76	36.46	45.70	0.44	0.05	0.01	8.60	0.32	0.00	0.83	94.16
		JJ-A12		1.19	35.74	46.29	0.59	0.00	0.00	9.58	0.32	0.01	1.11	94.82
				1.59	36.40	46.53	0.51	0.03	0.02	8.79	0.35	0.00	1.02	95.23
				1.64	36.10	46.58	0.56	0.03	0.03	8.76	0.41	0.00	0.97	95.06
		JJ-B11-1		1.58	35.78	46.15	0.68	0.03	0.04	8.71	0.27	0.01	1.14	94.39
		JJ-B11-2-3		1.30	34.68	45.42	0.63	0.03	0.00	9.04	0.33	0.04	0.92	92.38
				1.10	33.03	47.47	1.25	0.04	0.00	9.45	0.29	0.03	1.27	93.93
		JJ-B12-3-4		1.99	35.48	45.62	0.50	0.00	0.03	8.35	0.22	0.01	1.04	93.24
		JJ-B21-11		1.29	35.20	45.87	0.70	0.08	0.02	9.33	0.28	0.06	1.09	93.91
		JJ-B4-13		1.24	35.18	46.09	0.74	0.02	0.01	9.13	0.26	0.04	1.28	94.00
				1.83	35.19	45.60	0.68	0.05	0.07	8.61	0.23	0.02	1.49	93.77
		JJ-B4-14		1.46	34.69	45.76	0.74	0.00	0.02	8.93	0.29	0.05	1.23	93.15
		JJ-B-4-15		1.43	33.90	46.49	1.00	0.02	0.03	8.76	0.35	0.00	1.74	93.71
				0.26	36.43	44.77	0.58	0.58	0.00	9.67	0.45	0.01	1.78	94.51
		JJ-B4-16		0.15	29.33	48.71	2.59	0.04	0.02	10.52	0.23	0.00	3.77	95.35
				1.77	35.77	45.28	0.49	0.00	0.00	8.33	0.30	0.05	1.47	93.47
	Kyanite	12-015		1.33	34.80	46.26	0.59	0.00	0.00	9.49	0.19	0.06	2.37	95.10
				1.36	33.98	46.15	0.87	0.03	0.00	9.14	0.26	0.00	3.12	94.90
				1.44	34.33	45.72	0.85	0.00	0.02	9.20	0.34	0.00	2.96	94.87
				1.31	34.29	45.94	0.87	0.02	0.00	9.15	0.28	0.03	3.29	95.18
				1.44	34.09	45.46	0.84	0.03	0.02	9.23	0.24	0.02	3.23	94.61
	Sillimanite	13-018		0.27	29.41	46.56	1.97	0.04	0.00	10.64	0.27	0.03	4.08	93.25
				0.26	30.16	46.92	1.92	0.00	0.03	10.71	0.09	0.00	4.08	94.16
				0.33	34.30	44.96	0.73	0.03	0.17	10.43	0.44	0.07	2.38	93.84
				0.31	29.56	46.02	2.04	0.02	0.05	10.58	0.18	0.01	4.63	93.41
Chlorite	Chlorite	12-030		0.01	22.62	23.98	11.62	0.00	0.23	0.03	0.10	0.03	30.12	88.74
				0.03	21.78	23.72	11.02	0.08	0.32	0.01	0.03	0.01	30.32	87.33
				0.03	22.36	24.24	11.70	0.06	0.30	0.04	0.07	0.07	30.13	89.01
	Biotie	12-027		0.00	21.77	24.71	11.02	0.06	0.46	0.00	0.11	0.02	31.62	89.77
				0.06	20.79	25.50	11.29	0.08	0.30	0.04	0.09	0.00	30.63	88.77
	Garnet	12-001-CR		0.01	22.19	24.52	10.75	0.10	0.24	0.00	0.02	0.05	30.79	88.68
				0.06	22.59	24.28	12.02	0.07	0.36	0.01	0.07	0.04	29.66	89.15
				0.00	22.13	25.39	14.50	0.04	0.41	0.03	0.06	0.02	25.86	88.45
		12-001-S		0.02	22.69	24.78	14.42	0.05	0.41	0.04	0.11	0.05	26.23	88.79
		13-001A (in garnet)		0.03	20.69	25.85	11.45	0.11	0.46	0.11	0.06	0.00	28.41	87.16
		13-001B		0.03	19.81	26.11	12.99	0.09	0.09	0.01	0.08	0.07	27.86	87.13
				0.02	23.02	23.71	11.37	0.06	0.20	0.03	0.08	0.08	28.70	87.27
	Staurolite	12-003A		0.04	23.55	25.00	16.92	0.02	0.10	0.00	0.11	0.06	21.08	86.88
		12-003B		0.00	23.32	24.86	16.32	0.04	0.05	0.03	0.10	0.00	22.35	87.07
		JJ-A11		0.05	23.19	25.17	14.39	0.02	0.04	0.02	0.10	0.01	25.53	88.52
		JJ-A12		0.04	20.48	25.27	12.20	0.02	0.10	0.08	0.08	0.05	26.03	84.36
		JJ-B11-2-3		0.04	21.59	25.01	12.77	0.01	0.07	0.10	0.02	0.00	28.14	87.75
		JJ-B11-2-3		0.00	21.97	24.98	12.46	0.02	0.03	0.04	0.04	0.00	27.53	87.06
		JJ-B11-8		0.02	23.45	25.46	14.10	0.03	0.00	0.03	0.11	0.00	24.88	88.07
		JJ-B11-10		0.00	23.13	25.29	14.63	0.00	0.11	0.00	0.08	0.05	24.20	87.48
		JJ-B21-10		0.13	20.37	27.81	16.34	0.08	0.34	0.24	0.22	0.03	21.99	87.54
		JJ-B21-10		0.01	19.51	30.54	15.69	0.07	0.10	1.16	0.44	0.05	19.72	87.28
		JJ-B21-10		0.01	20.22	27.04	17.35	0.01	0.12	0.09	0.10	0.09	21.52	86.56
		JJ-B21-11		0.04	23.81	25.09	16.47	0.05	0.21	0.03	0.06	0.09	21.25	87.09
		JJ-B21-11		0.04	20.06	28.63	16.59	0.04	0.17	1.24	0.23	0.08	21.14	88.22
		JJ-B41-6		2.41	31.07	36.25	4.99	0.08	0.03	0.02	0.34	0.01	10.55	85.75
	Kyanite	12-015		0.02	22.35	25.54	16.51	0.05	0.85	0.02	0.07	0.05	22.23	87.70
	Sillimanite	12-008		2.24	30.10	37.29	6.25	0.64	0.05	0.03	0.52	0.03	10.16	87.37
		13-018		1.88	32.96	35.75	6.48	0.84	0.04	0.03	0.69	0.00	7.13	85.79
				0.01	20.74	25.44	15.31	0.06	0.26	0.03	0.06	0.00	24.46	86.37
Biotite	Biotite	12-027		0.05	19.56	34.10	7.76	0.05	0.16	7.87	1.64	0.05	23.75	94.99
				0.04	19.34	34.75	7.28	0.02	0.21	8.53	1.62	0.03	24.23	96.04
				0.10	19.19	35.00	7.62	0.03	0.13	8.62	1.47	0.00	23.77	95.93

Mineral	Met. zone	Sample	Comment	Na2O	Al2O3	SiO2	MgO	CaO	MnO	K2O	TiO2	Cr2O3	FeO	Total
	Garnet	12-001-CR		0.04	19.21	34.95	8.80	0.05	0.26	9.28	1.62	0.02	20.50	94.72
				0.00	19.42	35.35	9.23	0.05	0.26	9.06	1.85	0.06	20.80	96.08
				0.12	19.09	35.44	9.53	0.01	0.20	9.16	2.03	0.03	20.12	95.74
				0.08	18.97	35.75	9.30	0.02	0.15	8.98	1.70	0.04	19.85	94.85
				0.12	19.11	36.01	9.16	0.04	0.25	9.14	1.79	0.04	20.11	95.77
		12-001-S		0.15	18.50	37.13	9.39	0.09	0.32	8.60	1.52	0.00	21.51	97.21
				0.11	18.19	35.49	9.51	0.00	0.19	8.99	1.56	0.05	20.86	94.95
				0.07	19.07	34.90	9.23	0.05	0.21	8.72	1.77	0.00	20.52	94.54
				0.16	18.97	35.76	9.10	0.07	0.14	9.07	1.81	0.04	20.32	95.44
				0.15	19.18	35.54	9.28	0.05	0.25	9.21	1.58	0.05	20.39	95.67
		13-001A		0.09	18.95	33.37	8.79	0.10	0.11	7.27	1.35	0.04	22.07	92.15
				0.27	18.66	35.34	8.96	0.15	0.04	7.97	1.41	0.03	20.77	93.64
				0.18	18.56	34.48	8.50	0.02	0.03	8.95	1.56	0.00	21.38	93.66
		13-001B		0.19	18.28	34.55	7.95	0.01	0.08	9.22	1.62	0.00	22.26	94.22
				0.07	18.33	34.81	7.91	0.02	0.12	9.24	1.84	0.08	21.88	94.38
	Staurolite	12-003A		0.07	18.56	34.35	11.15	0.06	0.16	7.66	1.62	0.09	19.52	93.24
				0.24	19.00	35.25	11.46	0.01	0.05	8.78	1.48	0.07	16.27	92.60
		12-003B		0.36	19.17	36.54	11.27	0.00	0.01	8.41	1.57	0.04	17.76	95.13
				0.43	19.39	35.86	11.15	0.07	0.03	8.69	1.56	0.06	17.84	95.07
				0.06	19.13	36.13	11.06	0.00	0.02	9.14	1.53	0.03	19.20	96.30
				0.20	19.61	36.51	11.14	0.01	0.00	9.14	1.45	0.01	17.93	96.00
		JJ-A11		0.20	19.49	35.68	9.54	0.00	0.04	9.20	1.62	0.03	19.36	95.21
				0.08	20.11	36.09	8.84	0.00	0.07	9.19	0.32	0.00	19.67	94.44
		JJ-A12		0.20	19.31	35.77	8.99	0.03	0.05	9.06	1.39	0.02	19.78	94.60
				0.15	19.15	36.50	8.81	0.07	0.07	8.96	1.00	0.03	19.35	94.19
		JJ-B11-1		0.42	19.24	35.25	9.68	0.04	0.01	8.78	1.57	0.03	19.65	94.77
				0.26	19.19	35.43	9.63	0.06	0.06	8.86	1.54	0.00	19.36	94.45
				0.11	18.71	33.39	9.30	0.06	0.00	7.59	1.29	0.01	21.39	91.84
		JJ-B11-10		0.04	18.78	34.13	9.31	0.01	0.11	8.36	1.36	0.18	21.73	93.99
				0.08	19.49	35.78	8.36	0.00	0.08	9.56	1.60	0.14	20.51	95.58
		JJ-B11-23		0.14	19.20	35.35	8.66	0.01	0.00	9.13	1.57	0.04	19.89	93.98
		JJ-B1-18		0.13	19.19	34.90	9.00	0.02	0.04	8.52	1.43	0.12	20.15	93.53
				0.25	20.99	34.64	9.27	0.20	0.00	5.28	1.45	0.02	17.47	89.59
		JJ-B12-3-4		0.16	19.34	35.26	8.79	0.00	0.04	9.20	1.64	0.02	20.21	94.72
				0.13	19.23	34.12	8.73	0.02	0.00	8.35	1.43	0.05	21.89	93.97
				0.10	19.43	31.91	9.11	0.06	0.07	4.57	1.00	0.02	25.20	91.47
				0.10	20.17	35.00	7.73	0.00	0.00	8.81	1.65	0.04	20.61	94.12
		JJ-B21-10		0.15	18.69	35.41	11.72	0.05	0.04	7.90	1.42	0.01	17.18	92.68
		JJ-B21-11		0.08	19.87	32.48	12.57	0.15	0.22	5.41	1.08	0.09	19.33	91.29
		JJ-B21-8		0.25	19.19	36.04	11.91	0.07	0.07	9.04	1.47	0.04	16.35	94.50
				0.19	18.53	36.30	10.87	0.21	0.16	7.53	1.40	0.00	18.01	93.27
		JJ-B41-3		0.02	18.89	32.94	10.92	0.01	0.00	6.00	1.35	0.03	23.16	93.31
				0.02	19.35	30.50	10.39	0.01	0.11	5.04	1.28	0.06	24.34	91.10
		JJ-B41-4		0.24	19.28	34.89	10.39	0.04	0.03	9.24	1.45	0.03	17.97	93.63
				0.21	20.38	35.21	9.68	0.00	0.02	9.12	1.69	0.04	18.26	94.62
		JJ-B41-5		0.21	20.24	36.26	10.17	0.02	0.07	9.29	1.66	0.12	17.37	95.44
		JJ-B41-6		0.08	18.70	32.65	8.13	0.04	0.09	7.10	1.47	0.07	23.92	92.23
				0.21	18.80	34.98	8.45	0.00	0.12	9.01	1.44	0.00	21.25	94.30
	Sillimanite	13-018		0.16	16.34	35.73	8.97	0.02	0.14	8.93	2.41	0.00	20.42	93.14
Garnet	Garnet	12-001-S	core	0.10	20.99	37.01	1.30	5.49	13.77	0.00	0.36	0.02	22.65	101.69
			rim	0.00	20.96	37.71	1.90	3.46	8.51	0.01	0.09	0.00	29.11	101.75
			core	0.00	21.13	36.41	1.33	5.80	11.93	0.00	0.13	0.00	24.17	100.90
			rim	0.01	21.48	36.98	1.97	3.37	8.53	0.01	0.05	0.03	28.89	101.32
			core	0.00	21.14	37.74	1.71	3.16	9.45	0.02	0.19	0.00	28.37	101.78
			rim	0.00	20.91	37.60	1.77	2.68	9.53	0.00	0.02	0.00	28.72	101.23
		13-001A	core	0.02	21.28	37.51	1.56	4.78	6.84	0.01	0.08	0.03	29.01	101.13
			rim	0.03	21.35	37.57	1.65	3.88	6.26	0.03	0.07	0.01	30.04	100.88
		13-001B	core	0.03	21.15	37.77	1.26	5.04	8.29	0.01	0.12	0.06	27.04	100.76
			rim	0.02	21.23	37.61	1.67	3.85	5.61	0.00	0.02	0.03	30.54	100.57
			core	0.00	21.16	37.41	1.45	4.09	7.79	0.01	0.15	0.00	28.80	100.85
			rim	0.00	21.49	37.59	1.67	3.69	4.71	0.01	0.03	0.01	32.12	101.31
	Staurolite	12-003B	core	0.11	21.14	37.48	1.59	3.57	10.36	0.01	0.15	0.02	27.72	102.15
			rim	0.00	21.51	37.24	3.11	2.99	3.06	0.00	0.09	0.00	33.65	101.65
			core	0.10	21.03	37.31	1.68	4.30	9.39	0.01	0.15	0.01	28.00	101.98
			rim	0.04	21.29	37.55	2.53	3.53	3.85	0.00	0.08	0.00	33.13	102.00
			core	0.09	21.30	37.28	1.72	3.40	9.81	0.01	0.08	0.07	28.61	102.37
			rim	0.00	21.56	37.36	3.04	2.68	3.48	0.02	0.05	0.06	33.68	101.93
			core	0.08	21.28	37.54	1.59	3.72	10.70	0.01	0.12	0.00	27.51	102.55
			rim	0.04	21.13	37.43	2.22	3.36	5.92	0.00	0.09	0.03	32.02	102.25
			core	0.01	21.01	37.32	1.63	4.30	11.21	0.01	0.08	0.02	26.12	101.72
			rim	0.00	21.16	37.31	2.69	2.99	3.70	0.01	0.07	0.00	33.34	101.27
		JJ-A11	core	0.00	20.56	37.40	1.87	2.42	6.17	0.00	0.08	0.01	31.67	100.18
			rim	0.02	20.65	37.90	2.41	1.76	2.02	0.07	0.08	0.01	35.24	100.25
		JJ-A12	core	0.00	20.14	37.66	1.51	2.80	7.75	0.00	0.09	0.00	29.44	99.39
			rim	0.07	20.51	38.39	2.59	1.96	1.75	0.03	0.07	0.05	35.09	100.53
		JJ-B11-1	core	0.01	20.52	37.90	2.48	2.27	1.54	0.00	0.07	0.01	35.20	100.11
			rim	0.07	20.59	37.64	2.47	1.66	0.57	0.04	0.08	0.03	36.93	100.19
		JJ-B11-2-3	core	0.07	20.72	37.51	1.31	2.87	7.08	0.00	0.10	0.00	31.13	101.12
			rim	0.02	20.72	37.75	2.82	1.80	0.35	0.02	0.01	0.04	37.07	100.81
		JJ-B11-8	core	0.04	19.70	37.33	1.10	4.39	7.90	0.00	0.20	0.00	27.25	97.94
			rim	0.00	20.51	37.83	2.57	1.64	1.07	0.02	0.02	0.03	35.96	99.93
			core	0.01	20.26	37.91	2.42	2.31	2.49	0.00	0.05	0.00	33.95	99.43
			rim	0.00	20.19	37.80	2.25	1.63	1.36	0.02	0.05	0.03	35.98	99.41
			core	0.03	20.42	38.31	1.74	2.50	5.67	0.00	0.02	0.00	32.40	101.16
			rim	0.04	20.62	37.97	2.61	1.57	1.10	0.01	0.00	0.00	35.73	99.84

Mineral	Met. zone	Sample	Comment	Na2O	Al2O3	SiO2	MgO	CaO	MnO	K2O	TiO2	Cr2O3	FeO	Total
			core	0.05	20.12	36.98	2.58	1.92	1.43	0.02	0.06	0.02	35.09	98.43
			rim	0.02	20.65	38.15	2.62	1.51	1.07	0.00	0.02	0.03	35.82	100.00
		JJ-B11-10	core	0.03	21.43	37.86	2.13	3.48	3.56	0.00	0.09	0.03	32.63	101.25
			rim	0.06	21.36	38.16	2.27	1.69	1.40	0.05	0.04	0.03	35.69	100.74
		JJ-B12-3-4	core	0.04	20.42	37.98	1.30	2.89	7.21	0.02	0.06	0.00	30.80	100.81
			rim	0.00	20.52	37.24	2.00	2.39	1.23	0.00	0.06	0.06	36.52	100.11
			core	0.04	20.63	37.73	2.72	1.61	0.31	0.04	0.05	0.04	36.83	100.01
			rim	0.03	20.33	37.76	2.51	1.52	0.39	0.05	0.04	0.05	37.22	100.05
		JJ-B21-10	core	0.03	20.28	38.07	1.93	6.09	11.50	0.00	0.17	0.03	22.12	100.26
			rim	0.05	20.65	38.08	2.47	6.47	6.86	0.00	0.11	0.04	25.78	100.51
		JJ-B21-8	core	0.00	21.04	38.45	2.19	3.52	10.15	0.01	0.06	0.02	26.01	101.45
			rim	0.01	20.98	37.89	2.82	2.30	5.50	0.04	0.00	0.00	30.28	99.95
		JJ-B21-11	core	0.05	20.55	37.98	2.26	4.15	9.09	0.00	0.09	0.07	26.60	100.94
			rim	0.10	21.09	38.13	2.93	2.53	6.07	0.03	0.01	0.07	30.36	101.43
		JJ-B41-3	core	0.00	20.68	38.14	2.20	2.60	2.63	0.00	0.07	0.09	33.72	100.17
			rim	0.00	20.30	37.96	2.37	1.89	1.03	0.03	0.02	0.07	35.86	99.68
		JJ-B41-4	core	0.04	20.42	37.46	1.64	3.41	5.41	0.01	0.11	0.00	31.77	100.31
			rim	0.00	20.88	37.54	2.70	1.83	0.88	0.01	0.02	0.01	35.83	100.00
		JJ-B41-5	core	0.03	20.44	37.99	1.73	3.33	4.80	0.01	0.06	0.03	32.67	101.10
			rim	0.03	20.73	37.68	2.44	1.91	0.90	0.04	0.04	0.05	36.30	100.44
		JJ-B41-6	core	0.00	20.44	38.13	1.55	3.59	6.91	0.00	0.08	0.02	29.42	100.15
			rim	0.01	20.81	37.97	2.86	2.14	0.80	0.04	0.03	0.04	35.93	100.67
	Kyanite	12-015	core	0.00	21.43	37.63	4.18	2.76	18.10	0.01	0.06	0.02	17.35	101.55
			rim	0.00	21.54	37.59	3.79	2.24	18.52	0.07	0.04	0.07	17.43	101.28
			core	0.10	21.10	37.58	4.39	1.69	18.70	0.04	0.00	0.02	17.92	101.54
			rim	0.01	21.54	37.42	3.71	1.60	19.19	0.09	0.03	0.00	17.35	100.94
Staurolite	Staurolite	12-003A		0.0245	53.86	28.42	1.78	0	0.1396	0.0147	0.6255	0.0366	11.67	96.571
				0.0111	53.26	27.98	1.97	0	0.1278	0.0013	0.4302	0	11.97	95.7505
		12-003B-st		0.0068	55.49	27.69	1.78	0.049	0.2162	0.0094	0.7047	0.0271	12.81	98.7833
				0	55.26	28.05	1.76	0.0154	0.1915	0	0.663	0.0181	12.43	98.3881
				0	55.15	27.93	1.5129	0.0148	0.136	0.0038	0.8428	0.0497	12.8	98.4401
				0.0218	55.58	28.67	1.4364	0.0403	0.2253	0.0155	0.503	0.0227	11.68	98.1951
				0.0246	56.33	28.11	1.3513	0	0.1148	0.0003	0.5009	0.0317	12.53	98.9937
		JJ-B11-1		0.012	54.997	28.546	0.839	0.002	0.065	0	0.589	0.011	12.426	97.4871
				0.018	54.937	28.277	0.803	0.007	0.034	0.022	0.472	0.016	11.694	96.2801
		JJB11-2-3		0	56.102	28.082	0.821	0.024	0	0.001	0.37	0.036	12.117	97.5531
				0	55.122	28.383	0.607	0	0.085	0.018	0.42	0.02	12.171	96.826
				0	55.172	28.074	0.746	0.031	0.049	0.018	0.69	0.057	12.281	97.1181
				0.009	56.135	27.907	0.678	0	0.048	0.004	0.462	0.005	12.251	97.499
		JJ-B11-8		0	55.204	27.898	0.983	0.007	0.099	0	0.389	0.039	12.018	96.6371
				0	54.824	27.642	0.938	0.047	0.063	0	0.389	0.011	12.004	95.9181
				0.031	54.736	27.824	1.116	0.005	0.045	0.021	0.474	0	11.859	96.1111
				0.008	55.013	28.303	1	0	0.018	0	0.48	0.079	11.7	96.6011
				0.019	54.246	28.211	1.572	0	0.088	0.012	0.737	0.027	12.159	97.071
				0.024	54.605	28.459	0.969	0	0.101	0.011	0.548	0.069	11.745	96.5311
		JJ-B12-3-4		0.013	54.983	27.931	0.774	0	0.104	0.01	0.451	0.023	11.859	96.1481
				0.024	54.343	27.894	1.176	0.013	0.004	0.014	0.581	0.046	12.542	96.6371
		JJ-B21-11		0.009	54.533	28.014	1.982	0.001	0.352	0	0.664	0.073	12.395	98.023
				0.047	55.291	28.158	1.562	0.017	0.323	0	0.455	0.059	11.275	97.187
				0.016	54.221	28.375	1.691	0.071	0.269	0.039	0.473	0.084	11.383	96.6221
				0.037	54.773	28.169	1.476	0.062	0.325	0.015	0.54	0.03	11.376	96.803
				0.003	55.179	28.038	1.004	0.123	0.388	0.003	0.423	0.029	11.513	96.703
				0.017	55.005	28.489	1.507	0.02	0.276	0.001	0.581	0.098	11.379	97.3731
		JJ-B41-3		0.019	54.231	27.695	1.339	0.012	0.053	0.012	0.611	0.014	12.089	96.0751
		JJ-B41-4		0.009	54.704	28.143	1.209	0	0.017	0.014	0.395	0.014	11.982	96.4871
				0	54.403	27.898	1.429	0.027	0.027	0.018	0.608	0.039	11.951	96.4001
				0.01	54.879	27.967	1.648	0.008	0.057	0	0.395	0.009	12.024	96.9971
				0.033	54.397	28.335	0.996	0	0.03	0.017	0.534	0.039	11.797	96.178
		JJ-B41-5		0.034	54.844	28.353	1.272	0.037	0.031	0.008	0.461	0.016	11.867	96.9231
				0.048	55.584	28.155	0.866	0	0.094	0.021	0.475	0.041	11.861	97.1451
		JJ-B41-6		0	54.982	27.819	1.327	0.006	0.027	0.011	0.559	0	11.721	96.452
				0.017	54.357	28.71	1.072	0.016	0	0.012	0.3	0	11.881	96.3651
				0.009	55.231	27.936	0.705	0.022	0.157	0.012	0.493	0	11.728	96.2931
				0	54.467	28.542	0.8	0.011	0.091	0.026	0.736	0.052	11.647	96.3721
				0.03	54.973	28.608	1.1	0.01	0.05	0.04	0.534	0.036	11.573	96.9541
Plagioclase	Garnet	13-001A		5.90	27.18	56.19	0.00	9.21	0.03	0.23	0.02	0.00	0.24	98.99
		13-001B		8.16	24.57	61.10	0.01	5.84	0.05	0.07	0.00	0.02	0.07	99.89
				7.46	24.80	59.50	0.02	6.69	0.01	0.07	0.01	0.01	0.27	98.82
	Staurolite	12-003A		8.35	24.41	60.89	0.03	5.84	0.01	0.07	0.01	0.02	0.34	99.97
		JJ-A11		8.40	24.14	61.98	0.01	4.48	0.02	0.42	0.00	0.00	0.01	99.45
				10.28	20.55	66.42	0.01	1.63	0.00	0.07	0.10	0.04	0.44	99.53
		JJ-B11-10		8.54	24.74	61.90	0.00	5.47	0.04	0.07	0.00	0.00	0.02	100.77
		JJ-B21-8		7.30	25.56	59.53	0.01	7.20	0.00	0.06	0.00	0.00	0.19	99.84
		JJ-B21-10		6.79	26.14	57.89	0.00	8.10	0.03	0.08	0.00	0.02	0.03	99.08
				6.85	25.91	57.97	0.02	8.26	0.01	0.07	0.08	0.04	0.04	99.23
				6.81	26.16	58.04	0.04	8.00	0.08	0.07	0.00	0.02	0.01	99.23
		JJ-B41-3		8.09	24.67	60.75	0.00	5.91	0.00	0.09	0.02	0.00	0.08	99.61
				7.59	24.89	60.85	0.04	6.42	0.00	0.12	0.03	0.01	0.15	100.09
		JJ-B41-4		8.34	23.99	61.45	0.04	5.27	0.06	0.12	0.04	0.02	0.11	99.43
		JJ-B41-6		7.47	24.99	59.91	0.01	5.59	0.00	0.52	0.02	0.00	0.23	98.74
				8.11	24.18	61.62	0.00	5.69	0.00	0.07	0.02	0.00	0.09	99.77
				7.57	25.09	60.27	0.01	6.22	0.00	0.05	0.00	0.03	0.31	99.55
	Sillimanite	12-008		10.47	21.04	66.43	0.00	0.57	0.00	0.73	0.00	0.00	0.02	99.27
		13-018		10.71	20.40	68.15	0.01	0.64	0.04	0.08	0.02	0.01	0.09	100.14
				10.87	19.80	67.17	0.00	0.54	0.00	0.08	0.03	0.00	0.11	98.59

Table 6. Oxygen isotope ratios

Met. zone	Sample	Analysed phase	Comment	d18O
Chlorite	12-031	Quartz	country rock	14.31
		Quartz	vein	13.99
Biotite	12-020	Quartz	country rock	13.69
		Quartz	vein	14.72
	12-024	Quartz	country rock	13.10
		Quartz	vein	13.01
	12-028	Quartz	country rock	12.47
		Quartz	vein	13.58
Garnet	12-001	Quartz	41 mm from vein	13.29
		Quartz	24 mm from vein	13.27
		Quartz	16.5 mm from vein	13.21
		Quartz	11.5 mm from vein	13.28
		Quartz	3.5 mm from vein	13.04
		Quartz		13.07
		Quartz	vein	12.91
		Quartz		13.01
Kyanite	12-015	Kyanite	29 mm from vein	10.12
		Kyanite	18 mm from vein	9.99
		Kyanite	10 mm from vein	10.11
		Kyanite	6 mm from vein	10.15
		Kyanite	4 mm from vein	10.04
		Quartz	vein	13.02